

SYNTHESIS AND CHARACTERISATION OF METAL (Fe, Ga, Y) DOPED ALUMINA AND GALLIUM OXIDE NANOSTRUCTURES

by

Yanyan Zhao

*(Bachelor of Chemical Engineering, Zhengzhou University, China;
Master of Biochemical Engineering, Beijing University of Chemical
Technology, China.)*



Inorganic Material Research Group
School of Physical and Chemical Sciences
Queensland University of Technology

*This thesis is submitted in partial fulfillment of the requirements of the
degree of Doctor of Philosophy.*

May, 2008

Queensland University of Technology

DOCTOR OF PHILOSOPHY THESIS EXAMINATION

CANDIDATE NAME: Yanyan ZHAO
PRINCIPAL SUPERVISOR: Prof. Ray L. FROST
ASSOCIATE SUPERVISOR: Dr. Wayde N. MARTENS
CO-SUPERVISOR: A/Prof. H. ZHU

Under the requirements of PhD regulation 9.2, the above candidate was examined orally by the Faculty of Science. The members of the panel set up for this examination recommend that the thesis be accepted by the University and forwarded to the appointed Committee for examination.

Name	Signature
Panel chairman
Panel Member
Panel Member

Under the requirements of PhD regulation 9.15, it is hereby certified that the thesis of the above named candidate has been examined. I recommend on behalf of the Thesis Examination Committee that the thesis be accepted in fulfilment of the conditions for the award of the degree of Doctor of Philosophy.

Name
Signature.....
(Chair of Examiners, External Thesis Examination Committee)

This work is dedicated to my boyfriend Shiyi Li.

KEYWORDS

Alumina

Boehmite

Iron

Gallium

Yttrium

Gallium oxide

Gallium oxide hydroxide

Surfactant

Nanofibres

Nanotubes

Nanosheets

Nanorods

Hydrothermal treatment

X-ray diffraction

Transmission electron microscopy

N₂ adsorption/desorption

BET Surface area

Pore size distribution

Thermal decomposition

Thermogravimetric analysis

Infrared spectroscopy

Raman spectroscopy

ABBREVIATIONS

XRD	X-ray diffraction
SEM	Scanning electron microscopy
TEM	Transmission electron microscopy
IR	Infrared spectroscopy
BET	Brunauer, Emmett and Teller
TG	Thermogravimetric analysis
CRTA	Controlled rate thermal analysis
PEO	Poly(ethylene oxide), C₁₂₋₁₄H₂₅₋₂₉O (CH₂CH₂O)₇H
CTAB	N-cetyl-N,N,N-trimethylammonium bromide
EDX	Energy dispersive X-ray analysis
SAED	Small area electron diffraction

ABSTRACT

It is well known that nanostructures possess unique electronic, optical, magnetic, ferroelectric and piezoelectric properties that are often superior to traditional bulk materials. In particular, one dimensional (1D) nanostructured inorganic materials including nanofibres, nanotubes and nanobelts have attracted considerable attention due to their distinctive geometries, novel physical and chemical properties, combined effects and their applications to numerous areas. Metal ion doping is a promising technique which can be utilized to control the properties of materials by intentionally introducing impurities or defects into a material.

γ -Alumina (Al_2O_3), is one of the most important oxides due to its high surface area, mesoporous properties, chemical and thermal properties and its broad applications in adsorbents, composite materials, ceramics, catalysts and catalyst supports. γ -Alumina has been studied intensively over a long period of time. Recently, considerable work has been carried out on the synthesis of 1D γ -alumina nanostructures under various hydrothermal conditions; however, research on the doping of alumina nanostructures has not been forthcoming. Boehmite ($\gamma\text{-AlOOH}$) is a crucial precursor for the preparation of γ -Alumina and the morphology and size of the resultant alumina can be manipulated by controlling the growth of AlOOH.

Gallium (Ga) is in the same group in the periodic table as aluminum. β -Gallium (III) oxide ($\beta\text{-Ga}_2\text{O}_3$), a wide band gap semiconductor, has long been known to exhibit conduction, luminescence and catalytic properties. Numerous techniques have been employed on the synthesis of gallium oxide in the early research. However, these techniques are plagued by inevitable problems. It is of great interest to explore the synthesis of gallium oxide via a low temperature hydrothermal route, which is economically efficient and environmentally friendly.

The overall objectives of this study were: 1) the investigation of the effect of dopants on the morphology, size and properties of metal ion doped 1D alumina nanostructures by introducing dopant to the AlOOH structure; 2) the investigation of impacts of hydrothermal conditions and surfactants on the crystal growth of gallium

oxide nanostructures. To achieve the above objectives, trivalent metal elements such as iron, gallium and yttrium were employed as dopants in the study of doped alumina nanostructures. In addition, the effect of various parameters that may affect the growth of gallium oxide crystals including temperature, pH, and the experimental procedure as well as different types of surfactants were systematically investigated.

The main contributions of this study are: 1) the systematic and in-depth investigation of the crystal growth and the morphology control of iron, gallium and yttrium doped boehmite (AlOOH) under varying hydrothermal conditions, as a result, a new soft-chemistry synthesis route for the preparation of one dimensional alumina/boehmite nanofibres and nanotubes was invented; 2) systematic investigation of the crystal growth and morphology and size changes of gallium oxide hydroxide (GaOOH) under varying hydrothermal conditions with and without surfactant at low temperature; We invented a green hydrothermal route for the preparation of α -GaOOH or β -GaOOH micro- to nano-scaled particles; invented a simple hydrothermal route for the direct preparation of γ -Ga₂O₃ from aqueous media at low temperature without any calcination.

The study provided detailed synthesis routes as well as quantitative property data of final products which are necessary for their potential industrial applications in the future. The following are the main areas and findings presented in the study:

- **Fe doped boehmite nanostructures**

This work was undertaken at 120°C using PEO surfactant through a hydrothermal synthesis route by adding fresh iron doped aluminium hydrate at regular intervals of 2 days. The effect of dopant iron, iron percentage and experimental procedure on the morphology and size of boehmite were systematically studied. Iron doped boehmite nanofibres were formed in all samples with iron contents no more than 10%. Nanosheets and nanotubes together with an iron rich phase were formed in 20% iron doped boehmite sample. A change in synthesis procedure resulted in the formation of hematite large crystals. The resultant nanomaterials were characterized by a combination of XRD, TEM, EDX, SAED and N₂ adsorption analysis.

- **Growth of pure boehmite nanofibres/nanotubes**

The growth of pure boehmite nanofibres/nanotubes under different hydrothermal conditions at 100°C with and without PEO surfactant was systematically studied to provide further information for the following studies of the growth of Ga and Y doped boehmite. Results showed that adding fresh aluminium hydrate precipitate in a regular interval resulted in the formation of a mixture of long and short 1D boehmite nanostructures rather than the formation of relatively longer nanofibres/nanotubes. The detailed discussion and mechanism on the growth of boehmite nanostructure were presented. The resultant boehmite samples were also characterized by N₂ adsorption to provide further information on the surface properties to support the proposed mechanism.

- **Ga doped boehmite nanostructures**

Based on this study on the growth of pure boehmite nanofibre/nanotubes, gallium doped boehmite nanotubes were prepared via hydrothermal treatment at 100°C in the presence of PEO surfactant without adding any fresh aluminium hydrate precipitate during the hydrothermal treatment. The effect of dopant gallium, gallium percentage, temperature and experimental procedure on the morphology and size of boehmite was systematically studied. Various morphologies of boehmite nanostructures were formed with the increase in the doping gallium content and the change in synthesis procedure. The resultant gallium doped boehmite nanostructures were characterized by TEM, XRD, EDX, SAED, N₂ adsorption and TGA.

- **Y doped boehmite nanostructures**

Following the same synthesis route as that for gallium doped boehmite, yttrium doped boehmite nanostructures were prepared at 100°C in the presence of PEO surfactant. From the study on iron and gallium doped boehmite nanostructures, it was noted both iron and gallium cannot grow with boehmite nanostructure if iron nitrate and gallium nitrate were not mixed with aluminium nitrate before dissolving in water, in particular, gallium and aluminium are 100% miscible.

Therefore, it's not necessary to study the mixing procedure or synthesis route on the formation of yttrium doped boehmite nanostructures in this work. The effect of dopant yttrium, yttrium percentage, temperature and surfactant on the morphology and size of boehmite were systematically studied. Nanofibres were formed in all samples with varying doped Y% treated at 100°C; large $Y(OH)_3$ crystals were also formed at high doping Y percentage. Treatment at elevated temperatures resulted in remarkable changes in size and morphology for samples with the same doping Y content. The resultant yttrium doped boehmite nanostructures were characterized by TEM, XRD, EDX, SAED, N_2 adsorption and TGA.

- **The synthesis of Gallium oxide hydroxide and gallium oxide with surfactant**

In this study, the growth of gallium oxide hydroxide under various hydrothermal conditions in the presence of different types of surfactants was systematically studied. Nano- to micro-sized gallium oxide hydroxide was prepared. The effect of surfactant and synthesis procedure on the morphology of the resultant gallium oxide hydroxide was studied. β -gallium oxide nanorods were derived from gallium oxide hydroxide by calcination at 900°C and the initial morphology was retained. γ -gallium oxide nanotubes up to 65 nm in length, with internal and external diameters of around 0.8 and 3.0 nm, were synthesized directly in solution with and without surfactant. The resultant nano- to micro-sized structures were characterized by XRD, TEM, SAED, EDX and N_2 adsorption.

- **The synthesis of gallium oxide hydroxide without surfactant**

The aim of this study is to explore a green synthesis route for the preparation of gallium oxide hydroxide or gallium oxide via hydrothermal treatment at low temperature. Micro to nano sized GaOOH nanorods and particles were prepared under varying hydrothermal conditions without any surfactant. The resultant GaOOH nanomaterials were characterized by XRD, TEM, SAED, EDX, TG and FT-IR. The growth mechanism of GaOOH crystals was proposed.

PUBLICATIONS AND CONFERENCE PRESENTATIONS

1. Zhao, Yanyan; Martens, Wayde N.; Bostrom, Thor E.; Zhu, Huai Yong; Frost, Ray L.. **Synthesis, Characterization, and Surface Properties of Iron-Doped Boehmite Nanofibers.** *Langmuir* (2007), 23(4), 2110-2116.
2. Zhao, Yanyan; Frost, Ray L.; Martens, Wayde N.; Zhu, Huai Yong. **Growth and Surface Properties of Boehmite Nanofibers and Nanotubes at Low Temperatures Using a Hydrothermal Synthesis Route.** *Langmuir* (2007), 23(19), 9850-9859
3. Zhao, Yanyan; Frost, Ray L.; Martens, Wayde N.. **Gallium-Doped Boehmite Nanotubes and Nanoribbons. A TEM, EDX, XRD, BET, and TG Study.** *Journal of Physical Chemistry C* (2007), 111(14), 5313-5324.
4. Zhao, Yanyan; Frost, Ray L.; Martens, Wayde N.. **Synthesis and Characterization of Gallium Oxide Nanostructures via a Soft-chemistry Route.** *Journal of Physical Chemistry C.* (2007), 111(44), 16290-16299.
5. Zhao, Yanyan; Frost, Ray L.; Jin Yang; Martens, Wayde N.. **Size and Morphology Control of Gallium Oxide Hydroxide GaO(OH) Nano- to Micro-sized particles by Soft-chemistry Route without Surfactant.** *Journal of Physical Chemistry C.* (2008), 112(10), 3568-3579.
6. Zhao, Yanyan; Frost, Ray L.. **Synthesis and Surface Characterization of Yttrium Doped Boehmite Nanofibres.** *Journal of Colloid and Interface Science.* (2008), 326(1), 289-299.
7. Zhao, Yanyan; Frost, Ray L.. **XRD, TEM and thermal analysis of Yttrium doped boehmite nanofibres.** *Journal of Nanoscience and Nanotechnology.* (2008), Accepted
8. Zhao, Yanyan; Yang, Jing; Frost, Ray L.. **Dynamic and Controlled rate thermal analysis, surface analysis and infrared emission of Ga doped boehmite nanofibres and nanosheets.** *Thermochimica Acta.* Under review.
9. Zhao, Yanyan; Frost, Ray L.; Martens, Wayde N.; Zhu, Huai Yong. **XRD, TEM and Thermal Analysis of Fe Doped Boehmite Nanofibres and Nanosheets.** *Journal of Thermal Analysis and Calorimetry,* (2007), 90(3), 755-760.
10. Zhao, Yanyan; Frost, Ray L.; Vágvölgyi, Veronika; Martens, Wayde N.; Kristóf, János; Horváth, Erzsébet. **XRD, TEM and Thermal Analysis of**

Yttrium Doped Boehmite Nanofibres and Nanosheets. *Journal of Thermal Analysis and Calorimetry*, (2008), 94(1), 219-226.

11. Zhao, Yanyan; Yang, Jing; Frost, Ray L. **Raman Spectroscopy of the Transition of α -gallium Oxyhydroxide to β -gallium Oxide Nanorods.** *Journal of Raman Spectroscopy* (2008), 39(10), 1327-1331.
12. Zhao, Yanyan; Frost, Ray L. **Raman spectroscopy and characterization of α -gallium oxyhydroxide and β -gallium oxide nanorods.** *Journal of Raman Spectroscopy* (2008), 39(10), 1494-1501.
13. Zhao, Yanyan; Martens, Wayde N.; Zhu, Huaiyong; Frost, Ray L.. **Synthesis and Characterisation of Iron Doped Boehmite Nanofibres, Nanotubes and Nanosheets.** *2006 International Conference Of Nanoscience and Nanotechnology*, Brisbane, Australia, 2006. Published in the proceeding.

TABLE OF CONTENTS

KEYWORDS	4
ABBREVIATIONS	5
ABSTRACT	6
PUBLICATIONS AND CONFERENCE PRESENTATIONS	10
STATEMENT OF ORIGINALITY	15
ACKNOWLEDGEMENTS	16
CHAPTER 1	17
Introduction and Literature review.....	17
1.1 Introduction.....	17
1.2 Synthesis of aluminum based 1D nanostructure	19
1.2.1 The importance of alumina	19
1.2.2 The importance of boehmite for the fabrication of alumina nanostructure.....	19
1.2.3 Studies on the synthesis of boehmite or alumina nanostructures.....	20
1.2.3.1 Without surfactant.....	20
1.2.3.2 With surfactant.....	23
1.2.4 Others studies related to this project	26
1.3 Synthesis of gallium based 1D nanostructure	28
1.3.1. The importance of gallium oxide.....	28
1.3.2 Studies on the synthesis of gallium oxide hydroxide and gallium oxide nanostructures.....	28
1.3.2.1 Investigations on the growth of GaOOH and Ga ₂ O ₃ nanostructures via hydrothermal reaction.....	29
1.3.3 Other studies related to this project.....	32

1.4	Summary	33
1.5	References	35
CHAPTER 2		39
Synthesis, Characterization, and Surface Properties of Iron-Doped Boehmite Nanofibers		
CHAPTER 3		49
Growth and Surface Properties of Boehmite Nanofibres and Nanotubes at Low Temperatures Using a Hydrothermal Synthesis Route		
CHAPTER 4		62
Gallium-Doped Boehmite Nanotubes and Nanoribbons: A TEM, EDX, XRD, BET, and TG Study		
CHAPTER 5		77
Synthesis and Surface Characterization of Yttrium Doped Boehmite Nanofibres		
CHAPTER 6		91
Synthesis and Characterization of Gallium Oxide Nanostructures via a Soft-chemistry Route		
CHAPTER 7		104
Size and Morphology Control of Gallium Oxide Hydroxide GaO(OH) Nano- to Micro-sized particles by Soft-chemistry Route without Surfactant		
CHAPTER 8		118
Summary and Conclusions.....		
8.1	Summary.....	118
8.2	Conclusions	122
CHAPTER 9		124
Additional support papers		

CHAPTER 9.1	126
Synthesis and Characterization of Iron Doped Boehmite Nanofibres, Nanotubes and Nanosheets	
CHAPTER 9.2	133
XRD, TEM and Thermal Analysis of Fe Doped Boehmite Nanofibres and Nanosheets	
CHAPTER 9.3	142
Raman Spectroscopy of the Transition of α -gallium Oxyhydroxide to β -gallium Oxide Nanorods	
CHAPTER 9.4	150
XRD, TEM and Thermal Analysis of Yttrium Doped Boehmite Nanofibres and Nanosheets	
CHAPTER 9.5	161
Raman Spectroscopy and Characterization of α -gallium Oxyhydroxide and β -gallium Oxide Nanorods	
CHAPTER 9.6	172
Dynamic and Controlled rate Thermal analysis, Surface Analysis and Infrared Emission of Ga Doped Boehmite Nanofibres and Nanosheets	

STATEMENT OF ORIGINALITY

The work contained in this thesis has not been previously submitted to meet requirements for an award at this or any other higher education institution. To the best of my knowledge and belief, the thesis contains no material previously published or written by another person except where due reference is made.

Signed _____

Date _____

ACKNOWLEDGEMENTS

I would like to thank my supervisory team: Prof. Ray Frost, Dr Wayde Martens and A/Prof. Huaiyong Zhu, for their patience, help and support throughout my PhD. It was a pleasure working with all of them.

I would have been impossible to conduct the necessary analysis of my samples without the help of the various technical and research staff in both QUT and UQ. My thanks go to: Dr Llew Rintoul, Dr Thor Bostrom, Tony Raftery, Lambert Bekessy, Dr Loc Doung and Dr Adrienne Chandler

My thanks also go to my fellow honors students and postgraduate students who have provided an interesting and supportive work environment during my time at QUT.

Thanks to IMRP and SPCS for their financial support.

And finally, I would also like to thank my mum Lanzhi Cheng, my dad Wenxing Zhao and my sister Yanling Zhao for their enthusiastic support.

CHAPTER 1

Introduction and Literature review

1.1 Introduction

One nanometre (nm) is one billionth of a meter, which is the size of a large molecule. A structure with at least one dimension between 1 and 100 nm is defined as a nanostructure. Nanoscale structures have unique properties [1, 2]. Most of their behavior cannot be described by classical mechanics, but can only be explained by quantum mechanics [3]. The most interesting and important property of nanostructures is that their chemical and physical properties are size and shape dependent. Due to quantum size effects, nanostructures possess unique electronic, optical and magnetic properties superior to traditional bulk materials. The size-dependent behavior of these nanostructures enables researchers to design and produce devices with particular or advanced properties, such as high performance electronic and optoelectronic devices by employing nanostructures as building blocks [4-6].

Although the interesting nanoscale effects have been recognized for a long time, it was not until the year of 1960 that scientists began to seriously move into this area [3]. Since the discovery of carbon nanotubes in 1991 [7], there have been significant efforts to synthesize nanostructures. However, the development on nanoscale research stayed at a very low rate until the year 2000 due to the lack of instrumentation suitable to manufacture and characterize such small structures. There are two basic approaches for nanofabrication. One is the top-down method; the other is the bottom-up method. In the past years, especially before the late 1980s, nanofabrication was mainly carried by the top-down method which starts with bulk material and cuts it until it is down to the nanoscale. Conversely, starting with individual atoms and building up to a nanostructure is called bottom-up nanofabrication [3].

In the past few years, supported by the advanced measuring and manufacturing techniques, nanotechnology is becoming one of the most interesting fields in today's

science, business and news. In Australia, nanotechnology is also a rapidly growing area of research, development and commercialization. It is supported by strong government commitment, business initiatives and international collaboration which will ensure the nation's place at the forefront of this emerging strategic industrial and scientific capability. According to a government report in 2005, combined with state and territory governments and private entities, up to AU\$100 million per annum is being invested for research and commercialization purposes [8]. The fundamental research work of nanotechnology in Australia is quickly leading to applications across a range of industries ranging from complex surface coatings to new forms of drug delivery and quantum computing devices [8].

A variety of materials including carbons, metals, glass, polymers and ceramics have been employed to produce nanomaterials or nanostructures. Based on the morphology, nanostructures can be roughly grouped into four categories [9]: zero-dimensional nanostructures; one-dimensional nanostructures; two-dimensional nanostructures and special nanomaterials. Spheres, cubes and platelets are some of the possible morphologies for nanoparticles; nanofibres, nanowires, nanoribbons, nanobelts and nanotubes are considered as one-dimensional nanostructures; nanofilms are the typical morphology for two-dimensional nanostructures; while some bulk materials with nanosized building blocks, such as nanograined ceramics and nanocomposites are classified as special nanomaterials.

Synthesis of inorganic nanostructures has been of great interest in material science and nanotechnology over the last decades [1, 2, 7]. Due to the distinctive geometries, novel physical and chemical properties, combined effects and their applications in numerous areas, one dimensional (1D) nanostructured inorganic materials (nanofibres, nanotubes, nanobelts and nanowires) have attracted considerable attention [10, 11].

This review will focus on the synthesis of 1D aluminum and gallium based nanostructures via a soft chemistry method.

1.2 Synthesis of aluminum based 1D nanostructure

1.2.1 The importance of alumina

Alumina (Al_2O_3), is one of the most important metal oxides and has been studied intensively over a long period of time because of its broad applications in adsorbent [12, 13], composite materials [14, 15], ceramics [16-18], catalysts and catalyst supports [19, 20]. At least seven transition alumina phases have been reported so far on the basis of ^{27}Al MAS NMR spectroscopy, powder X-ray diffraction (XRD) and other scattering techniques [21-25]. Among these, $\gamma\text{-Al}_2\text{O}_3$ is widely used in catalysis as an active phase and is characterized by having acidic sites which determines the activity and selectivity of the catalyst for specific catalytic reactions [26]. Due to its excellent thermal stability and chemical properties, γ -alumina has also been extensively used as carrier and support for a variety of industrial catalysts in many chemical processes including cracking, hydrocracking, and hydrodesulfurization of petroleum feedstock [19, 20, 27]. Since nanomaterials possess large surface areas, research into the nanochemistry of alumina based nanomaterials will lead to new catalysts.

1.2.2 The importance of boehmite for the fabrication of alumina nanostructure

Alumina is formed through the thermal dehydration of aluminum hydroxides and oxyhydroxides. Among the alumina precursors, boehmite ($\gamma\text{-AlOOH}$) is of special interest because its transformation into $\gamma\text{-Al}_2\text{O}_3$ is pseudomorphic which preserves the boehmite texture [28]. It was reported that $\gamma\text{-Al}_2\text{O}_3$ was formed through the dehydration of the boehmite at temperatures ranging from 400 to 700°C [21, 23, 28-30]. During heating, boehmite nanostructures undergo an isomorphous transformation to nanocrystalline alumina.

It is well known that the properties of nanostructured materials depend on their size and morphology. Therefore the investigation of morphology and size control of boehmite is of fundamental importance in designing the properties of alumina one

dimensional (1D) nanomaterial, such as nanofibres, nanowires, nanotubes and nanoribbons. This is of great interest due to their special properties for fabrication of nanodevices [10, 31-33]. Since boehmite nanofibres were first synthesised by John Bugosh in 1961 [34], intense effort has been devoted to the investigation of 1D boehmite nanostructures including nanofibres [35-41], nanobelts [42], nanorods [43] and nanotubes [37, 44] via hydrothermal routes.

1.2.3 Studies on the synthesis of boehmite or alumina nanostructures.

As discussed above, controlling the particle size and morphology is of great interest to improve the potentialities of alumina in catalysis. Various boehmite synthesis procedures have been investigated in the literature in order to control particle size and morphology as well as porosity of the resulting powders.

Boehmite can be obtained by several techniques including sol-gel [45-48], neutralization of acidic salts [35, 36], precipitation of aluminates [49], laser ablation [50] and template-based synthesis [51]. Because of significant advantages including controllable particle size, low temperature, cost-effectiveness and less-complicated techniques, sol-gel and the neutralization of acidic salts by direct addition of a base such as NaOH, NH₄OH or thermal decomposition of urea are the most usual ways. The size and morphology of the boehmite formed from the hydrolysates depend on the conditions such as pH, temperature, nature of salts and bases, pressure and also the ageing of the hydrolysates [52]. Ageing can affect the rates of peptisation of the alumina sols. Ageing of the oxy-hydroxides as gels causes structural changes in the sequence amorphous-pseudoboehmite-bayerite-gibbsite [53, 54]. The synthesis of boehmite or alumina nanostructure via hydrothermal or sol-gel methods can be roughly divided into two groups: with surfactant and without surfactant.

1.2.3.1 Without surfactant

In this study, fibrous boehmite precipitate as well as sol was prepared by hydrolysis of a basic aluminum chloride solution at 160°C with a reaction time ranging from 4 to 16 hours. The resulting boehmite consisted of stable colloidal fibrils, ~5 nm in diameter, which is physically analogous to linear, high molecular weight organic

molecules.

Morgado et al. [55] investigated the synthesis of boehmite from hydrolysed aluminum nitrate solutions and discussed the relationship between the synthesis conditions and the peptisation ability of the resulting boehmite gel. Boehmite was synthesized through neutralizing an aluminum nitrate solution with NH_4OH under various conditions, followed by an aging step at high OH/Al ratio and temperature. Two methods of adding the reactants were used in the neutralization step including sequential dosing with variable pH and simultaneous dosing with constant pH [55]. Two different temperatures (25°C and 85°C) were used as variable parameters in the neutralization step. It was reported that low temperature precipitation resulted in the formation of peptisable boehmite, whereas high temperatures combined with high OH/Al ratios (>3.0) led to nonpeptisable boehmite [55]. Randomly interconnected fibrils were formed in nonpeptisable boehmite samples. In particular, agglomerated fibril bundles were formed in the sample synthesized at 85°C via simultaneous dosing at a OH/Al ratio of 3.1 [55].

Martens et al. [56] investigated the structure and peptisation of boehmite and alumina prepared from Hydrolysis of tri-sec-butoxyaluminum (III) (ASB). The alumina hydrolysates were prepared by adding modified ASB solution into alkoxide water solution at a molar ratio of 1:100 alkoxide to water under vigorous stirring at different temperatures. Amorphous aluminum oxy hydroxide was formed on the hydrolysis of ASB in water at 25°C . This amorphous AlOOH underwent ageing and formed pseudoboehmite then bayerite via a dissolution-re-precipitation process. When alumina, precipitated from the action of water on ASB at 75°C , formed pseudoboehmite, no ageing process was observed. Boehmite nanofibres were formed after 2 hours ageing at 75°C .

Hochepped et al. [35, 36] studied the effect of precipitation condition including pH temperature and mixing procedure on the morphology and porosity of boehmite particles synthesized by precipitation of aluminum nitrates with soda. The results showed that one-step synthesis at 60°C , pH 9 led to a crystallized boehmite phase where polycrystalline boehmite nanofibres were formed; two-step synthesis by temperature and pH jumps to 60°C , pH 9 resulted in the formation of an isolable

amorphous hydroxide firstly, and then the amorphous phase subsequently transformed into porous boehmite constituted by the agglomeration of irregular boehmite nanocrystals [36]. It was also reported that the mixing procedure did affect the morphology of resultant boehmite by keeping the identical aging condition (T 60°C, pH 9, 2 hours aging) [35]. Injection of nitrate aluminum solution into soda and injection of soda to nitrate aluminum solution led to microporous boehmite and bayerite respectively; whereas double jet procedure resulted in the formation of boehmite nanofibres [35].

Kuiri et al. [57] reported a solution-based chemical synthesis of boehmite nanofibres and alumina nanorods by a modified sol-gel process in the presence of organic solvent. The conventional process for alumina synthesis includes hydrolysis of the aluminum alkoxide at about 80°C, followed by a series of synthesis steps such as peptisation in mild acidic condition, solvent evaporation, drying, and calcination [57]. In this study, boehmite nanorods were synthesized by the following steps: 1) Preparing aluminum isopropoxide in anhydrous ethanol under magnetic stirring; 2) Adding ethanol solution with 4% water into it; 3) Reacting for 15 h to form a viscous liquid; 4) calcinating at 600°C for 4 hours [57]. The length of the resulting boehmite/alumina nanorods were up to 10 µm whereas the diameter varied.

Bokhimi et al. [58] investigated the properties of colloidal particles in a sol prepared with aluminum tri-sec-butoxide and 2-propanol containing different concentrations of sulphuric acid. The particles were nanocapsules with diameters between 10 and 50 nm and shells 3.5 nm thick. Boehmite nanofibres were formed at low sulphate ions where the nanocapsules interacted with each other leading to the reorganization of atoms. High sulphate ions diminished the interaction by covering all the nanocapsules in the sample [58]. Therefore the morphology of boehmite can be controlled by adjusting the concentration of sulphate, consequently, control the texture of the sample when it was calcined.

Zhang et al. [59] reported a template-free preparation method for the synthesis of boehmite nanowires. The boehmite nanowires in this study were prepared using AlCl₃ and Na₂B₄O₇ as precursors and hydrothermally treated at 200°C for 24 hours. The resulting nanowires with an average diameter of ~20 nm are arrayed in an

ordered fashion and are closely packed together. It was reported that the morphology and size of the AlOOH strongly depend on alkali salts $\text{Na}_2\text{B}_4\text{O}_7$. Without $\text{Na}_2\text{B}_4\text{O}_7$, no precipitate was observed. Irregular nanowires were observed when $\text{Na}_2\text{B}_4\text{O}_7$ was replaced by NaOH. The authors proposed that adding $\text{Na}_2\text{B}_4\text{O}_7$ in this system increased the chemical potential of the solution which would be advantageous for 1D nanostructure growth [60]. Shen et al. [43] synthesized boehmite nanorods using $\text{Al}(\text{NO}_3)_3$ and NH_4OH as precursors thermally treated at 200°C for up to 48 hours via a steam-assisted solid wet-gel route. After five hours calcination at 600°C , $\gamma\text{-Al}_2\text{O}_3$ nanorods with clear-cut edges were obtained.

Lepot et al. [61] prepared platelet-shaped nanostructures together with a small amount of fibular γ -boehmite and γ -alumina nanoparticles by hydrothermal treatment using aluminum iso-propoxide as precursor without using any surfactant. Irregular shaped γ -boehmite nanoparticles were prepared by Potdar et al. [62] using aluminum nitrate and sodium carbonate as starting materials at 70°C . The catalytic property of the resultant γ -alumina was tested.

1.2.3.2 With surfactant

Kuang et al. [44] reported the formation of tubular boehmite and alumina nanostructures using AlCl_3 and NaOH as precursors at 120°C via hydrothermal treatment in the presence of a cationic N-cetyl-N,N,N-trimethylammonium bromide (CTAB) surfactant. The resulting nanotubes are typically 30~70 nm in length, 3~4 nm and 5~6 nm for inner and outer diameters respectively. The BET surface areas of the boehmite AlOOH and γ -alumina are 137.5 and 205.5 $\text{m}^2 \text{g}^{-1}$, respectively. The authors proposed that $\text{CTA}^+ \text{-AlO}_2^-$ ion pairs are formed initially by electrostatic interaction between the CTAB surfactant and the NaAlO_2 in aqueous solution, followed by the formation of ordered lamellar structures via the assembly of $\text{CTA}^+ \text{-AlO}_2^-$ ion pairs under the hydrothermal conditions. These lamellar sheets began to loosen at the sheet edge and roll into separate scrolls with increasing reaction temperature.

Zhang et al. [38, 63] synthesized porous lath to rod shaped alumina nanoparticles by ageing an aqueous mixture of $[\text{Al}_{13}\text{O}_4(\text{OH})_{24}(\text{H}_2\text{O})_{12}]\text{Cl}_7$ with a nonionic tri-block

Pluronic P84 ((EO)₁₉(PO)₃₉(EO)₁₉) surfactant at 150°C. After calcination, mesostructured aluminas, composed of γ -Al₂O₃ walls were formed. The results indicated that the key to obtaining these structures is the formation of a mesostructured surfactant/boehmite precursor, assembled through the hydrolysis of an aluminum cation, oligomer, or molecule in the presence of a nonionic surfactant [38, 63].

Lee et al. [37] studied the effect of surfactants on the morphology of boehmite/alumina by using tri-sec-butoxide as precursor hydrothermally treated at 150°C for 72 hours followed by 4 hours calcination at 500°C in the flow of air. Cationic, anionic, neutral and nonionic surfactants were employed for this study. Using cationic and noionic surfactant led to the formation of isolated individual and branched nanotubes. Nanofibres and nanorods were formed for samples synthesized with anionic and neutral surfactant respectively. Lee et al. [37] also compared synthesis methods with and without organic solvent (1-butanol). It was reported that with organic solvent, mesoporous alumina molecular sieves with a wormhole like morphology were formed [64] whereas nanofibres were formed under the same condition but without organic solvent in Lee and co-workers study. Based on the research of Lee et al. [37], Kim et al. [65] reported the preparation of lithium doped alumina nanotubes, 3.6~6.9 nm in diameter and 100~400 nm in length. Since the Li ions in this material appeared to be highly mobile at moderate conditions, the lithium alumina could be a promising candidate as a solid ionic conductor [65].

Zhu et al. [66] prepared fibrous crystallites of γ -alumina about 3-4 nm thick and 30-60 nm long by introducing nonionic poly(ethylene oxide) surfactant to aluminum hydrate colloids. Results showed that the surfactant can effectively direct the crystal growth of boehmite and the crystal morphology of the final γ -alumina crystallites. Boehmite nanofibres stack randomly, resulting in a structure with a low contact area between the fibers but with a very large porosity. Such a structure exhibits strong resistance to sintering when heated to high temperatures. Zhu et al. [40] also reported a novel approach for the growth of the boehmite nanofibers. When fresh aluminum hydrate precipitate was added at regular interval to the initial mixture of boehmite and PEO surfactant at 373 K, the nanofibers grow from 40 to 50 nm long to over 100 nm. The results indicate that the surfactant micelles play an important role in the

nanofiber growth: directing the assembly of aluminum hydrate particles through hydrogen bonding with the hydroxyls on the surface of aluminum hydrate particles [40]. Meanwhile a gradual improvement in the crystallinity of the fibers during growth is observed and attributed to the Ostwald ripening process. Using such an approach, the size and morphology of boehmite nanofibres can be precisely controlled through soft chemical methods [66]. This novel approach could be useful for low temperature, aqueous syntheses of other oxide nanomaterials with tailorable structural specificity such as size, dimension and morphology. This method has been applied to the synthesis of FeOOH 1D nanostructures and iron doped boehmite nanostructures by Frost's group [67].

Gao et al. [42] prepared 10 nm wide single crystal boehmite nanobelts by a simple and efficient 'molecule tailoring lamella' route. In this study, anionic surfactant AOT was employed. Different size nanobelts can be obtained by only changing the concentration of the tailoring agent. Gao et al. [42] proposed that when the anionic surfactant is used in the formation of the lamellar hydroxyl inorganic-surfactant mesostructures, the surfactant will interact with the hydrogen atom of the hydroxyl and gradually break the hydrogen bonds resulting in splitting of the lamellar structures and produce thin and narrow belt-like nanostructures.

Kim et al. [68] prepared high surface area boehmite nanofibres and nanosheets via a simple sol-gel route using aluminum iso-propoxide, acetic acid and 2-propanol as the Al precursor, solvent and hydrolysis rate controller, respectively. The surface area of the resulting boehmite nanostructures was $\sim 442.9 \text{ m}^2\text{g}^{-1}$ by digestion of precipitate at 80°C for 20 hours.

Liu et al. [69] synthesized mesoporous γ -aluminas via hydrothermal processing using boehmite sol as precursors and non-ionic surfactant $\text{EO}_{20}\text{PO}_{70}\text{EO}_{20}$ as the structure-directing agent. Nanofibres were observed in the boehmite sol and the resultant γ -alumina. The properties of Fe and Pb loaded alumina catalysts were also investigated.

Besides these 1D boehmite or alumina nanostructures, Naskar et al. [70] reported the preparation of uniform spherical boehmite nanoparticles at the presence of

surfactant through two-reverse emulsion approach and the average particles size of boehmite was around 10 nm. Zhang et al. [71] synthesized flower-like three dimensional boehmite nanoarchitectures using AlCl_3 as the precursor via hydrothermal treatment in a mixed ethanol-water solution without employing templates or matrixes. In his study, AlCl_3 ethanol-water solutions were treated at 200°C for 72 hours followed by annealing the AlOOH nanoarchitectures in air atmosphere at 1000°C for 5 hours after which $\theta\text{-Al}_2\text{O}_3$ flowerlike nanoarchitectures were obtained [71].

1.2.4 Others studies related to this project

To a large extent, the key for fabrication of functional catalysts, ceramics and nanostructures is manipulation of the surface and interfacial energies. As for alumina, the transformation from γ -alumina (defect spinel structures) into the α -alumina (corundum structure) leads to a dramatic decrease in surface area. Therefore, the major challenge for alumina in applications as catalyst supports and ceramic precursors is to retain large surface areas during high-temperature annealing. In order to manipulate the phase transformation temperature and surface area of alumina, Castro et al. [72] investigated the relationship between dopants and surface energy and thermodynamic stability of γ -alumina by using Zr and Mg as additives. Results showed that dopants changed the pattern of phase transformation and densification. Zr doped γ -alumina showed a higher energy of the hydroxylated surface than that of pure γ -alumina but showed a lower energy of the anhydrous surface. Mg additions did not significantly change surface energies but decreases the energetic instability of the γ -alumina phase. Djuričić et al. [73] also studied the morphology and thermal stability of Zr doped alumina prepared by homogeneous precipitation from an aqueous salt solution followed by calcination in air. Boehmite nanofibres and nanosheets with irregular shape were formed after hydrothermal treatment. The results showed that zirconia was insoluble in $\alpha\text{-Al}_2\text{O}_3$ so that phase transformation to $\alpha\text{-Al}_2\text{O}_3$ was accompanied by a phase separation to form an alumina-zirconia nanocomposite. The thermal stability of the transition phases was increased both by the dopant and by hydrothermal treatment.

Xue et al. [14] synthesized Fe-Al₂O₃ nanocomposite by reducing a mixture of FeOOH and AlOOH dry gel at different temperatures in a hydrogen atmosphere and studied the magnetic properties of the Fe-Al₂O₃ nanocomposite. The results showed that the magnetic properties of the nanocomposite can be controlled by the concentration and size of the Fe nanoparticles.

Van Bruggen [74] successfully prepared colloidal core-shell rods with adjustable aspect ratios. In this study, colloidal boehmite nanorods were used as cores for the preparation of rods with a silica shell. The results showed that the silica/boehmite nanorods are stable in various solvents including water, ethanol, propenol and dimethylformamide (DMF).

Among those non-reducible oxide supporting Au catalysts, Au/ γ -Al₂O₃ is of great interest for both practical application and academic study. Han et al. [75] studied the catalytic properties of Au nanoparticles supported on 1D γ -Al₂O₃ nanofibres and commercial γ -Al₂O₃ during CO oxidation at low temperature. The results showed that the activity of the Au catalysts supported by γ -Al₂O₃ nanofibres was remarkably higher than that supported by commercial γ -Al₂O₃. It was also reported that tiny modifications of the structure of γ -Al₂O₃ matrix may have a strong influence on the structure and activity of the Au nanoparticles.

Alumina coating of particles has been used in many fields such as ceramics, battery materials, phosphors, magnetic materials and pigments. A layer of alumina oxide coating can increase the amount of -OH groups on the particle surface which can improve the dispersibility of the particles in aqueous solution and provide more active sites for further organic modification. Wu et al. [76] synthesized hydrous alumina coated TiO₂ particles via aqueous precipitation.

Petre et al. [77] reported that gallium-containing catalysts exhibit very interesting catalytic properties in the selective catalytic reduction (SCR) of NO_x with hydrocarbons in the presence of oxygen and in the dehydrogenation and/or aromatization of alkanes. Different oxide matrices have been tested in Petre et al.'s study [77] as supports for gallium oxide. In particular, alumina-supported gallium oxide is the most promising candidate for practical applications due to its high

activity, selectivity and hydrothermal stability.

1.3 Synthesis of gallium based 1D nanostructure

1.3.1. The importance of gallium oxide

Gallium (III) oxide, also known as gallia, is a chemical which may be fired into ceramic material with high melting point of about 1900°C. It behaves like an insulator at room temperature and as a semi-conductor above 800°C owing to its wide band gap [78].

Gallium oxide can crystallize forming the polymorphs α , β , γ , δ and ϵ , similar to alumina. Among these five modifications, β -Ga₂O₃ is the only thermodynamically stable polymorph and has a monoclinic structure where Ga³⁺ ions occupy both distorted tetrahedral and distorted octahedral sites. β -Ga₂O₃ is a wide band gap semiconductor ($E_g = 4.9$ eV) and has long been known to exhibit both conduction and luminescence properties [79, 80]. β -Ga₂O₃ is chemically and thermally stable and is useful for insulating oxide layers for all gallium-based semiconductors [81, 82]. Also, β -Ga₂O₃ has potential application in optoelectronic devices including flat-panel displays, solar energy conversion devices, optical limiters for ultraviolet light, and high-temperature stable oxygen gas sensors [81, 83-89]. Furthermore, gallium oxide can be employed as a catalyst [77, 90, 91]. In particular, a large surface area/volume ratio is necessary for both sensor and catalyst applications. Low-dimensional structures which possess large surface area/volume ratios, such as nanowires, nanoribbons, nanotubes and nanosheets display interesting properties which can be exploited in fabricating the next generation of optoelectronic and sensing devices.

1.3.2 Studies on the synthesis of gallium oxide hydroxide and gallium oxide nanostructures.

It is noted that the recent studies on the synthesis of one-dimensional gallium oxide nanostructures usually involves several techniques such as physical evaporation via a

vapour-solid process [79, 83, 92-94], chemical vapour deposition [95-98], thermal evaporation [99], implantation-assisted synthesis [100], arc discharge [81], catalyst-assisted methods [82, 86, 101], oxidation milling of GaN powder [102], laser ablation [103], thermal annealing [104, 105] and microwave plasma [106, 107]. However, these methods face several kinds of problems. Firstly, they are time consuming and complex procedures through which some other nanostructures are needed to induce and direct the growth of the gallium oxide nanostructure and this leads to troubles in purification; secondly, high operation temperatures, usually around 1300°C or even above 1600°C are required; thirdly, introducing Ni, C and expensive elements (such as Au) as catalyst may influence the properties of the target materials and those are difficult to remove from the gallium oxide nanostructures. It is of great interest to explore the synthesis of gallium oxide hydroxide or oxide via a low temperature hydrothermal route, which is economically efficient and environmentally friendly.

Gallium oxide can be obtained by dehydration of gallium oxide hydroxide (GaOOH). As with aluminum, the chemical, microstructure and physical properties and morphology of gallium oxide depends on its precursor which means that it is possible to control the properties of gallium oxide by varying the precipitation chemistry of the corresponding precursor [108].

Here we mainly focus the synthesis of gallium oxide hydroxide and gallium oxide via hydrothermal routes.

1.3.2.1 Investigations on the growth of GaOOH and Ga₂O₃ nanostructures via hydrothermal reaction.

Similar to aluminum, the chemical, micro-structural and physical properties and morphology of gallium oxide depend on its precursor which means that it is possible to control the properties of gallium oxide by varying the precipitation chemistry of the corresponding precursor. It is well known that the important precursor for synthesis of gallium oxide is gallium oxyhydroxide (GaOOH). Thus, studies on the synthesis of GaOOH in solution are primary and important steps for preparation of gallium oxide via hydrothermal route.

- ***Studies on the synthesis of GaOOH precipitate in solution***

The precipitation of GaOOH from solutions has been studied for a long time. In 1939, Laubengayer et al. [109] synthesized α -GaOOH from a gel by the hydrolysis of gallium nitrate or gallium chloride after calcination at temperatures between 110 and 300°C. Gimblett [110] monitored the hydrolysis of $\text{Ga}(\text{ClO}_4)_3$ solutions and the formation of the solid phase at 50°C using turbid metric and pH measurements. The crystalline phase was identified as gallium oxyhydroxide. Sato et al. [111] studied GaOOH precipitates prepared by mixing gallium chloride and various alkalis including NaOH, KOH, NH_4OH , NaHCO_3 and Na_2CO_3 . These authors reported that the freshly precipitated precursor obtained at pH values varying between 6 and 10 were all X-ray amorphous and converted to crystalline α -GaOOH with an orthorhombic crystal structure similar to that of diaspore (α - AlOOH) after about one day of ageing. Yada et al. [112] investigated the precipitation process induced by heating the aqueous system of GaCl_3 +urea+sodium dodecyl sulphate (SDS). A templated mesophase with hexagonal and lamellar structures were formed. Jung et al. [113] studied GaOOH precipitate synthesized by adding urea to an aqueous solution of gallium nitrate where the mole ratio of gallium salt to urea was 1:3, followed by stirring overnight at 80-90°C. The resulting GaOOH possessed a rod-like morphology.

- ***Studies on synthesis of GaOOH or Ga₂O₃ nanostructures via hydrothermal route***

Although a great effort has been devoted to investigate the synthesis of GaOOH precipitate in solution, little work has been carried out to synthesize gallium oxide hydroxide and gallium oxide nanostructures based on aqueous solution system, in particular one dimensional (1D) nanostructures via hydrothermal routes based on aqueous solution systems.

Hamada et al. [114] reported the formation of mono-dispersed GaOOH particles with diameters of ~100 nm in the presence of sulphate by hydrolysis at elevated temperatures. Avivi et al. [115] synthesized scroll-like layered gallium oxide

hydroxide GaOOH using sonochemical reduction.

Tas et al. [116] produced GaOOH quadrilateral prisms and spindle-like nanoparticles by forced hydrolysis of Ga^{3+} ions in pure water or in the presence of decomposing urea. After calcination at high temperature, the spindles lose their morphology and the quadrilateral prisms maintain their morphology but with some nanoscale pores on them.

Ristić et al. [117] studied the application of sol-gel methods in the synthesis of gallium oxyhydroxide and gallium oxide by hydrolysis of gallium isopropoxide and GaCl_3 in the presence of tetramethylammonium hydroxide in water solution. A completely amorphous precipitate was obtained by hydrolysis of gallium isopropoxide in pure water at room temperature. Nanosized $\alpha\text{-Ga}_2\text{O}_3$ particles (10~20 nm) were formed by heating the gallium oxyhydroxide at 500°C . These authors reported that the size and morphology of the particles in the samples strongly depended on the starting chemicals and the conditions of the experiment.

Cheng et al. [118] prepared Ga_2O_3 nanotubes by immersing alumina membranes in amorphous $\text{Ga}_2\text{O}_3 \cdot n\text{H}_2\text{O}$ sol, followed by drying and heating at 500°C . Amorphous $\text{Ga}_2\text{O}_3 \cdot n\text{H}_2\text{O}$ gel was precipitated from ethanolic solution of $\text{Ga}(\text{NO}_3)_3$ using ammonia solution, then the precipitate was thermally treated to obtain $\gamma\text{-Ga}_2\text{O}_3$ or $\beta\text{-Ga}_2\text{O}_3$.

Most recently, Zhang et al. [119] prepared GaOOH nanorods through a facile large-scale hydrothermal process from $\text{GaCl}_3\text{-H}_2\text{O-NaOH}$ solutions under suitable pH conditions. Results showed that the aspect ratio of the nanorods could be modulated from 1:7 to 1:15 using diethyleneglycol (DEG) and water mixed solvent. The pH value variation in water resulted in different nucleation rates, which led to different structures from quadrilateral nanorods to nanorods arrays. $\beta\text{-Ga}_2\text{O}_3$ was obtained by dehydration of GaOOH nanorods at 900°C in air. The resulting $\beta\text{-Ga}_2\text{O}_3$ retained the morphology of precursor GaOOH.

Liu et al. [120] prepared gallium oxide nanorods by the conversion of gallium oxide hydroxide nanorods. In this study, gallium oxide hydroxide nanorods were

synthesized via a hydrothermal route using gallium oxide as the gallium source and NaN_3 and aqueous hydrazine as the alkaline and complexing reagents. It was also reported that single crystal $\alpha\text{-Ga}_2\text{O}_3$ and $\beta\text{-Ga}_2\text{O}_3$ nanorods can be selectively obtained by thermal decomposition.

1.3.3 Other studies related to this project

Luminescence is an attractive property of $\beta\text{-Ga}_2\text{O}_3$. $\beta\text{-Ga}_2\text{O}_3$ can exhibit UV, blue, and green emissions depending on the sample preparation conditions and the nature of the defects upon photo-excitation through the band gap. Because Cr^{3+} has excellent ability of substitution for Ga^{3+} in $\beta\text{-Ga}_2\text{O}_3$, Fujihara et al. [121] studied luminescence of Cr doped as well as undoped $\beta\text{-Ga}_2\text{O}_3$. It was demonstrated that the green emission from $\beta\text{-Ga}_2\text{O}_3$ is quenched by the inclusion of Cr^{3+} ions and the material exhibits the red emission instead under UV excitation. The results showed that $\beta\text{-Ga}_2\text{O}_3$ is a good host material to produce characteristic luminescence of transition metal ions under UV excitation across the band gap.

Otero Arean et al. [122] prepared mesoporous $\gamma\text{-Ga}_2\text{O}_3$ by calcining a gallium oxide gel at 773 K. The gallium oxide employed in this study was obtained by adding ammonia to an ethanolic solution of gallium nitrate. Nitrogen adsorption-desorption at 77 K showed the material had a BET surface area of $120 \text{ m}^2\text{g}^{-1}$ and a most frequent pore radius of 2.1 nm. Yada et al. [112] prepared yttrium doped mesoporous gallium oxide by using sodium dodecyl sulphate ($\text{C}_{12}\text{H}_{25}\text{OSO}_3\text{Na}$) as the templating agent. It was reported that the structural stability of mesoporous gallium oxide was remarkably increased by introducing yttrium.

Song et al. [123, 124] synthesized manganese doped gallium oxide nanowires via the thermal evaporation method. The field and temperature dependence of the magnetization revealed the obvious hysteresis loop and large magnitude of Curie-Weiss temperature, corresponding to a strong antiferromagnetic super exchange interaction between the manganese ions. A broad green emission band was observed owing to the ${}^4\text{T}_1\text{-}{}^6\text{A}_1$ transition in Mn^{2+} (3d^5) ions. Since $\beta\text{-Ga}_2\text{O}_3$ has a large dielectric capacitance and high electrical resistivity, Mn-doped gallium oxide

nanowires with ferromagnetic characteristics have potential applications in high-frequency microwave devices, storage magnetic cores and nanoscale magneto-optical electronic devices.

1.4 Summary

In the past few decades, syntheses of nanostructures, in particular, one dimensional nanostructures have been of great interest due to their distinctive geometries, novel physical and chemical properties, combined effects and their application in numerous areas especially in the fabrication of nanodevices. Self-assembly, sol-gel, physical evaporation, chemical vapor deposition, microwave plasma, laser ablation and hydrothermal techniques are commonly used to fabricate 1D nanostructures. Among these techniques, hydrothermal synthesis technique is extensively used because of its economic efficiency and because it is environmentally friendly.

As for alumina based nanostructures, considerable studies have been performed on the synthesis of 1D boehmite nanostructures with/without surfactant. Various surfactants including nonionic, cationic, anionic and neutral surfactants were used as templates or directing agents in different studies. Current studies reveal that hydrothermal conditions such as pH, temperature and the type of surfactant strongly affect the morphology of the resultant boehmite nanostructures. It is noted from this literature that high hydrothermal temperatures (150 ~180°C) would be preferable for the growth of nanorods and nanobelts whereas low temperature (<150°C) for nanofibres and nanotubes. Also, surfactants have a greater effect on the growth of boehmite nanostructures at low hydrothermal temperatures than at high temperatures. Although considerable work has been done on the growth of boehmite, the mechanism for the formation of 1D boehmite nanostructures remains unclear. Size and morphology control is still a hot topic in this area. In addition, little effort has been devoted to synthesis of doped boehmite which may possess interesting properties, therefore leading to more potential applications.

As for gallium based nanostructures, limited studies were carried out on the synthesis of gallium oxide hydroxide and gallium oxide 1D nanostructures. It is noted that

gallium nanostructures synthesized via hydrothermal routes are usually much bigger and thicker than those obtained by other techniques such as physical evaporation and chemical vapor deposition. Although various precursors and hydrothermal conditions were investigated, the morphologies of the resultant GaOOH or Ga₂O₃ were somehow similar. The size and morphology control of GaOOH and Ga₂O₃ via hydrothermal route remains challenging. It can be expected from investigations on the properties of doped gallium oxide nanostructured or bulk materials that when doped with some elements, gallium oxide hydroxide or gallium oxide could possess interesting properties leading to more potential applications.

1.5 References

1. Fendler, J.H. and F.C. Meldrum, *Adv. Mater.*, 1995. **7**(7): p. 607-32.
2. Lakshmi, B.B., C.J. Patrissi, and C.R. Martin, *Chem. Mater.*, 1997. **9**(11): p. 2544-2550.
3. Ratner, M. and D. Ratner, *Nanotechnology: a gentle introduction to the next big idea*. 2002, New Jersey: Bernard Goodwin.
4. Ho, H.P., et al., *Chem. Phys. Lett.*, 2003. **382**(5-6): p. 573-577.
5. He, J., et al., *Mater. Lett.*, 2006. **60**: p. 150-153.
6. Kuykendall, T., et al., *Nature Mater.*, 2004. **3**: p. 524-528.
7. Iijima, S., *Nature*, 1991. **354**: p. 56-58.
8. *Australian nanotechnology: capability & commercial potential*. 2005, nanostructural analysis network organization.
9. Cao, G.Z., *Nanostructures & Nanomaterials: synthesis, properties & applications*. 2004, London: Imperial College Press.
10. Gudixsen, M.S., et al., *Nature*, 2002. **415**: p. 617-620.
11. Yu, T., et al., *Angew. Chem. Int. Ed.*, 2005. **44**: p. 2-6.
12. Nedez, C., et al., *Langmuir*, 1996. **12**(16): p. 3927-3931.
13. Burkat, V.S., et al., *Light Met.*, 1985: p. 1443-8.
14. Xue, D.S., et al., *J. Mater. Sci. Lett.*, 2003. **22**(24): p. 1817-1820.
15. Chen, Y., L. Jin, and Y. Xie, *J. Sol-Gel Sci. Technol.*, 1998. **13**(1/2/3): p. 735-738.
16. Okada, K., et al., *J. Mater. Res.*, 1994. **9**(7): p. 1709-13.
17. Ananthakumar, S., V. Raja, and K.G.K. Warriar, *Mater. Lett.*, 2000. **43**(4): p. 174-179.
18. Philipse, A.P., A.-M. Nechifor, and C. Patmamanoharan, *Langmuir*, 1994. **10**(12): p. 4451-8.
19. Nedez, C., J.-l. Le Loarer, and B. Taxil, *Alumina, its preparation, and use as catalyst, catalyst support, and adsorbent*. 1999, (Institut Francais du Petrole, Fr.). Appl.: EP. p. 8
20. Le Loarer, J.-L., H. Nussbaum, and D. Bortzmeyer, *Alumina extrudates, methods for preparing and use as catalysts or catalyst supports*. 1998, (Rhodia Chimie, Fr.). Appl.: WO. p. 44.
21. Ruan, H.D., et al., *Spectrochim. Acta A*, 2002. **58A**(2): p. 265-272.
22. Martens, W.N., et al., *Thermochim. Acta*, 2001. **374**(1): p. 31-43.
23. Ruan, H.D., R.L. Frost, and J.T. Klopogge, *Appl. Spectrosc.*, 2001. **55**(2): p. 190-196.
24. Frost, R.L., et al., *Thermochim. Acta*, 1999. **329**(1): p. 47-56.
25. Szetu, J., J.T. Klopogge, and R.L. Frost. *Infrared emission spectroscopy of alumina phases and gels*. in *3rd Australian Conference on Vibrational Spectroscopy*. 1998. University of Melbourne, Australia.
26. Valente, J.S., X. Bokhimi, and F. Hernandez, *Langmuir*, 2003. **19**: p. 3583.
27. Misra, C., *Industrial alumina chemicals*. ACS Monograph 184. 1986, Washington DC: American Chemical Society.
28. Guzman-Castillo, M.L., et al., *J. Phys. Chem. B*, 2001. **105**(11): p. 2099-2106.
29. Klopogge, J.T., H.D. Ruan, and R.L. Frost, *J. Mater. Sci.*, 2002. **37**(6): p. 1121-1129.
30. Frost, R.L., et al., *Appl. Spectrosc.*, 1999. **53**(5): p. 572-582.
31. Duan, X., et al., *Nature*, 2001. **409**(6816): p. 66-9.
32. Hu, J., et al., *Science*, 2001. **292**(5524): p. 2060-2063.
33. Puentes, V.F., K.M. Krishnan, and A.P. Alivisatos, *Science*, 2001. **291**(5511): p. 2115-2117.
34. Bugosh, J., *J. Phys. Chem.*, 1961. **65**: p. 1789-92.
35. Hochepped, J.F., O. Ilioukhina, and M.H. Berger, *Mater. Lett.*, 2003. **57**(19): p.

- 2817-2822.
36. Hochepped, J.F. and P. Nortier, Powder Technol., 2002. **128**(2-3): p. 268-275.
 37. Lee, H.C., et al., J. Am. Chem. Soc., 2003. **125**(10): p. 2882-2883.
 38. Zhang, Z., et al., J. Am. Chem. Soc., 2002. **124**(8): p. 1592-1593.
 39. Zhao, Y., et al., Langmuir, 2007. **23**(19): p. 9850-9859.
 40. Zhu, H.Y., et al., J. Phys. Chem. B., 2004. **108**(14): p. 4245-4247.
 41. Zhu, H.Y., et al., Microporous and Mesoporous Mater., 2005. **85**(3): p. 226-233.
 42. Gao, P., et al., J. Cryst. Growth, 2005. **285**(4): p. 555-560.
 43. Shen, S.C., et al., J. Phys. Chem. C, 2007. **111**(2): p. 700-707.
 44. Kuang, D., et al., J. Mater. Chem., 2003. **13**(4): p. 660-662.
 45. Buining, P.A., et al., J. Am. Ceram. Soc., 1991. **74**(6): p. 1303-1307.
 46. Chiou, Y.H., M.T. Tsai, and H.C. Shih, J. Mater. Sci., 1994. **29**: p. 2378-2388.
 47. Fukui, T. and M. Hori, J. Mater. Sci., 1995. **30**: p. 1794-1800.
 48. Imose, M., et al., J. Am. Ceram. Soc., 1998. **81**(6): p. 1537-1540.
 49. Van Straten, H.A., B.T.W. Holtkamp, and P.L. de Bruyn, J. Colloid Interface Sci., 1984. **98**(2): p. 342-362.
 50. Lee, Y.P., Y.H. Liu, and C.-S. Yeh, Phys. Chem. Chem. Phys., 1999. **1**: p. 4681-4686.
 51. Deng, D., et al., Langmuir, 2008. **24**: p. 368-370.
 52. Calvet, E., et al., Bull. Soc. Chim. Fr., 1953: p. 99.
 53. Yoldas, B.B., J. Appl. Chem. Biotechnol., 1973. **23**: p. 803.
 54. Martens, W.N., et al., J. Mater. Chem., 2001. **11**: p. 1681-1686.
 55. Morgado, E., Y.L. Lam, and L.F. Nazar, J. Colloid Interface Sci., 1997. **188**(2): p. 257-269.
 56. Martens, W.N., *The Structure and Peptisation of Alumina Prepared From the Hydrolysis of Trisecbutoxyaluminium (III)*, in *Instrumental and Developmental Chemistry, School of Physical Sciences*. 2001, Queensland University of Technology: Brisbane. p. 93.
 57. Kuiry, S.C., et al., J. Phys. Chem. B, 2005. **109**(9): p. 3868-3872.
 58. Bokhimi, X., A. Morales, and J.S. Valente, J. Phys. Chem. C, 2007. **111**(1): p. 103-107.
 59. Zhang, J., et al., J. Phys. Chem. B, 2006. **110**(43): p. 21680-21683.
 60. Wang, X. and Y.D. Li, Angew. Chem. Int. Ed, 2002. **41**: p. 4790.
 61. Lepot, N., et al., Ceram. Int., 2007. **In Press, Corrected Proof**: p. 1249.
 62. Potdar, H.S., et al., Appl. Catal. A, 2007. **321**(2): p. 109-116.
 63. Zhang, Z. and T.J. Pinnavaia, J. Am. Chem. Soc., 2002. **124**(41): p. 12294-12301.
 64. Bagshaw, S.A. and T.J. Pinnavaia, Angew. Chem. Int. Ed., 1996. **35**(10): p. 1102-1105.
 65. Kim, H.J., et al., J. Am. Chem. Soc., 2003. **125**(44): p. 13354-13355.
 66. Zhu, H.Y., J. D. Riches, and J.C. Barry., Chem. Mater., 2002. **14**: p. 2086-2093.
 67. Frost, R., et al., Mater. Lett., 2005. **59**(17): p. 2238-2241.
 68. Kim, S.-M., et al., Mater. Chem. Phys., 2007. **104**(1): p. 56-61.
 69. Liu, Q., et al., Microporous and Mesoporous Mater., 2008. **111**(1-3): p. 323-333.
 70. Naskar, M.K. and M. Chatterjee, J. Am. Ceram. Soc., 2005. **88**(12): p. 3322-3326.
 71. Zhang, J., et al., J. Phys. Chem. B, 2006. **110**(29): p. 14249-14252.
 72. Castro, R.H.R., et al., Chem. Mater., 2006. **18**: p. 1867-1872.
 73. Djuricic, B., et al., J. Mater. Sci., 1997. **32**(3): p. 589-601.
 74. Van Bruggen, M.P.B., Langmuir, 1998. **14**(9): p. 2245-2255.
 75. Han, Y., et al., J. Am. Chem. Soc., 2007: p. In Press.
 76. Wu, H.X., T.J. Wang, and Y. Jin, Ind. Eng. Chem. Res., 2006. **45**: p. 5274-5278.
 77. Petre, A.L., et al., Thermochim. Acta, 2001. **379**(1-2): p. 177-185.
 78. Gowtham, S., A. Costales, and R. Pandey, Chem. Phys. Lett., 2006. **431**(4-6): p. 358-363.
 79. Wu, W.C., et al., Chem. Phys. Lett., 2000. **328**: p. 5-9.
 80. Fu, L., et al., J. Phys. Chem. B, 2004. **108**(35): p. 13074-13078.
 81. Choi, Y.C., et al., Adv. Mater., 2000. **12**: p. 746-750.

82. Gao, Y.H., et al., *Appl. Phys. Lett.*, 2002. **81**(12): p. 2267-2269.
83. Dai, Z.R., Z.W. Pan, and Z.L. Wang, *J. Phys. Chem. B.*, 2002. **106**: p. 902-904.
84. Edwards, D.D., et al., *Appl. Phys. Lett.*, 1997. **70**: p. 1706.
85. Hu, J.Q., Y. Bando, and Z.W. Liu, *Adv. Mater.*, 2003. **15**: p. 1000-1003.
86. Liang, C.H., et al., *Appl. Phys. Lett.*, 2001. **78**: p. 3202-3204.
87. Ma, R. and Y. Bando, *Chem. Phys. Lett.*, 2003. **367**: p. 219-222.
88. Ogita, M., et al., *Appl. Surf. Sci.*, 1999. **142**(1-4): p. 188-191.
89. Weh, T., et al., *Sens. Actuators B*, 2001. **78**(1-3): p. 202-207.
90. Nakagawa, K., et al., *J. Catal.*, 2001. **203**(1): p. 87-93.
91. Xu, B., et al., *J. Catal.*, 2006. **239**(2): p. 470-477.
92. Gundiah, G., A. Govindaraj, and C.N.R. Rao, *Chem. Phys. Lett.*, 2002. **351**(3-4): p. 189-194.
93. Fu, L., et al., *Chem. Mater.*, 2003. **15**(22): p. 4287-4291.
94. Zhang, H.Z., et al., *Solid State Commun.*, 1999. **109**(11): p. 677-682.
95. Zhu, F., et al., *Appl. Surf. Sci.*, 2006. **252**(22): p. 7930-7933.
96. Kim, N.H., et al., *Mater. Sci. Eng. B*, 2004. **111**: p. 131-134.
97. Johnson, M.C., et al., *Cryst. Growth Des.*, 2006. **6**(8): p. 1936-1941.
98. Choi, K., et al., *J. Colloid Interface Sci.*, 2008. **313-314**: p. 60-65.
99. Xiang, X., et al., *Chem. Phys. Lett.*, 2003. **378**(5-6): p. 660-664.
100. Lo, K.C., et al., *Surf. Coat. Technol.*, 2007. **201**(15): p. 6804-6807.
101. Chun, H.J., et al., *J. Phys. Chem. B*, 2003. **107**: p. 9042-9046.
102. Kim, B.C., et al., *Appl. Phys. Lett.*, 2002. **80**(2): p. 481.
103. Huang, C.-C., C.-S. Yeh, and C.-J. Ho, *J. Phys. Chem. B*, 2004. **108**: p. 4940-4945.
104. Jung, W.-S., H.U. Joo, and B.-K. Min, *Physica E*, 2007. **36**(2): p. 226-230.
105. Xiao, H.-D., et al., *Mater. Chem. Phys.*, 2007. **101**(1): p. 99-102.
106. Sharma, S. and M.K. Sunkara, *J. Am. Chem. Soc.*, 2002. **124**: p. 12288-12293.
107. Zhu, F., et al., *Solid State Commun.*, 2006. **137**(4): p. 177-181.
108. Zhao, Y., R.L. Frost, and W.N. Martens, *J. Phys. Chem. C*, 2007. **111**(44): p. 16290-16299.
109. Laubengayer, A.W. and H.R. Engle, *J. Am. Chem. Soc.*, 1939. **61**: p. 1210-1214.
110. Gimblett, F.G.R., *J. Inorg. Nucl. Chem.*, 1971. **33**: p. 2887.
111. Sato, T. and T. Nakamura, *J. Chem. Tech. Biotechnol.*, 1982. **32**: p. 469-475.
112. Yada, M., et al., *J. Chem. Soc.*, 1998. **Dalton Trans**: p. 1547.
113. Jung, W.-S. and B.-K. Min, *Mater. Lett.*, 2004. **58**: p. 3058-3062.
114. Hamada, S., K. Bando, and Y. Kudo, *Bull. Chem. Soc. Jpn.*, 1986. **59**: p. 2063-2069.
115. Avivi, S., et al., *J. Am. Chem. Soc.*, 1999. **121**(17): p. 4196-4199.
116. Tas, A.C., Peter J. Majewski, and F. Aldinger, *J. Am. Chem. Soc.*, 2002. **85**(6): p. 1421-1429.
117. Ristic, M., S. Popovic, and S. Music, *Mater. Lett.*, 2005. **59**: p. 1227-1233.
118. Cheng, B. and E.T. Samulski, *J. Mater. Chem.*, 2001. **11**: p. 2901.
119. Zhang, J., et al., *J. Cryst. Growth*, 2005. **280**(1-2): p. 99-106.
120. Liu, X., et al., *J. Alloys Compd.*, 2007. **439**: p. 275-278.
121. Fujihara, S. and Y. Shibata, *J. Lumin.*, 2006. **121**(2): p. 470-474.
122. Otero Arean, C., et al., *Microporous and Mesoporous Mater.*, 2000. **40**(1-3): p. 35-42.
123. Song, Y.P., et al., *Physica E*, 2006. **31**(1): p. 67-71.
124. Song, Y.P., et al., *Phys. Lett. A*, 2006. **351**(4-5): p. 302-307.



STATEMENT OF CONTRIBUTION

The authors listed below have certified that:

1. They meet the criteria for authorship in that they have participated in the conception, execution, or interpretation, of at least that part of the publication in their field of expertise;
2. They take public responsibility for their part of the publication, except for the responsible author who accepts overall responsibility for the publication;
3. There are no other authors of the publication according to these criteria;
4. Potential conflicts of interest have been disclosed to (a) granting bodies, (b) the editor or publisher of journals or other publications, and (c) the head of the responsible academic unit, and
5. They agree to the use of the publication in the student's thesis and its publication on the Australian Digital Thesis database consistent with any limitations set by publisher requirements.

In the case of this chapter:

Synthesis, Characterization, and Surface Properties of Iron-Doped Boehmite Nanofibers

Yanyan Zhao, Wayde N. Martens, Thor E. Bostrom, Huai Yong Zhu, and Ray L. Frost
Published in the Journal: Langmuir, 2007, 23(4), 2110-2116.

Contributor	Statement of contribution
Yanyan Zhao	Developed experimental design and scientific method; conducted experimental and most of the characterisation work; interpreted data; wrote manuscript.
Wayde N. Martens	Assisted with experimental design and data interpretation; Contributed to manuscript.
Thor E. Bostrom	Conducted SEM and TEM measurements, assisted with data interpretation
Huai Yong Zhu	Helped with the editing of the manuscript
Ray L. Frost	Assisted with data interpretation and problem solving throughout this research; helped with editing of manuscript

Principal Supervisor Confirmation

I have sighted email or other correspondence from all Co-authors confirming their certifying authorship.

Ray L. Frost

11/07/2008

Name

Signature

Date

CHAPTER 2

Synthesis, Characterization, and Surface Properties of Iron-Doped Boehmite Nanofibers

Yanyan Zhao, Wayde N. Martens, Thor E. Bostrom, Huai Yong Zhu, and Ray L. Frost

Yanyan Zhao Queensland University of Technology, Faculty of Science,
School of Physical and Chemical Science, Brisbane, Australia

Wayde N. Martens Queensland University of Technology, Faculty of Science, School
of Physical and Chemical Science, Brisbane, Australia

Thor E. Bostrom Queensland University of Technology, Faculty of Science,
School of Physical and Chemical Science, Brisbane, Australia

Huai Yong Zhu Queensland University of Technology, Faculty of Science,
School of Physical and Chemical Science, Brisbane, Australia

Ray L. Frost Queensland University of Technology, Faculty of Science,
School of Physical and Chemical Science, Brisbane, Australia

ABSTRACT

Iron-doped boehmite nanofibers with varying iron contents have been prepared at low temperatures using hydrothermal treatment in the presence of poly(ethylene oxide) surfactant. The resulting nanofibers were characterized by transmission electron microscopy (TEM), X-ray diffraction, energy-dispersive X-ray analysis, and N₂ adsorption. TEM images showed that the resulting nanostructures are predominantly nanofibers when the doped iron content is less than 5% (mol/mol); in contrast, nanosheets were formed when iron doping was above 4%. Nanotubes instead of nanofibres and iron-rich particles were observed in samples with 20% added iron. A detailed characterization and discussion on the iron-doped nanofibers is presented.

KEYWORDS: Boehmite; iron-doped; nanofibres; nanosheets; nanotubes; surfactant; hydrothermal treatment.

This article is not available here.
Please consult the hardcopy thesis
available from QUT Library



STATEMENT OF CONTRIBUTION

The authors listed below have certified that:

1. They meet the criteria for authorship in that they have participated in the conception, execution, or interpretation, of at least that part of the publication in their field of expertise;
2. They take public responsibility for their part of the publication, except for the responsible author who accepts overall responsibility for the publication;
3. There are no other authors of the publication according to these criteria;
4. Potential conflicts of interest have been disclosed to (a) granting bodies, (b) the editor or publisher of journals or other publications, and (c) the head of the responsible academic unit, and
5. They agree to the use of the publication in the student's thesis and its publication on the Australian Digital Thesis database consistent with any limitations set by publisher requirements.

In the case of this chapter:

Growth and Surface Properties of Boehmite Nanofibers and Nanotubes at Low Temperatures Using a Hydrothermal Synthesis Route

Yanyan Zhao, Ray L. Frost, Wayde N. Martens and Huai Yong Zhu
Published in the Journal: Langmuir, 2007, 23(19), 9850-9859

Contributor	Statement of contribution
Yanyan Zhao	Developed experimental design and scientific method; conducted experimental and characterisation work; interpreted data; wrote manuscript.
Ray L. Frost	Assisted with data interpretation and editing of the manuscript
Wayde N. Martens	Assisted with data interpretation and problem solving; helped with editing of the manuscript
Huai Yong Zhu	Helped with the editing of the manuscript.

Principal Supervisor Confirmation

I have sighted email or other correspondence from all Co-authors confirming their certifying authorship.

Ray L. Frost

11/07/2008

Name

Signature

Date

CHAPTER 3

Growth and Surface Properties of Boehmite Nanofibres and Nanotubes at Low Temperatures Using a Hydrothermal Synthesis Route

Yanyan Zhao, Ray L. Frost, Wayde N. Martens and Huai Yong Zhu

Yanyan Zhao	Queensland University of Technology, Faculty of Science, School of Physical and Chemical Science, Brisbane, Australia
Ray L. Frost	Queensland University of Technology, Faculty of Science, School of Physical and Chemical Science, Brisbane, Australia
Wayde N. Martens	Queensland University of Technology, Faculty of Science, School of Physical and Chemical Science, Brisbane, Australia
Huai Yong Zhu	Queensland University of Technology, Faculty of Science, School of Physical and Chemical Science, Brisbane, Australia

ABSTRACT

The growth of boehmite nanostructures at low temperature using a soft chemistry route with and without (PEO) surfactant is presented. Remarkably long boehmite 1D nanotubes/nanofibers were formed within a significantly short time by changing the reaction mechanism of aluminum hydroxide. By using the PEO surfactant as a templating agent, boehmite nanotubes up to 170 nm in length with internal and external diameters of 2-5 and 3-7 nm, respectively, were formed at 100°C. A slightly higher temperature (120°C) resulted in the formation of lath-like nanofibers with an average length of 250 nm. Using the cationic surfactant CTAB, nanotubes rather than nanofibers were formed at 120°C. Without surfactant, nanotubes counted for around 20% of the entire sample. A regular interval supply of fresh boehmite precipitate resulted in a larger crystallite size distribution of nanotubes. The morphology of nanotubes was more uniform in samples without the regular addition of aluminum hydroxide. Moreover, for the same hydrothermal time, the final nanotubes for nanomaterials without a regular interval supply of fresh aluminum hydroxide precipitate were longer than those with a regular aluminum hydroxide precipitate supply, which is in contrast to previously published results. Higher Al/PEO concentrations resulted in the formation of shorter nanotubes. A detailed characterization and mechanism are presented.

KEYWORDS: Boehmite; nanosheets; nanotubes; surfactant; hydrothermal treatment.

This article is not available here.
Please consult the hardcopy thesis
available from QUT Library



STATEMENT OF CONTRIBUTION

The authors listed below have certified that:

1. They meet the criteria for authorship in that they have participated in the conception, execution, or interpretation, of at least that part of the publication in their field of expertise;
2. They take public responsibility for their part of the publication, except for the responsible author who accepts overall responsibility for the publication;
3. There are no other authors of the publication according to these criteria;
4. Potential conflicts of interest have been disclosed to (a) granting bodies, (b) the editor or publisher of journals or other publications, and (c) the head of the responsible academic unit, and
5. They agree to the use of the publication in the student's thesis and its publication on the Australian Digital Thesis database consistent with any limitations set by publisher requirements.

In the case of this chapter:

Gallium-Doped Boehmite Nanotubes and Nanoribbons. A TEM, EDX, XRD, BET, and TG Study

Yanyan Zhao, Ray L. Frost and Wayde N. Martens

Published in the Journal of Physical and Chemistry C, 2007, 111(14), 5313-5324

Contributor	Statement of contribution
Yanyan Zhao	Developed experimental design and scientific method; conducted experimental and characterisation work; interpreted data; wrote manuscript.
Ray L. Frost	Assisted with data interpretation; contributed to manuscript, and helped with editing.
Wayde N. Martens	Assisted with data interpretation and editing of the manuscript

Principal Supervisor Confirmation

I have sighted email or other correspondence from all Co-authors confirming their certifying authorship.

Ray L. Frost

11/07/2008

Name

Signature

Date

CHAPTER 4

Gallium-Doped Boehmite Nanotubes and Nanoribbons: A TEM, EDX, XRD, BET, and TG Study

Yanyan Zhao, Ray L. Frost and Wayde N. Martens

Yanyan Zhao	Queensland University of Technology, Faculty of Science, School of Physical and Chemical Science, Brisbane, Australia
Ray L. Frost	Queensland University of Technology, Faculty of Science, School of Physical and Chemical Science, Brisbane, Australia
Wayde N. Martens	Queensland University of Technology, Faculty of Science, School of Physical and Chemical Science, Brisbane, Australia

ABSTRACT

Gallium-doped boehmite nanostructures with varying Ga content have been prepared at low temperatures via a soft-chemistry route in the presence of poly(ethylene oxide) (PEO) surfactant. The effect of Ga content, hydrothermal temperature, and mixing procedures on the growth of boehmite nanostructures was systematically studied. The resultant boehmite nanostructures were characterized by transmission electron microscopy (TEM), energy-dispersive X-ray (EDX) microanalysis, X-ray diffraction (XRD), N₂ adsorption, and thermogravimetric analysis (TGA). Nanotubes with an average length of ~ 90 nm and internal and external diameters of 2-5 nm and 3-7 nm, respectively, were formed when the added Ga molar percentage was ≤5%; when the added Ga percentage was >10%, an amorphous phase dominated the sample with a mixture of nanosheets, nanotubes, and nanoribbons being formed. Synthesis at slightly higher temperatures (120°C) for an added Ga molar percentage of 5% resulted in longer nanotubes. For high-Ga-content boehmites, large crystals were formed when hydrothermally treated at 120°C. The detailed characterization of the resultant Ga-doped boehmite nanostructures is presented.

KEYWORDS: Boehmite; gallium-doped; nanotubes; nanosheets; nanoribbons; surfactant; hydrothermal treatment.

This article is not available here.
Please consult the hardcopy thesis
available from QUT Library



STATEMENT OF CONTRIBUTION

The authors listed below have certified that:

1. They meet the criteria for authorship in that they have participated in the conception, execution, or interpretation, of at least that part of the publication in their field of expertise;
2. They take public responsibility for their part of the publication, except for the responsible author who accepts overall responsibility for the publication;
3. There are no other authors of the publication according to these criteria;
4. Potential conflicts of interest have been disclosed to (a) granting bodies, (b) the editor or publisher of journals or other publications, and (c) the head of the responsible academic unit, and
5. They agree to the use of the publication in the student's thesis and its publication on the Australian Digital Thesis database consistent with any limitations set by publisher requirements.

In the case of this chapter:

Synthesis and Surface Characterization of Yttrium Doped Boehmite Nanofibres

Yanyan Zhao, Ray L. Frost

Published in the Journal of Colloid and Interface Science, 2008, 326(1), 289-299

Contributor	Statement of contribution
Yanyan Zhao	Developed experimental design and scientific method; conducted experimental and characterisation work; interpreted data; wrote manuscript.
Ray L. Frost	Contributed to manuscript and helped with manuscript editing

Principal Supervisor Confirmation

I have sighted email or other correspondence from all Co-authors confirming their certifying authorship.

Ray L. Frost

11/07/2008

Name

Signature

Date

CHAPTER 5

Synthesis and Surface Characterization of Yttrium Doped Boehmite Nanofibres

Yanyan Zhao, Ray L. Frost

Yanyan Zhao Queensland University of Technology, Faculty of Science,
School of Physical and Chemical Science, Brisbane, Australia

Ray L. Frost Queensland University of Technology, Faculty of Science,
School of Physical and Chemical Science, Brisbane, Australia

ABSTRACT

Yttrium doped boehmite nanofibres with varying yttrium content have been synthesized at low temperatures using a soft-chemistry route in the presence of poly(ethylene oxide) (PEO) surfactant. The effect of yttrium content and hydrothermal temperature on the growth of boehmite nanostructures was systematically studied. Nanofibres were formed in all samples with varying doped Y% treated at 100°C; large $Y(OH)_3$ crystals were also formed at high yttrium doping. Treatment at elevated temperatures resulted in a remarkable changes in size and morphology for samples with the same doped Y content. The resultant nanofibres were characterized by X-ray diffraction (XRD), transmission electron microscopy (TEM), selected area electron diffraction (SAED), energy-dispersive X-ray analysis (EDX), N_2 adsorption and thermogravimetric analysis. The detailed characterization and discussion on the Y doped nanostructures is presented.

KEYWORDS: Boehmite; surface characterisation; nanofibre; surface area; transmission electron microscopy.

This article is not available here.
Please consult the hardcopy thesis
available from QUT Library



STATEMENT OF CONTRIBUTION

The authors listed below have certified that:

1. They meet the criteria for authorship in that they have participated in the conception, execution, or interpretation, of at least that part of the publication in their field of expertise;
2. They take public responsibility for their part of the publication, except for the responsible author who accepts overall responsibility for the publication;
3. There are no other authors of the publication according to these criteria;
4. Potential conflicts of interest have been disclosed to (a) granting bodies, (b) the editor or publisher of journals or other publications, and (c) the head of the responsible academic unit, and
5. They agree to the use of the publication in the student's thesis and its publication on the Australian Digital Thesis database consistent with any limitations set by publisher requirements.

In the case of this chapter:

Synthesis and Characterization of Gallium Oxide Nanostructures via a Soft-chemistry Route

Yanyan Zhao, Ray L. Frost and Wayde N. Martens

Published in the Journal of Physical Chemistry C, 2007, 111(44), 16290-16299

Contributor	Statement of contribution
Yanyan Zhao	Developed experimental design and scientific method; conducted experimental and characterisation work; interpreted data; wrote manuscript.
Ray L. Frost	Assisted with data interpretation and manuscript editing.
Wayde N. Martens	Assisted with data interpretation and manuscript editing.

Principal Supervisor Confirmation

I have sighted email or other correspondence from all Co-authors confirming their certifying authorship.

Ray L. Frost

11/07/2008

Name

Signature

Date

CHAPTER 6

Synthesis and Characterization of Gallium Oxide Nanostructures via a Soft-chemistry Route

Yanyan Zhao, Ray L. Frost and Wayde N. Martens

Yanyan Zhao	Queensland University of Technology, Faculty of Science, School of Physical and Chemical Science, Brisbane, Australia
Ray L. Frost	Queensland University of Technology, Faculty of Science, School of Physical and Chemical Science, Brisbane, Australia
Wayde N. Martens	Queensland University of Technology, Faculty of Science, School of Physical and Chemical Science, Brisbane, Australia

ABSTRACT

Nano- to micro-sized gallium oxide was prepared with and without surfactant via a hydrothermal route at low temperature through different synthesis procedures. Rodlike GaOOH crystals with average length of $\sim 2.5 \mu\text{m}$ and width of $1.5 \mu\text{m}$ were prepared when the initial molar ratio of Ga to OH was 1:3. $\beta\text{-Ga}_2\text{O}_3$ materials were derived from GaOOH by calcination at 900°C , and the initial morphology was retained. $\gamma\text{-Ga}_2\text{O}_3$ nanotubes up to 65 nm in length, with internal and external diameters of around 0.8 and 3 nm, were achieved directly in solution with and without surfactant under hydrothermal treatment condition at 100°C when the initial molar ratio of Ga to OH was 1:5. The combination of X-ray diffraction (XRD), transmission electron microscopy (TEM), N_2 adsorption, small area electron diffraction (SAED), and energy dispersive X-ray analysis (EDX) were employed to characterize the resulting nano- to micro-sized structures. Cationic and nonionic surfactants were used in this study. Detailed results are presented.

KEYWORDS: Gallium oxide; gallium oxide hydroxide; nanotubes; nanorods; surfactant; hydrothermal treatment.

This article is not available here.
Please consult the hardcopy thesis
available from QUT Library



STATEMENT OF CONTRIBUTION

The authors listed below have certified that:

1. They meet the criteria for authorship in that they have participated in the conception, execution, or interpretation, of at least that part of the publication in their field of expertise;
2. They take public responsibility for their part of the publication, except for the responsible author who accepts overall responsibility for the publication;
3. There are no other authors of the publication according to these criteria;
4. Potential conflicts of interest have been disclosed to (a) granting bodies, (b) the editor or publisher of journals or other publications, and (c) the head of the responsible academic unit, and
5. They agree to the use of the publication in the student's thesis and its publication on the Australian Digital Thesis database consistent with any limitations set by publisher requirements.

In the case of this chapter:

Size and Morphology Control of Gallium Oxide Hydroxide GaO(OH) Nano-to Micro-sized particles by Soft-chemistry Route without Surfactant

Yanyan Zhao, Ray L. Frost, Jing Yang and Wayde N. Martens

Published in the Journal of Physical Chemistry C, 2008, 112(10), 3568-3579.

Contributor	Statement of contribution
Yanyan Zhao	Developed experimental design and scientific method; conducted experimental and characterisation work; interpreted data; wrote manuscript.
Ray L. Frost	Assisted with data interpretation and manuscript editing
Jing Yang	Assisted with manuscript editing.
Wayde N. Martens	Assisted with data interpretation and manuscript editing.

Principal Supervisor Confirmation

I have sighted email or other correspondence from all Co-authors confirming their certifying authorship.

Ray L. Frost

11/07/2008

Name

Signature

Date

CHAPTER 7

Size and Morphology Control of Gallium Oxide Hydroxide GaO(OH) Nano- to Micro-sized particles by Soft-chemistry Route without Surfactant

Yanyan Zhao, Ray L. Frost, Jing Yang and Wayde N. Martens

Yanyan Zhao Queensland University of Technology, Faculty of Science,
School of Physical and Chemical Science, Brisbane, Australia

Ray L. Frost Queensland University of Technology, Faculty of Science,
School of Physical and Chemical Science, Brisbane, Australia

Jing Yang Queensland University of Technology, Faculty of Science,
School of Physical and Chemical Science, Brisbane, Australia

Wayde N. Martens Queensland University of Technology, Faculty of Science,
School of Physical and Chemical Science, Brisbane, Australia

ABSTRACT

Micro to nano sized GaOOH nanorods and particles were prepared under varying hydrothermal conditions without any surfactant and additive using gallium nitrate and sodium hydroxide as starting materials. The combination of X-ray Diffraction (XRD), Transmission Electron Microscopy (TEM), Small Area Electron Diffraction (SAED) and Energy Dispersive X-ray analysis (EDX), Thermogravimetric analysis (TG) and FT-IR were employed to characterize the resulting gallium oxide hydroxide nanorods. Detailed results and the possible growth mechanism were presented.

KEYWORDS: Gallium oxide hydroxide; nanoparticles; nanorods; hydrothermal treatment.

This article is not available here.
Please consult the hardcopy thesis
available from QUT Library

CHAPTER 8

Summary and Conclusions

8.1 Summary

This study investigated the following themes:

- 1) The growth of one dimensional pure boehmite nanostructure via hydrothermal treatment at low temperatures with and without surfactant.
- 2) The preparation of doped one dimensional boehmite nanostructures via hydrothermal synthesis route at low temperature in the presence of surfactant using iron, gallium and yttrium as dopants.
- 3) The preparation of gallium hydroxide and gallium oxide nanostructures at different hydrothermal conditions with and without surfactant.

In the study on theme 1, the effect of surfactant, water and temperature on the morphology of boehmite nanostructures was systematically investigated to reveal the growth mechanism of boehmite nanostructures. Nonionic surfactant PEO and cationic surfactant CTAB were employed in this study. The molar ratio of the starting materials and hydrothermal temperature were varied and the surface properties of the resultant boehmite samples were also investigated to provide detailed information on the growth of pure boehmite nanostructures. The results prove that the entire sample was nanotubes after two days hydrothermal treatment at 100°C. With the increase in hydrothermal time, there is an obvious improvement in homogeneity and uniformity in the morphology and size of boehmite nanotubes due to Ostwald ripening process. A regular supply of fresh aluminium hydrate precipitate during the hydrothermal process resulted in the formation of a mixture of short and long nanotubes rather than stimulating the growth of longer nanotubes where the added fresh aluminium precipitate was expected to be employed as building blocks to improve the elongation of existing nanotubes. Surfactant PEO acted as a directing agent for the elongation of nanotubes rather than a template for the formation of nanotubes. Few nanotubes and a large fraction of nanosheets were formed in the absence of

surfactant PEO or at very low concentration of PEO. The average crystallite sizes along the b crystallographic direction of the resultant boehmite samples indicate the same result as observed in TEM images. Surface analysis of boehmite samples is also in agreement with XRD and TEM results. A slight increase in hydrothermal temperature from 100 to 120°C resulted in the formation of longer lath-like nanofibres together with a small fraction of nanotubes in the presence of nonionic surfactant PEO. The entire sample was found to be nanotubes when using cationic surfactant CTAB instead of PEO treated at the same temperature of 120 °C.

As for the studies on theme 2, the effect of various dopants, percentage of introduced dopant, hydrothermal temperature, mixing procedure on the morphology and properties the resultant boehmite nanostructures were systematically investigated.

- **Fe doped boehmite nanostructures**

This study investigated the morphology and property change of iron doped boehmite nanostructures with doped iron no more than 20%. Nanofibres were formed when the doped iron less than 5%. Nanosheets and nanofibres were formed for 10% iron doped sample. When the doped iron percentage was 20%, nanotubes, nanosheets and iron rich particles were formed. Instead of forming iron doped boehmite nanostructures, hematite crystals were formed if iron was introduced after the formation of aluminium hydrate precipitate. There was a linear relationship between added iron and actual iron in samples before hydrothermal treatment. An obvious miscibility gap was observed for samples with varying iron content after hydrothermal treatment showing the maximum aluminium that can be substituted by iron under this hydrothermal condition is around 4.4%. Compared with pure boehmite nanofibres, there is a remarkable decrease in the BET surface area and an increase in the BET average pore diameters for iron doped boehmite samples.

- **Ga doped boehmite nanostructures**

Doped with gallium, the resultant samples with no more than 5% gallium content turned out to be nanotubes. Doped with 10% gallium, a mixture of nanosheets, nanotubes and nanoribbons was formed in which nanosheets with bevelled ends

counted for around 80% of the entire sample. An amorphous phase together with a small fraction of nanotubes, nanoribbons and large crystals was observed in 20% gallium doped samples. Doped with 5% of gallium, a higher hydrothermal temperature of 120°C led to the formation of remarkable longer nanotubes which is 2~3 times longer than that prepared at 100°C; whereas a higher hydrothermal temperature of 120°C resulted in the formation of large crystals for 20% gallium doped sample. There is a linear relationship between the added and actual gallium content both for samples before and after hydrothermal treatment indicating the difference in solubility and miscibility between Ga and Al chemicals. Although pure gallium and aluminium are totally miscible, only 60-70% of the added gallium content can substitute some of the aluminium to form gallium doped boehmite nanostructures and gallium oxide hydroxide crystals and boehmite nanofibres grow separately when gallium hydrate and aluminium hydrate precipitate were prepared separately and mixed afterwards. The BET surface area decreased and the BET average pore diameters increase with an increase in hydrothermal duration. Compared with pure boehmite nanostructures prepared at the same hydrothermal condition, gallium doped boehmite samples have remarkably larger BET surface area and smaller BET average pore diameters. Gallium doped boehmite nanostructures thermally decomposed at a higher temperature than that of the pure boehmite nanostructures.

- **Y doped boehmite nanostructures**

The entire samples were nanofibres when the doped yttrium percentage is no more than 5%. Yttrium hydroxide large crystals together with nanofibres were formed in 10 and 20% yttrium doped samples. With 5% yttrium, increasing temperature led to changes in morphology and size of the resulting nanostructures. At 120°C, nanosheets as well as nanofibres were formed; at 150°C, nanosheets, nanofibres and nanorods were presented; at 180°C, large nanosheets and nanorods as well as square large crystals formed. Interestingly, the large crystals formed in 180°C were of a combination of $Y(OH)_3$ and Y_2O_3 phase where the Y_2O_3 phase may result from the breakdown of the hydroxide. In addition, pure boehmite nanorods were formed in the absence of surfactant at 180°C indicating that the presence of water is necessary for the growth of boehmite nanostructures but the creation of additional steam does not

help the formation of nanorods. The BET surface area, pore volume of Y doped boehmite samples were remarkably larger than that of pure boehmite, whereas the mean pore diameter of the doped sample was much smaller than that of pure boehmite sample when doped yttrium percentage was no more than 10%.

The study on the theme 3 investigated the effect of hydrothermal conditions including the molar ratio of the starting materials, pH, temperature, hydrothermal duration, and surfactant on the morphology and size of the resultant gallium oxide hydroxide and gallium oxide crystals.

- **The effect of surfactant on the morphology of GaOOH and Ga₂O₃ nanostructures under different hydrothermal conditions**

When the initial molar ratio of Ga to OH is 1:3, the growth of GaOOH crystals mainly occurred during ageing; stirring during ageing resulted in the formation of layered structured GaOOH nanorods; there is little difference in morphology and size between GaOOH crystals prepared with and without surfactants. β -Ga₂O₃ can be obtained by calcination of the GaOOH crystals at 900°C. The rodlike morphology of GaOOH was retained, but the surface properties including mesoporosity, pore size distribution of the resultant β -Ga₂O₃ prepared with different surfactants are very much different. When the initial molar ratio of Ga to OH is 1:5, γ -Ga₂O₃ nanotubes with lengths up to 65 nm were obtained directly from the solution at 100°C. More nanotubes were formed in the presence of surfactant. The surfactant played an important role in the growth of γ -Ga₂O₃ nanotubes by serving as a directing agent.

- **The effect of hydrothermal conditions on the morphology of GaOOH in the absence of surfactant**

GaO(OH) nanoparticles via a simple green softchemistry route have been synthesized and the size and morphology changes under varying hydrothermal conditions were systematically investigated. Results show that temperature and pH strongly affected the size and morphology of the resultant GaO(OH) crystals. The higher the treatment temperature, the larger the crystallite size and faster the crystal growth rate. The aspect ratio of the GaO(OH) crystals dramatically dropped at high

temperature (180°C) and gradually decreased at low temperature (100°C) with an increase in pH. Spindle-like, rod-like, and round are favorable shapes for the initial freshly precipitated GaO(OH) particles during reaction at pH 5, 7, and 10, respectively, at room temperature. However, rod-like could be the most stable shape at higher temperatures of 100 and 180°C regardless of the pH. At acidic and neutral conditions, large GaO(OH) rods were formed by consuming amorphous small particles, whereas in basic conditions GaO(OH) rods were most likely formed by the oriented aggregation and emergence of small rod arrays. A higher hydrothermal temperature resulted in sharper DTG curves of GaO(OH). A lower treatment temperature led to the appearance of additional DTG peaks which are attributed to other GaO(OH) phases.

8.2 Conclusions

Nanofibres and nanotubes are preferable morphologies for pure boehmite under different hydrothermal conditions at the relatively low temperature of 120°C in the presence of a surfactant. Irregular shaped nanosheets and few nanotubes were formed without surfactant. The morphology of the resultant boehmite one dimensional nanostructures can be controlled by using different types of surfactant. There is little effect of dopants on the morphology of boehmite nanostructures when the percentage of dopants is less than 5%. When the percentage of dopants is more than 10%, a numerous morphologies including nanosheets, nanoribbons, nanorods, large crystals and even amorphous phases are present in boehmite samples doped with different dopants. A slightly higher hydrothermal temperature lead to the formation of longer one dimensional nanostructure for low dopant content boehmite samples whereas large crystals are preferable for high dopant content samples. However, when the hydrothermal temperature is more than 150°C, a remarkable change in morphology for samples with low dopant content occurs. During the growth of pure or doped boehmite nanostructure, surfactants act as directing agents rather than templates. The surface properties and thermal decomposition behaviour are changed when doped with various dopants.

Gallium oxide hydroxide can be prepared via hydrothermal treatment at low temperature with and without surfactant. Rod-like nanorods with different length to

width ratio are the popular morphology for gallium oxides hydroxides prepared via hydrothermal treatment regardless what surfactant is used. The surfactant has little effect on the overall morphology of the resultant gallium oxide hydroxide; however, a significant difference in surface properties occur for β -gallium oxide samples derived from the calcination of gallium oxide hydroxide prepared with different types of surfactant. The length to width ratio of gallium oxide hydroxide nanorods can be tailored by changing the hydrothermal conditions such as pH and temperature. In addition, γ -gallium oxide nanotubes can be prepared directly from hydrothermal treatment at a low temperature without calcination.

CHAPTER 9

Additional support papers

The following papers are supporting studies which were conducted parallel with this thesis:

- 9.1 Zhao, Yanyan; Martens, Wayde N.; Zhu, Huaiyong; Frost, Ray L.. **Synthesis and Characterisation of Iron Doped Boehmite Nanofibres, Nanotubes and Nanosheets.** *2006 International Conference Of Nanoscience and Nanotechnology*, Brisbane, Australia, 2006. Published in the proceeding.
- 9.2 Zhao, Yanyan; Frost, Ray L.; Martens, Wayde N.; Zhu, Huai Yong.. **XRD, TEM and Thermal Analysis of Fe Doped Boehmite Nanofibres and Nanosheets.** *Journal of Thermal Analysis and Calorimetry*, (2007), 90(3), 755-760.
- 9.3 Zhao, Yanyan; Jing Yang and Ray L. Frost. **Raman Spectroscopy of the Transition of α -gallium Oxyhydroxide to β -gallium Oxide Nanorods.** *Journal of Raman spectroscopy*, (2008), 39(10), 1327-1331.
- 9.4 Zhao, Yanyan; Frost, Ray L.; Vágvölgyi, Veronika; Martens, Wayde N.; Kristóf, János; Horváth, Erzsébet. **XRD, TEM and Thermal Analysis of Yttrium Doped Boehmite Nanofibres and Nanosheets.** *Journal of Thermal Analysis and Calorimetry*, (2008), 94(1), 219-226
- 9.5 Zhao, Yanyan; Frost, Ray L. **Raman spectroscopy and characterization of α -gallium oxyhydroxide and β -gallium oxide nanorods.** *Journal of Raman Spectroscopy* (2008), 39(10), 1494-1501
- 9.6 Zhao, Yanyan; Yang, Jing; Frost, Ray L.. **Dynamic and Controlled rate thermal analysis, surface analysis and infrared emission of Ga doped boehmite nanofibres and nanosheets.** *Thermochimica Acta*. (2008), Under review



STATEMENT OF CONTRIBUTION

The authors listed below have certified that:

1. They meet the criteria for authorship in that they have participated in the conception, execution, or interpretation, of at least that part of the publication in their field of expertise;
2. They take public responsibility for their part of the publication, except for the responsible author who accepts overall responsibility for the publication;
3. There are no other authors of the publication according to these criteria;
4. Potential conflicts of interest have been disclosed to (a) granting bodies, (b) the editor or publisher of journals or other publications, and (c) the head of the responsible academic unit, and
5. They agree to the use of the publication in the student's thesis and its publication on the Australian Digital Thesis database consistent with any limitations set by publisher requirements.

In the case of this chapter:

Synthesis and Characterization of Iron Doped Boehmite Nanofibres, Nanotubes and Nanosheets

Yanyan Zhao, Wayde N. Martens, Huai Yong Zhu and Ray L. Frost
Published in the ICCON 2006 proceedings, 2006, Brisbane, Australia.

Contributor	Statement of contribution
Yanyan Zhao	Developed experimental design and scientific method; conducted experimental and most of the characterisation work; interpreted data; wrote manuscript.
Wayde N. Martens	Assisted with experimental design and data interpretation; Contributed to manuscript.
Huai Yong Zhu	Helped with the editing of the manuscript
Ray L. Frost	Assisted with data interpretation and problem solving throughout this research; helped with editing of manuscript

Principal Supervisor Confirmation

I have sighted email or other correspondence from all Co-authors confirming their certifying authorship.

Ray L. Frost

11/07/2008

Name

Signature

Date

CHAPTER 9.1

Synthesis and Characterization of Iron Doped Boehmite Nanofibres, Nanotubes and Nanosheets

Yanyan Zhao, Wayde N. Martens, Huai Yong Zhu, and Ray L. Frost

Yanyan Zhao Queensland University of Technology, Faculty of Science,
School of Physical and Chemical Science, Brisbane, Australia

Wayde N. Martens Queensland University of Technology, Faculty of Science,
School of Physical and Chemical Science, Brisbane, Australia

Huai Yong Zhu Queensland University of Technology, Faculty of Science,
School of Physical and Chemical Science, Brisbane, Australia

Ray L. Frost Queensland University of Technology, Faculty of Science,
School of Physical and Chemical Science, Brisbane, Australia

ABSTRACT

The modification of nanostructured materials is of great interest due to controllable and unusual properties inherent in such materials. In this paper, iron doped boehmite nanofibres, nanotubes and nanosheets with varying iron content have been prepared through low temperature hydrothermal treatment in the presence of poly (ethylene oxide) surfactant. The combination of transmission electron microscopy (TEM), X-ray diffraction (XRD), energy dispersive X-ray analysis (EDX) and N₂ adsorption were employed to characterize the resulting nanostructures. TEM images showed that the resulting nanostructures are predominantly nanofibres when iron content is less than 5% (mol/mol); in contrast nanosheets were formed when iron doping was above 5%. Nanotubes instead of nanofibres and iron rich particles were observed in samples with 20% added iron. XRD showed that the iron doped nanostructures are boehmite (γ -AlOOH), with EDX analysis indicating the maximum

Iron content in the boehmite nanostructures is about 4.3%. Nitrogen adsorption results indicate a lowering of the surface area for the iron doped phase in comparison to that of undoped boehmite nanofibres. Further study is required to determine the magnetic and optical properties of the iron doped boehmite nanostructures for their prospective applications. A detailed characterization of the iron doped nanofibres is presented.

KEYWORDS- Nanofibres; hydrothermal synthesis; boehmite

Synthesis and characterisation of iron doped boehmite nanofibres, nanotubes and nanosheets

Yanyan Zhao, Wayde N. Martens, Huaiyong Zhu, Ray L. Frost*

School of Physical and Chemical Sciences

PO Box 2434 GPO, Brisbane, QLD 4001

Email: r.frost@qut.edu.au

Ph: +61 7 3864 2407 Fax: +61 7 3864 1804

Abstract—The modification of nanostructured materials is of great interest due to controllable and unusual properties inherent in such materials. In this paper, iron doped boehmite nanofibres, nanotubes and nanosheets with varying iron content have been prepared through low temperature hydrothermal treatment in the presence of poly (ethylene oxide) surfactant. The combination of transmission electron microscopy (TEM), X-ray diffraction (XRD), energy dispersive X-ray analysis (EDX) and N₂ adsorption were employed to characterize the resulting nanostructures. TEM images showed that the resulting nanostructures are predominantly nanofibres when iron content is less than 5 % (mol/mol); in contrast nanosheets were formed when iron doping was above 5%. Nanotubes instead of nanofibres and iron rich particles were observed in samples with 20 % added iron. XRD showed that the iron doped nanostructures are boehmite (γ -AlOOH), with EDX analysis indicating the maximum iron content in the boehmite nanostructures is about 4.3%. Nitrogen adsorption results indicate a lowering of the surface area for the iron doped phase in comparison to that of undoped boehmite nanofibres. Further study is required to determine the magnetic and optical properties of the iron doped boehmite nanostructures for their prospective applications. A detailed characterization of the iron doped nanofibres is presented.

Keywords- nanofibres; hydrothermal synthesis; boehmite

INTRODUCTION

Synthesis of inorganic nanostructures has been of great interest in material science and nanotechnology over the last few decades [1-3]. In particular, one dimensional (1D) nanostructured inorganic materials nanofibres, nanotubes, nanobelts and nanowires, have attracted considerable attention due to their distinctive geometries, novel physical and chemical properties and potential application in various areas [4].

Alumina has high surface area and mesoporous properties, making it a versatile material. Due to alumina chemical and thermal stability, it has been extensively used as supports for a variety of industrial catalysts at both low and high temperatures. Further applications of alumina include adsorbents [5, 6], composites [7, 8] and ceramics [9-11]. Boehmite (γ -AlOOH), an oxyhydroxide of alumina, is a crucial precursor for preparing γ -alumina and is also the most

commonly used precursor in the sol-gel technique for preparing high-purity and high-strength monolithic α -alumina ceramics. Such ceramics have been employed as substrates for electronic circuits, abrasives, high-temperature refractory materials, fibres and thin films [12].

Metal ion doping is a promising technique which can be utilised to control the properties of materials by intentionally introducing impurities or defects into a material. Doping can influence three main properties: surface morphology, nanocrystal shape and growth in solution [13]. Studies have shown that the doping of ZnO [14, 15], GaN [16], CdS [17, 18], MgB₂ [19] with ions such as Mn, Cu, Co, Ni and Ti can impart photoluminescence, magnetic and ferromagnetic properties to the parent material. Recently, considerable work has been conducted on the optical properties of transition metal ion doped alumina [20-22], while to our best knowledge, little work has been undertaken on the doping of boehmite.

Interesting new synthesis methods, using 'soft' chemical treatments, based upon the use of surfactants, have been elucidated by Zhu et al. [23]. The surfactant was able to direct formation and growth of boehmite fibres, rather than acting as templates for the synthesis of mesoporous materials [24]. It was reported that much higher Al concentrations and lower temperatures could be used in comparison to traditional methods for the synthesis of boehmite nanofibres. Such an approach is an efficient means of producing nanofibres in large quantity. The growth of boehmite nanofibres can be improved by the addition of freshly precipitated aluminum hydrate, with fibres growing to over 100 nm long when reaction conditions are well-controlled.

In this work, we investigate iron doped boehmite nanostructures including nanofibres, nanotubes and nanosheets based on the soft chemistry synthetic approach. A series of iron doped boehmite nanostructures with varying iron content have been systematically studied with XRD, SEM EDS, TEM and N₂ absorption. The resulting iron doped boehmite nanostructures possess both optical and magnetic properties which will enable further specifically designed industrial applications.

I. MATERIALS AND METHODS

A. Materials

Analytical grade NaOH pellets (Chem-Supply, 98% pure), $\text{Al}(\text{NO}_3)_3 \cdot 9\text{H}_2\text{O}$ and $\text{Fe}(\text{NO}_3)_3 \cdot 9\text{H}_2\text{O}$ were used in this work to prepare the iron doped aluminium hydrate precipitate. Nonionic PEO surfactant Tergitol 15-S-7 ($\text{C}_{12-14}\text{H}_{25-29}\text{O}(\text{CH}_2\text{CH}_2\text{O})_7\text{H}$, Aldrich) with average molecular weight of $\sim 508 \text{ g}\cdot\text{mol}^{-1}$ was used in hydrothermal processing.

B. Preparation

1) The preparation of precipitate

Aqueous solutions of $\text{Al}(\text{NO}_3)_3$ and $\text{Fe}(\text{NO}_3)_3$ were prepared in molar ratios of 100:0, 99:1, 98:2, 97:3, 96:4, 95:5, 90:10 and 80:20, with a total metal ion concentration of $0.56 \text{ mol}\cdot\text{l}^{-1}$. This solution was heated to 80°C and a NaOH solution ($5 \text{ mol}\cdot\text{L}^{-1}$) was then added at a rate of $5 \text{ ml}\cdot\text{min}^{-1}$, before ageing for three hours with constant stirring through out. The precipitate was then recovered by centrifugation and washed with pure water four times. This precipitate was divided into five equal parts for hydrothermal processing and characterization.

2) Hydrothermal synthesis

PEO surfactant was mixed with one part of the resulting precipitate and ultra pure water. This mixture was stirred, transferred into an autoclave and hydrothermal treated at 120°C . The molar ratio of the starting materials for hydrothermal processing is 1: 0.4: 16 (Al:PEO:H₂O). The remaining three parts of fresh precipitate was added in to the autoclave every two days. The final product was washed by water then acetone before drying in air at 80°C .

II. CHARACTERISATION

A. X-Ray diffraction

XRD analyses were performed on a PANalytical X'Pert PRO X-ray diffractometer, with a Cu X-ray tube ($\lambda = 1.54\text{\AA}$), operating at 45 kV and 35 mA. Samples were analyzed utilising Bragg-Brentano geometry over a range of $3 - 75^\circ 2\theta$.

B. Transmission electron microscopy

A Philips CM 200 transmission electron microscopy (TEM) at 200KV was used to investigate the nanostructure of the boehmite nanofibres. All samples were dispersed in absolute ethanol solution, coated on carbon coated films and dried in an oven at 60°C for 10 mins for TEM studies.

C. SEM EDX analysis

The samples were crushed and coated with a thin layer of evaporated carbon and analysed in a JEOL 840A analytical SEM operating at 15 kV. The EDX analysis was performed using a JEOL 2300 microanalyser. Approximately 4 mm^2 area was analysed in order to produce representative sample areas.

D. Surface analysis

N_2 adsorption/desorption isotherms were measured at liquid nitrogen temperature (77.3 K), using a gas sorption analyzer

(Quantachrome, Autosorb-1). The specific surface area was calculated by the BET equation.

III. RESULTS AND DISCUSSION

A. X-Ray diffraction analysis

The XRD patterns of fresh precipitates with different iron content after 3 hours ageing. All the resulting material was identified as boehmite $\gamma\text{-AlOOH}$ except for a minor amount of bayerite formed in 0% and 1% samples. The peak broadening presented in these XRD patterns indicates that the aged precipitates are poorly crystalline before hydrothermal processing. Crystallite sizes along the *c* crystallographic direction as calculated from the Debye-Scherrer equation show that the crystallite sizes vary initial from 15.5 nm in pure aluminum precipitates, to a constant $\sim 22 \text{ nm}$ with iron doping. Crystallite sizes calculated along the *b* crystallographic direction however are seen vary from 6.1 nm largely to 6.4 (1% Fe) then gradually to 6.9 nm in the 20 % iron samples. The initial size increases are due to the influence of the iron on the growth of crystallites. The gradual change observed along the *b* direction may be related to an increased attraction of ions from solution to the surface of the precipitate.

As can be seen in Fig.1, the diffraction peaks in the XRD patterns for 1 % iron doped boehmite nanostructures become sharper with the increase in hydrothermal time, indicating a gradual increase in crystallinity of structures during soft chemical treatment. The increasing sharpness of peaks in XRD pattern were also observe for pure boehmite nanofibre growth [24]. Crystallite sizes are seen to vary gradually over 8 days from 6.5 to 11.2 nm (*b*) and 23.6 to 37.9 nm (*c*). These size increase can not to be correlated to the sizes of the fibers, sheets and tube detected in the TEM images as discussed later.

Compared with that of precipitate, the decrease intensity of bayerite peaks in final product (8 days samples) suggests a part of bayerite phase was converted into boehmite phase during hydrothermal treatment. In contrast, for undoped sample, bayerite phase can not be observed in the final product which indicates all the bayerite observed in precipitate was converted into boehmite after hydrothermal treatment. Such results are explained via Oswald ripening of boehmite, the phase most stable under the reaction conditions in this study.

Final crystallite sizes have been calculated and show a gradual increase in crystallite dimension with increasing iron content along the *b* (7.7 to 9.71 nm) and *a* (22.9 to 36.0 nm) crystallographic directions. This indicates that iron doping increases the crystallite sizes of the resultant materials.

Lattice cell parameters *a* and *b* were calculated from the XRD results. The results show that *a* remains constant for all samples while *b* varies with the change in composition and decreased during hydrothermal treatment. This change in *b* is related to the hydration of the boehmite basal spacing, with large values indicating a high amount of hydration as compared to small values.

B. EDX analysis

The relationship between added and actual iron content is shown in Fig.2. In this study a miscibility gap was observed for Fe and Al oxy hydroxides, as detected from the difference between concentrations of iron in the fibers (TEM) and the bulk material (SEM).

C. TEM results

After 8 days hydrothermal treatment, samples with varying iron content were examined by TEM. Nanofibres were observed in samples with added iron content up to 10%. For 20% iron added sample shown in Fig. 3, nanotubes of 40~100nm in length and 5~10nm in diameter were formed.

The iron doped boehmite fibres were up to 250 nm long while their width varied with iron content. Nanosheets were formed in samples with added iron percentage no less than 4%. It was noted that as the iron was increased, more sheets were formed. Similar heterogeneous morphology was also observed in a study of Zr doped alumina [25]. Small area electron diffraction patterns for sheets and fibres found in 10% added iron samples indicate the resulting nanofibres are made from a limited number of crystallites while the nanosheets contain numerous crystallites. In addition, the dark particles were examined by EDX via TEM and were found to be an iron rich phase. These results combined with the results of XRD indicate nanofibers are composed of 2-3 crystallites, indicating growth mainly occurs when fresh precipitate is added. Our results affirm the results of Zhu et al. [15].

D. Surface analysis

N_2 adsorption/desorption isotherms for undoped boehmite nanofibres, 10 and 20% iron added samples were examined. BET surface area for these three samples are 278.92, 157.23, 165.02 m^2g^{-1} respectively. The surface area of the undoped fibers is higher than that of iron doped samples due to the changes in morphology. The formation of nanotubes and iron rich particles may contribute to the higher surface area for 20% sample than that of 10% sample.

IV. CONCLUSIONS

Iron doped boehmite nanofibres, nanotubes and nanosheets were prepared using low temperature soft chemical hydrothermal treatment. The iron content in resulting boehmite nanostructures was found to be limited to a maximum of 4.3%. Fibers or needles were formed in low iron doped samples. With the increasing iron content lead to the formation of nanosheets. Nanotubes were formed when added iron content is up to 20%. Mechanistic reasons for variation in products need further investigation.

The motivation for the synthesis of iron doped boehmite nanofibres are several fold: (a) these new materials have special magnetic properties which will enable their use in drug delivery (b) the materials may have special optical properties for example the materials will absorb in the near-infrared region. (c) boehmite and its thermally activated materials are often used as catalysts. The presence of iron in the boehmite

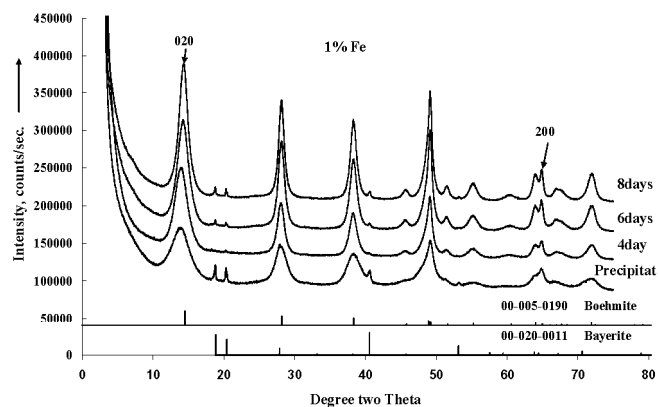


Figure 1. X-ray diffraction patterns of samples with 1% of iron added after 4, 6, 8 days hydrothermal processing.

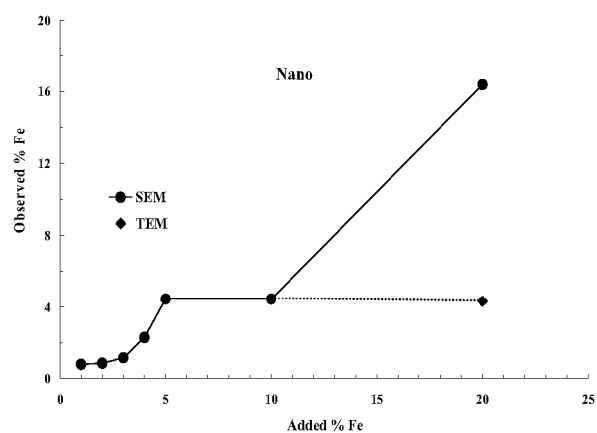


Figure 2. Observed iron content in samples that were hydrothermal processed for 8 days after washing as a function of original added iron content

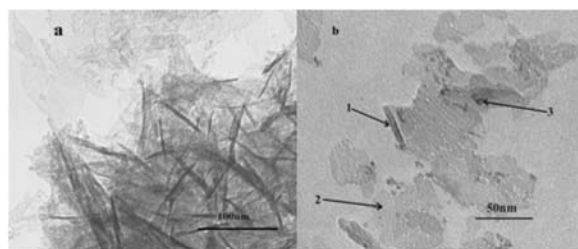


Figure 3. TEM image showing the detailed morphology of samples with 10% (a) and 20% (b) added iron after 8 days hydrothermal processing

nanomaterials enable their magnetic separation from other materials in the catalytic processes.

ACKNOWLEDGMENT

The financial and infra-structure support of the Queensland University of Technology, Inorganic Materials Research Program is gratefully acknowledged. Ms Yanyan Zhao is grateful for a QUT International Doctoral Scholarship (QIDS).

REFERENCES

- [1] J. H. Fendler and F. C. Meldrum, "The colloid chemical approach to nanostructured materials," *Advanced Materials (Weinheim, Germany)*, vol. 7, pp. 607-32, 1995.
- [2] S. Iijima, "Helical microtubules of graphitic carbon," *Nature*, vol. 354, pp. 56-58, 1991.
- [3] B. B. Lakshmi, C. J. Patrissi, and C. R. Martin, "Sol-gel template synthesis of semiconductor oxide micro- and nanostructures," *Chemistry of Materials*, vol. 9, pp. 2544-2550, 1997.
- [4] M. S. Gudiksen, L. J. Lauhon, J. Wang, D. C. Smith, and C. M. Lieber, "Growth of nanowire superlattice structures for nanoscale photonics and electronics," *Nature*, vol. 415, pp. 617-620, 2002.
- [5] C. Nedez, J.-P. Boitiaux, C. J. Cameron, and B. Didillon, "Optimization of the textural characteristics of an alumina to capture contaminants in natural gas," *Langmuir*, vol. 12, pp. 3927-3931, 1996.
- [6] V. S. Burkat, V. S. Dudorova, V. S. Smola, and T. S. Chagina, "Physicochemical properties of alumina used for removing fluorides in the dry cleaning systems," *Light Metals (Warrendale, PA, United States)*, pp. 1443-8, 1985.
- [7] D. S. Xue, Y. L. Huang, Y. Ma, P. H. Zhou, Z. P. Niu, F. S. Li, R. Job, and W. R. Fahrner, "Magnetic properties of pure Fe-Al₂O₃ nanocomposites," *Journal of Materials Science Letters*, vol. 22, pp. 1817-1820, 2003.
- [8] Y. Chen, L. Jin, and Y. Xie, "Sol-Gel processing of organic-inorganic nanocomposite protective coatings," *Journal of Sol-Gel Science and Technology*, vol. 13, pp. 735-738, 1998.
- [9] K. Okada, A. Tanaka, S. Hayashi, K. Daimon, and N. Otsuka, "Porous alumina ceramics by spray-pyrolyzed powder from aluminum sulfate and aluminum nitrate solutions," *Journal of Materials Research*, vol. 9, pp. 1709-13, 1994.
- [10] S. Ananthakumar, V. Raja, and K. G. K. Warriar, "Effect of nanoparticulate boehmite sol as a dispersant for slurry compaction of alumina ceramics," *Materials Letters*, vol. 43, pp. 174-179, 2000.
- [11] A. P. Philips, A.-M. Nechifor, and C. Patmanoharan, "Isotropic and Birefringent Dispersions of Surface Modified Silica Rods with a Boehmite-Needle Core," *Langmuir*, vol. 10, pp. 4451-8, 1994.
- [12] C. Kaya, J. Y. He, X. Gu, and E. G. Butler, "Nanostructured ceramic powders by hydrothermal synthesis and their applications," *Microporous and Mesoporous Materials*, vol. 54, pp. 37-49, 2002.
- [13] S. C. Erwin, L. Zu, M. I. Haftel, A. L. Efros, T. A. Kennedy, and D. J. Norris, "Doping semiconductor nanocrystals," *Nature (London, United Kingdom)*, vol. 436, pp. 91-94, 2005.
- [14] J. Luo, J. K. Liang, Q. L. Liu, F. S. Liu, Y. Zhang, B. J. Sun, and G. H. Rao, "Structure and magnetic properties of Mn-doped ZnO nanoparticles," *Journal of Applied Physics*, vol. 97, pp. 086106/1-086106/3, 2005.
- [15] J. B. Cui and U. J. Gibson, "Electrodeposition and room temperature ferromagnetic anisotropy of Co and Ni-doped ZnO nanowire arrays," *Applied Physics Letters*, vol. 87, pp. 133108/1-133108/3, 2005.
- [16] Q. Wang, Q. Sun, and P. Jena, "Ferromagnetism in Mn-Doped GaN Nanowires," *Physical Review Letters*, vol. 95, pp. 167202/1-167202/4, 2005.
- [17] M. Sima, I. Enculescu, A. Ioncea, T. Visan, and C. Trautmann, "Manganese and copper doped CdS nanowire arrays preparation," *Chalcogenide Letters*, vol. 1, pp. 119-124, 2004.
- [18] V. Ghiordanescu, M. Sima, I. Enculescu, M. N. Grecu, L. Mihut, M. Secu, and R. Neumann, "Photoluminescence of manganese- and copper-doped CdS nanowires," *Physica Status Solidi A: Applications and Materials Science*, vol. 202, pp. 449-454, 2005.
- [19] S. Haigh, P. Kovac, T. A. Prikhna, Y. M. Savchuk, M. R. Kilburn, C. Salter, J. Hutchison, and C. Grovenor, "Chemical interactions in Ti doped MgB₂ superconducting bulk samples and wires," *Superconductor Science and Technology*, vol. 18, pp. 1190-1196, 2005.
- [20] B. Djuricic, S. Pickering, P. Glaude, D. McGarry, and P. Tambuser, "Thermal stability of transition phases in zirconia-doped alumina," *Journal of Materials Science*, vol. 32, pp. 589-601, 1997.
- [21] V. Saraswati and G. V. R. Rao, "Transmission characteristics of transport alumina," *Journal of Materials Science Letters*, vol. 5, pp. 1095-6, 1986.
- [22] V. Saraswati and G. V. Ramarao, "Optical properties of colored transparent alumina gel monolith glasses," *Bulletin of Materials Science*, vol. 9, pp. 193-202, 1987.
- [23] H. Y. Zhu, J. D. Riches, and J. C. Barry, "A-alumina nanofibers prepared from aluminum hydrate with poly(ethylene oxide) surfactant,," *Chem. Mater.*, vol. 14, pp. 2086-2093, 2002.
- [24] H. Y. Zhu, G. X. P., D. Y. Song, Y. Q. Bai, S. P. Ringer, Z. Gao, Y. X. Xi, W. Martens, J. D. Riches, and R. L. Frost, "Growth of boehmite nanofibers by assembling nanoparticles with surfactant micelles," *J. Phys. Chem. B*, vol. 108, pp. 4245-4247, 2004.
- [25] B. Djuricic, S. Pickering, P. Glaude, D. McGarry, and P. Tambuser, "Thermal stability of transition phases in zirconia-doped alumina," *Journal of materials science*, vol. 32, pp. 589-601, 1997.



STATEMENT OF CONTRIBUTION

The authors listed below have certified that:

1. They meet the criteria for authorship in that they have participated in the conception, execution, or interpretation, of at least that part of the publication in their field of expertise;
2. They take public responsibility for their part of the publication, except for the responsible author who accepts overall responsibility for the publication;
3. There are no other authors of the publication according to these criteria;
4. Potential conflicts of interest have been disclosed to (a) granting bodies, (b) the editor or publisher of journals or other publications, and (c) the head of the responsible academic unit, and
5. They agree to the use of the publication in the student's thesis and its publication on the Australian Digital Thesis database consistent with any limitations set by publisher requirements.

In the case of this chapter:

XRD, TEM and Thermal Analysis of Fe Doped Boehmite Nanofibres and Nanosheets

Yanyan Zhao, Ray L. Frost, Wayde N. Martens and Huai Yong Zhu

Published in the Journal of Thermal Analysis and Calorimetry, 2007, 90(3), 755-760

Contributor	Statement of contribution
Yanyan Zhao	Developed experimental design and scientific method; conducted experimental and most of the characterisation work; interpreted data; wrote manuscript.
Ray L. Frost	Assisted with data interpretation and problem solving throughout this research; wrote part of the manuscript, helped with editing of manuscript
Wayde N. Martens	Assisted with experimental design and data interpretation; Contributed to manuscript.
Huai Yong Zhu	Helped with the editing of the manuscript

Principal Supervisor Confirmation

I have sighted email or other correspondence from all Co-authors confirming their certifying authorship.

Ray L. Frost

11/07/2008

Name

Signature

Date

CHAPTER 9.2

XRD, TEM and Thermal Analysis of Fe Doped Boehmite Nanofibres and Nanosheets

Yanyan Zhao, Ray L. Frost, Wayde N. Martens and Huai Yong Zhu

Yanyan Zhao Queensland University of Technology, Faculty of Science,
School of Physical and Chemical Science, Brisbane, Australia

Ray L. Frost Queensland University of Technology, Faculty of Science,
School of Physical and Chemical Science, Brisbane, Australia

Wayde N. Martens Queensland University of Technology, Faculty of Science, School
of Physical and Chemical Science, Brisbane, Australia

Huai Yong Zhu Queensland University of Technology, Faculty of Science,
School of Physical and Chemical Science, Brisbane, Australia

Copyright 2008 Akadémiai Kiadó

Author version reproduced with the
permission of the publisher.

ABSTRACT

Iron doped boehmite nanofibres with varying iron content have been prepared at low temperatures using a hydrothermal treatment in the presence of poly(ethylene oxide) surfactant. The resultant nanofibres were characterized by X-ray diffraction (XRD), and transmission electron microscopy (TEM). TEM images showed the resulting nanostructures are predominantly nanofibres when Fe doping is no more than 5%; in contrast nanosheets were formed if Fe doping was above 5%. For the 10% Fe doped boehmite, a mixed morphology of nanofibres and nanosheets were obtained. Nanotubes instead of nanofibres were observed in samples with 20% added iron. The Fe doped boehmite and the subsequent nanofibres/nanotubes were analysed by thermogravimetric and differential thermogravimetric methods. Boehmite nanofibres decompose at higher temperatures than non-hydrothermally treated boehmite and nano-sheets decompose at lower temperatures than the nanofibres

KEYWORDS: acicular, boehmite, nanofibre, nanosheets, nanotube

XRD, TEM AND THERMAL ANALYSIS OF Fe DOPED BOEHMITE NANOFIBRES AND NANOSHEETS

Y. Zhao, R. L. Frost*, W. N. Martens and H. Y. Zhu

Inorganic Materials Research Program, School of Physical and Chemical Sciences, Queensland University of Technology, GPO Box 2434, Brisbane Queensland 4001, Australia

Iron doped boehmite nanofibres with varying iron content have been prepared at low temperatures using a hydrothermal treatment in the presence of poly(ethylene oxide) surfactant. The resultant nanofibres were characterized by X-ray diffraction (XRD), and transmission electron microscopy (TEM). TEM images showed the resulting nanostructures are predominantly nanofibres when Fe doping is no more than 5%; in contrast nanosheets were formed if Fe doping was above 5%. For the 10% Fe doped boehmite, a mixed morphology of nanofibres and nanosheets were obtained. Nanotubes instead of nanofibres were observed in samples with 20% added iron. The Fe doped boehmite and the subsequent nanofibres/nanotubes were analysed by thermogravimetric and differential thermogravimetric methods. Boehmite nanofibres decompose at higher temperatures than non-hydrothermally treated boehmite and nano-sheets decompose at lower temperatures than the nanofibres.

Keywords: *acicular, boehmite, nanofibre, nanosheets, nanotube*

Introduction

Recently, synthesis of inorganic nanoscale materials with special properties have been of great interest in material science [1, 2], because their intrinsic properties of nanoscale materials are mainly determined by their composition, structure, crystallinity, size and morphology [3]. In particular, one dimensional (1D) nanoscale inorganic materials including nanofibers, nanowires and nanotubes have attracted intensive interest due to their distinctive geometries, novel physical and chemical properties and potential applications in numerous areas [4].

Because of its high surface area, chemical and thermally stable properties and mesoporous properties, alumina has been extensively used as carrier and support for a variety of industrial catalysts at high temperature as well as low temperature. Alumina can be employed as catalyst [5], adsorbent [6, 7], composite materials [8, 9] and ceramics [10–12]. Boehmite (γ -AlOOH), a principal oxo hydroxide of aluminium, is a crucial precursor in sol–gel technique for preparing high-purity and high-strength monolithic α -alumina ceramics for use as substrates for electronic circuits, abrasive grains, high-temperature refractory materials, fibres and thin films [13]. Boehmite nanofibres were first synthesised by Bugosh [14] in 1961. Nanofibres can be used as molecular building units in the preparation of core/shell materials [10, 15]. Also, since the resulting alumina prepared

from boehmite can keep the original size and morphology after calcination, great effort has been devoted to the investigation of nanoscale boehmite materials, especially 1D nanostructures, such as nanofibres and nanotubes [16, 17].

Latterly, Zhu *et al.* [18] reported an interesting new synthesis method by using a surfactant. Rather than acting as templates as for the synthesis of mesoporous materials, the surfactant was able to direct formation of boehmite fibres [17]. It was also reported that a much higher Al concentration and lower temperatures can be used compared to traditional methods for the synthesis of boehmite nanofibres. This is an efficient approach of producing nanofibres in large quantity. The growth of boehmite nanofibres can be improved by a regular interval supply of fresh precipitate of aluminium hydrate and the fibres can grow to over 100 nm long when reaction conditions are well-controlled. It is well known that the necessity of later catalyst or absorbent separation is an important issue in industrial catalytic process and water treatment. Except for filtration technique, magnetic separation is another good method [19, 20]. To achieve magnetic property, doping with iron would be an ideal way. Besides, doped with iron, the resulting boehmite nanostructure may have special optical properties which will enable it to further industrial applications.

Thermal analysis has proved most useful for the analysis of minerals and related materials [21–30]. In this work, boehmite nanofibres based on Zhu's methodology were synthesised by introducing iron as dop-

* Author for correspondence: r.frost@qut.edu.au

ant and a series of iron doped boehmite nanofibres with varying iron content have been systematically studied using thermogravimetric techniques.

Experimental

Synthesis of Fe-doped boehmite nanofibres

The detailed experimental procedure is as follows. A total amount of 0.25 mol aluminium nitrate and ferric nitrate were mixed before being dissolved in ultra-pure water. To make a comparison, mixtures with iron molar percentage of 0, 1, 2, 3, 4, 5, 10 and 20% were prepared separately and then dissolved in ultra-pure water to form a solution with a metal ion to H₂O molar ratio of 1:100 and heated to 80°C. 5 mol L⁻¹ NaOH solution was then added dropwise at a constant rate of 5 mL min⁻¹ to form precipitate. After that it was aged for three hours with constant stirring at 80°C, the resulting precipitate was recovered by centrifugation, washed with pure water four times to remove sodium nitrate. The fresh precipitate was then split into five parts evenly for hydrothermal treatment and characterization. Water and non-ionic PEO surfactant Tergitol 15-S-7 (C₁₂₋₁₄H₂₅₋₂₉O (CH₂CH₂O)₇H, Aldrich) with average molecular mass of ~508 were mixed with the first part of precipitate at a metal:PEO:H₂O molar ratio of 1:0.4:16. The viscous mixture is stirred for 1 h at room temperature and then transferred into an autoclave and kept in oven at 120°C. The remaining three parts of fresh precipitate and the same amount of ultra-pure water were added into autoclave every two days. Accordingly, the molar ratio of metal:PEO:H₂O changed to 2:0.4:32, 3:0.4:48 and 4:0.4:64, respectively, after 2, 4, 6 days. The final product was washed by water first and then acetone and dried in air at 80°C.

Methods

X-ray diffraction

XRD analyses were performed on a PANalytical X'Pert PRO X-ray diffractometer (radius: 240.0 mm). Incident X-ray radiation was produced from a line focused PW3373/10 Cu X-ray tube, operating at 45 kV and 35 mA, wavelength of 1.540596 Å. The incident beam passed through a 0.04 rad, Soller slit, a 1/2° divergence slit, a 15 mm fixed mask and a 1° fixed anti-scatter slit. After interaction with the sample, the diffracted beam was detected by an X'Celerator RTMS detector. The detector was set in scanning mode, with an active length of 2.022 mm. Samples were analysed utilising Bragg–Brentano geometry over a range of 3–75° 2θ with a step size of 0.02° 2θ, with each step measured for 200 s.

TEM analysis

A Philips CM 200 transmission electron microscopy (TEM) at 200 kV was used to investigate the morphology of the boehmite nanofibres. All samples were dispersed in absolute ethanol solution and then dropped on copper grids coated with carbon film, dried in an oven at 60°C for 10 min for TEM studies.

Thermal analysis

Thermal decomposition of the Fe-doped boehmite was carried out in a TA[®] Instruments incorporated high-resolution thermogravimetric analyzer (series Q500) in a flowing nitrogen atmosphere (60 cm³ min⁻¹). Approximately 35 mg of each sample underwent thermal analysis, with a heating rate of 5°C min⁻¹, with resolution of 6 from 25 to 1000°C. With the isothermal, isobaric heating program of the instrument the furnace temperature was regulated precisely to provide a uniform rate of decomposition in the main decomposition stage.

Results and discussion

X-ray diffraction

The X-ray diffraction of the precipitated boehmite and the hydrothermally treated boehmite are shown in Figs 1a and b. The XRD patterns show the precipitates

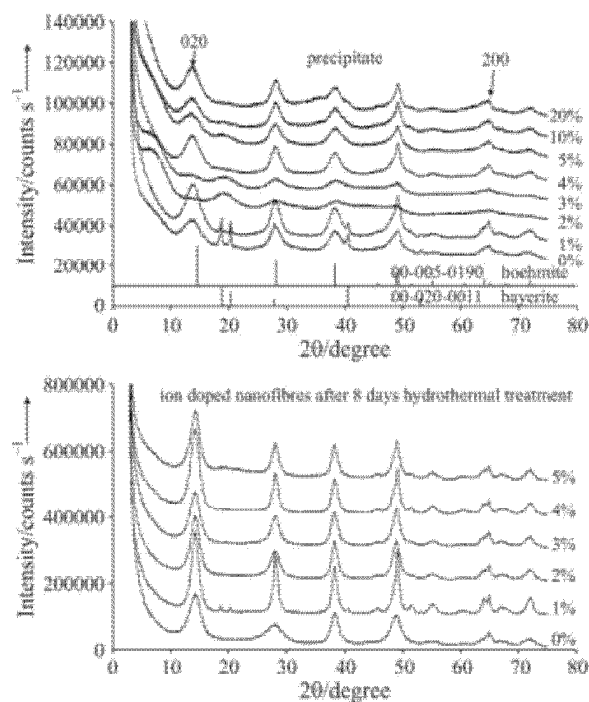


Fig. 1 a – Powder X-ray diffraction patterns of various % Fe doped boehmite and b – nanofibres

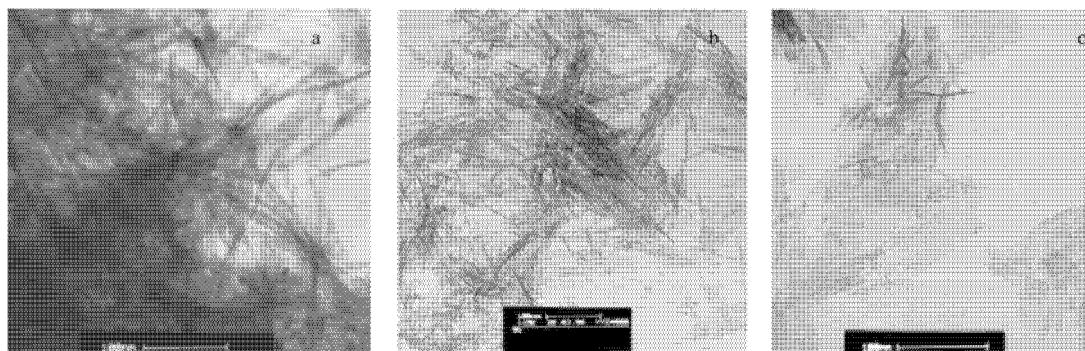


Fig. 2 TEM images of a – 3%, b – 5% and c– 10% Fe doped boehmite nanofibres

to be boehmite γ -AlOOH except for a minor amount of bayerite formed in 0 and 1% samples. By using the Debye–Scherrer equation the crystallite sizes vary initial from 15.5 nm in pure boehmite precipitates, to a constant value of \sim 22 nm with Fe doping. The XRD peaks in the patterns for 1% Fe doped boehmite nanostructures show decreased peak width with the increase in hydrothermal time, indicating a gradual increase in crystallinity of the nano-structures during the soft chemical treatment. The bayerite phase converts into boehmite with hydrothermal treatment.

Transmission electron microscopy

Typical transmission electron microscopy images for 3, 5 and 10% Fe doped nanofibres and nanosheets are shown in Figs 2a–c. The growth of pure boehmite nanofibres at 100°C has been systematically studied by Zhu *et al.* [17, 18, 31]. The average length of boehmite nanofibres after 8 days hydrothermal treatment was found to be \sim 92 nm. Hydrothermal treatment at 150°C resulted in the formation of 6 nm wide and 30 to 70 nm long lath like nanostructures [31]. In this work, boehmite nanostructures at 120°C were grown. As can be seen from Fig. 1a pure boehmite nanofibres with length up to 300 nm were synthesised, which is around three times long as that reported in a previous study [17].

As for iron doped samples, nanofibres were formed in samples with added iron content up to 10%. The iron doped boehmite fibres were up to 250 nm long while their width varied. Significant amounts of nanosheets were formed in samples with added iron percentage above 5%. Interestingly, most of the nanosheets formed have bevelled ends. As the iron doping was increased, more sheets formed; in particular, nanosheets are dominant in 10 and 20% iron doped samples. The nanofibres in these two samples aggregated in a parallel fashion forming bundle-like nanostructures resulting from increased surface charge of the nanostructure with increasing amounts of Fe. No nanofibres were observed in the 20% iron

doped sample; however, nanotubes of 40–100 nm in length and 5–10 nm in diameter were formed. The Fe content affects not only the growth of the nanofibres but also the aggregation of nanostructures. At low Fe content, nanofibres with regular shape were formed; at a higher iron content, nanofibres aggregated parallel resulting in the formation of nanosheets with pointed ends; at high Fe content, no fibres are formed and some of the sheets rolled to form nanotubes.

Thermogravimetric analysis

The thermogravimetric analysis and the differential thermal analysis of boehmite and Fe doped boehmite and their nanostructures with varying amounts of Fe from 0 to 20% are shown in Figs 3–5. The results of the

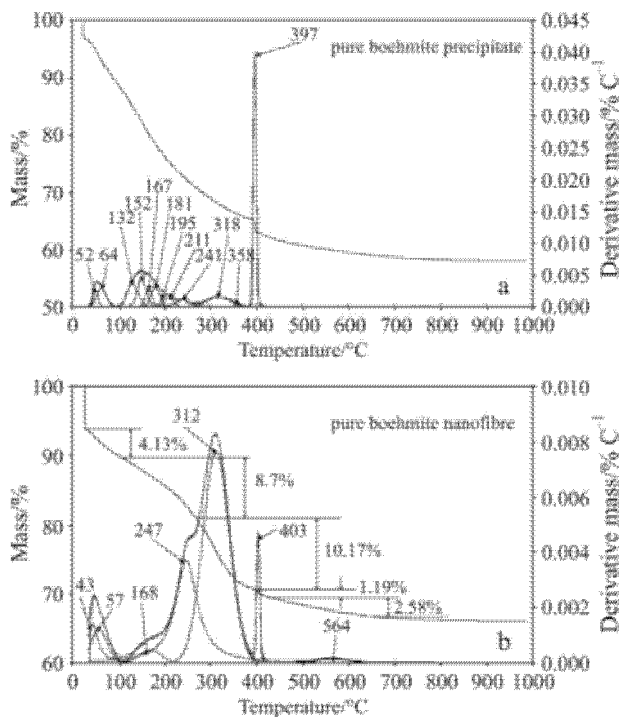
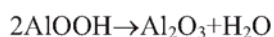


Fig. 3 Thermal analysis patterns of boehmite and boehmite nanofibres

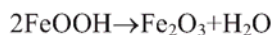
thermal analyses are reported in Table 1, including the results from other Fe doped boehmite compositions.

Pure boehmite shows four decomposition steps. The step which is characteristic of boehmite is the sharp DTG step at 397°C with a mass loss of 4.55%. The first mass loss occurs at around 50°C with a mass loss of 8.11%. This mass loss step is attributed to adsorbed water. The second mass loss step is observed at around 152°C and accounts for the major mass loss step with 18.15% mass loss. This mass loss is attributed to interstitial water trapped between the boehmite layers. The theoretical mass loss based upon the equation:



is 11.5%. In order to synthesize the boehmite nanofibres, the boehmite (precipitate) is hydrothermally treated at 120°C for 8 days. In comparison the thermal analysis of the boehmite nanofibres (Fig. 3b) shows a large thermal decomposition step at 247 and 312°C with a mass loss of 18.87%. It is concluded that the boehmite nanofibres thermally decompose at a higher temperature than boehmite. The sharp band at 403°C is attributed to boehmite in a non-fibre form.

The 1% Fe doped boehmite thermal decomposition shows an additional sharp mass loss of 12.15% is observed at 195°C. This mass loss is attributed to the decomposition of goethite according to the equation:



The boehmite precipitate decomposes over a temperature range from 229 to 364°C. In the 1% Fe doped

boehmite nanofibre the peak at 207°C is diminished in intensity with a 1.49% mass loss. This decomposition is attributed to the combustion of the surfactant molecules used to template the nanofibres. The boehmite nanofibre decomposes over the 343 to 383°C. There is a 13.90% mass loss over this temperature range. It is concluded that boehmite nanofibres decompose at temperatures higher than for untreated boehmite.

For the 2% Fe doped boehmite four decomposition steps are observed at 50°C (7.25%), 169°C (14.21%), 302°C (11.44%) and 447°C (1.90%). These thermal decomposition steps are attributed to (a) the loss of adsorbed water, (b) the decomposition of the surfactant, (c) the thermal decomposition of the goethite, (d) the decomposition of boehmite. The thermal decomposition at temperatures above 400°C is attributed to impurities. Step (c) is different to that of this step observed for the 1% Fe doped boehmite. It is possible that the goethite is an Al substituted goethite [32–34]. For the 2% Fe doped boehmite nanofibres two decomposition steps are observed at 245 and 335°C with mass losses of 7.35 and 13.98%.

The thermal decomposition of the 3% Fe doped boehmite and 3% Fe doped boehmite nanofibres are similar to that of the 2% Fe doped materials. For the 3% Fe doped boehmite nanofibre two mass loss steps are observed at 289 and 340°C with mass losses of 10.55 and 8.44%. For the 4% Fe doped boehmite thermal decomposition takes place over a wide temperature range from 269 to 374°C. Such a wide temperature range is indicative of ill defined and even amor-

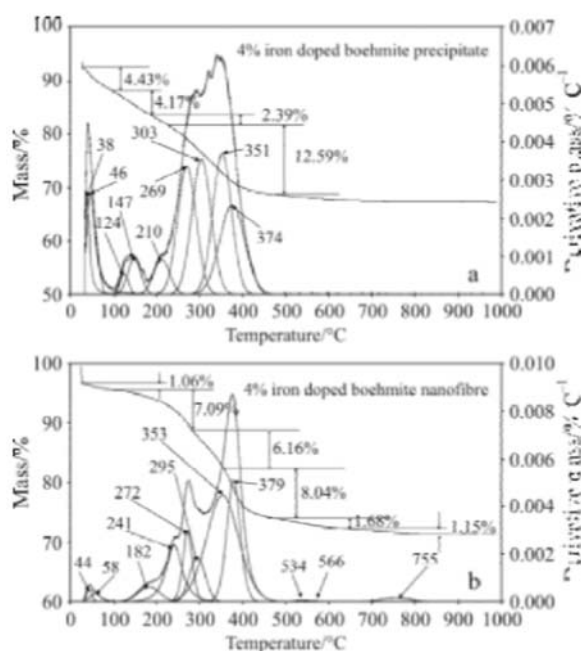


Fig. 4 Thermal analysis patterns of 4% Fe doped boehmite and boehmite nanofibres

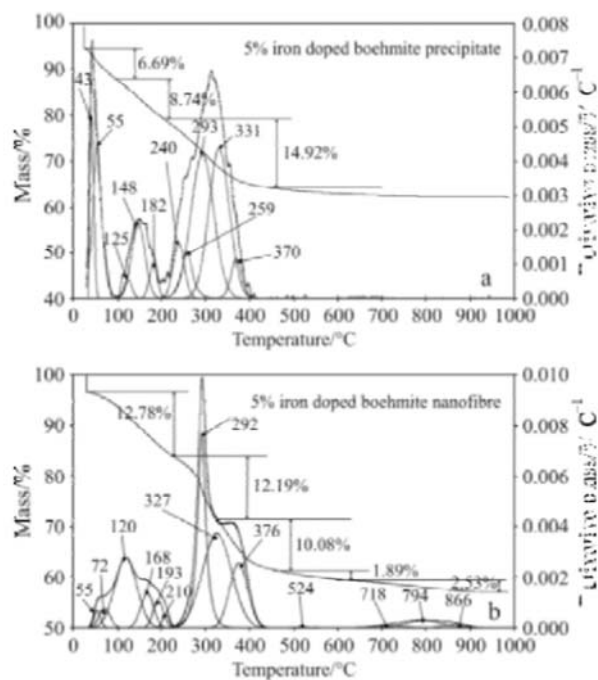


Fig. 5 Thermal analysis patterns of 5% Fe doped boehmite and boehmite nanofibres

Table 1 Results of the thermal analysis of boehmite and Fe doped boehmite and the equivalent nanofibres

Added Fe %	Decomposition step				
	First	Second	Third	Fourth	
Precipitate	0	8.11%/55°C	18.15%/152°C	4.92%/318°C	4.55%/397°C
	1	7.34%/50°C	12.15%/195°C	25.52%/348°C	–
	2	7.25%/50°C	14.21%/169°C	11.44%/302°C	1.90%/447°C
	3	6.88%/55°C	11.51%/171°C	13.74%/313°C	1.91%/702°C
	4	4.43%/46°C	4.17%/147°C	14.98%/327°C	–
	5	6.69%/50°C	8.74%/148°C	14.92%/351°C	–
	10	6.20%/50°C	10.15%/139–250°C	10.43%/337°C	–
	20	3.96%/50°C	7.99%/143–268°C	7.73%/350°C	–
	0	4.13%/50°C	8.70%/247°C	10.17%/312°C	1.19%/403°C
	1*	1.78%/50°C	1.37%/213°C	14.42%/384°C	–
Nanofibre	1	1.30%/50°C	1.49%/207°C	13.90%/383°C	–
	2	1.82%/50°C	7.35%/245°C	13.98%/335°C	–
	3	1.78%/50°C	10.55%/289°C	8.44%/340°C	–
	4	1.06%/50°C	7.09%/272°C	6.16%/353°C	8.04%/379°C
	5	12.78%/120°C	12.19%/292°C	10.08%/376°C	–
	10	1.00%/50°C	3.62%/230°C	4.04%/295°C	11.09%/376°C
	20	1.14%/50°C	–	–	17.40%/380°C

*hydrothermally treated for 6 days

phous boehmite materials (Figs 4a and b). The thermal decomposition at 241 and 272°C is attributed the combustion of the surfactant templating molecules. The temperature may be compared with the temperatures of 147 and 210°C for the 4% doped boehmite precipitate. For the 4% Fe doped boehmite nanofibres two decomposition steps at 272 and 379°C with mass losses of 7.09 and 14.20%. A similar set of results is observed for the 5% Fe doped boehmite precipitate and nanofibres. Three decomposition steps are observed for the 5% Fe doped boehmite precipitate at around 50, 150 and 351°C. For the 5% Fe doped boehmite nanofibres thermal decomposition steps are observed at 55, 120, 292 and 376°C.

As the concentration of Fe is increased the hydrothermally treated boehmite becomes a mixture of nanofibres and nanosheets. The 10% doped boehmite precipitate shows three decomposition steps at 139 to 179, 250 and 304 to 367°C. The hydrothermally treated boehmite shows three peaks at 230, 295 and 376°C. One possible assignment of these peaks is to (a) first decomposition step to goethite, (b) the decomposition of the surfactant and the third decomposition step to boehmite nanosheets. For the 20% Fe loaded boehmite the DTG patterns are similar to those of the 10% Fe doped sample. For the 20% Fe loaded boehmite nanomaterials a broad thermal decomposition is observed from 200 to 400°C with a maximum at 380°C.

Conclusions

Fe doped boehmite nanofibres 250 nm in length have been prepared at 120°C using soft chemical hydrothermal methodology using PEO as a surfactant directing agent. Fibres or needles were formed at low Fe doped samples. With the increasing iron content nanosheets are formed. Nanotubes were formed when added Fe content is increased to 20%.

Thermal analysis shows the non-treated boehmite decomposes in three steps at around 50, 150, 318 and at 397°C. The boehmite nanofibres thermally decompose at 50, 247, 312 and 403°C (Table 1). The first decomposition step is attributed to the loss of adsorbed water, the second to the loss of interstitial water and the third step to the dehydroxylation of the boehmite. In general the Fe doped boehmite nanofibres thermally decompose at higher temperatures than undoped boehmite. This is observed for both the loss of interstitial water and the dehydroxylation. For the Fe doped boehmite with Fe concentration above 5%, the thermal decomposition is of a mixed system consisting of both boehmite nanofibres and boehmite nanosheets.

Acknowledgements

The financial and infra-structure support of the Queensland University of Technology Inorganic Materials Research Program of the School of Physical and Chemical Sciences is gratefully acknowledged. The Australian Research Council (ARC) is thanked for funding the Thermal Analysis facility through a LIEF grant. One of the authors (YZ) is thankful for a Queensland University of Technology international doctoral scholarship (QIDS).

References

- J. H. Fendler and F. C. Meldrum, *Adv. Mater.* (Weinheim, Germany), 7 (1995) 607.
- B. B. Lakshmi, C. J. Patrissi and C. R. Martin, *Chem. Mater.*, 9 (1997) 2544.
- Y. Sun and Y. Xia, *Nature*, 298 (2002) 2176.
- M. S. Gudiksen, L. J. Lauhon, J. Wang, D. C. Smith and C. M. Lieber, *Nature*, 415 (2002) 617.
- J.-L. Le Loarer, H. Nussbaum and D. Bortzmeyer, (*Rhodia Chimie, Fr.*). Application: WO, 1998, p. 44.
- V. S. Burkat, V. S. Dudorova, V. S. Smola and T. S. Chagina, *Light Metals* (Warrendale, PA, United States), (1985) 1443.
- C. Nedez, J.-P. Boitiaux, C. J. Cameron and B. Didillon, *Langmuir*, 12 (1996) 3927.
- Y. Chen, L. Jin and Y. Xie, *J. Sol-Gel Sci. Technol.*, 13 (1998) 735.
- D. S. Xue, Y. L. Huang, Y. Ma, P. H. Zhou, Z. P. Niu, F. S. Li, R. Job and W. R. Fahrner, *J. Mater. Sci. Lett.*, 22 (2003) 1817.
- A. P. Philipse, A.-M. Nechifor and C. Patmamanoharan, *Langmuir*, 10 (1994) 4451.
- K. Okada, A. Tanaka, S. Hayashi, K. Daimon and N. Otsuka, *J. Mater. Res.*, 9 (1994) 1709.
- S. Ananthakumar, V. Raja and K. G. K. Warriar, *Mater. Lett.*, 43 (2000) 174.
- C. Kaya, J. Y. He, X. Gu and E. G. Butler, *Microporous Mesoporous Mater.*, 54 (2002) 37.
- J. Bugosh, *J. Phys. Chem.*, 65 (1961) 1789.
- M. P. B. Van Bruggen, *Langmuir*, 14 (1998) 2245.
- D. Kuang, Y. Fang, H. Liu, C. Frommen and D. Fenske, *J. Mater. Chem.*, 13 (2003) 660.
- H. Y. Zhu, D. Y. Song, Y. Q. Bai, S. P. Ringer, Z. Gao, Y. X. Xi, W. Martens, J. D. Riches and R. L. Frost, *J. Phys. Chem. B*, 108 (2004) 4245.
- H. Y. Zhu, J. D. Riches and J. C. Barry, *Chem. Mater.*, 14 (2002) 2086.
- L. Wood and J. Lindley, (Imperial Chemical Industries Ltd., UK), Application: EP EP, 1980, p. 21.
- W. Teunissen, A. A. Bol and J. W. Geus, *Catal. Today*, 48 (1999) 329.
- J. M. Bouzaid, R. L. Frost, A. W. Musumeci and W. N. Martens, *J. Therm. Anal. Cal.*, 86 (2006) 745.
- R. L. Frost, J. M. Bouzaid, A. W. Musumeci, J. T. Klopogge and W. N. Martens, *J. Therm. Anal. Cal.*, 86 (2006) 437.
- R. L. Frost, J. Kristof, W. N. Martens, M. L. Weier and E. Horvath, *J. Therm. Anal. Cal.*, 83 (2006) 675.
- R. L. Frost, A. W. Musumeci, J. T. Klopogge, M. L. Weier, M. O. Adebajo and W. Martens, *J. Therm. Anal. Cal.*, 86 (2006) 205.
- R. L. Frost, R.-A. Wills, J. T. Klopogge and W. Martens, *J. Therm. Anal. Cal.*, 84 (2006) 489.
- R. L. Frost, R.-A. Wills, J. T. Klopogge and W. N. Martens, *J. Therm. Anal. Cal.*, 83 (2006) 213.
- R. L. Frost, J. Kristof, M. L. Weier, W. N. Martens and E. Horvath, *J. Therm. Anal. Cal.*, 79 (2005) 721.
- R. L. Frost, M. L. Weier and W. Martens, *J. Therm. Anal. Cal.*, 82 (2005) 115.
- R. L. Frost, M. L. Weier and W. Martens, *J. Therm. Anal. Cal.*, 82 (2005) 373.
- Y.-H. Lin, M. O. Adebajo, R. L. Frost and J. T. Klopogge, *J. Therm. Anal. Cal.*, 81 (2005) 83.
- H. Y. Zhu, X. P. Gao, D. Y. Song, S. P. Ringer, Y. X. Xi and R. L. Frost, *Microporous Mesoporous Mater.*, 85 (2005) 226.
- H. D. Ruan, R. L. Frost and J. T. Klopogge, *Spectrochim. Acta, Part A*, 57A (2001) 2575.
- H. D. Ruan, R. L. Frost, J. T. Klopogge and L. Duong, *Spectrochim. Acta, Part A*, 58A (2002) 479.
- H. D. Ruan, R. L. Frost, J. T. Klopogge and L. Duong, *Spectrochim. Acta, Part A*, 58A (2002) 479.

Received: November 7, 2006

Accepted: February 22, 2007

OnlineFirst: June 28, 2007

DOI: 10.1007/s10973-006-8248-0



STATEMENT OF CONTRIBUTION

The authors listed below have certified that:

1. They meet the criteria for authorship in that they have participated in the conception, execution, or interpretation, of at least that part of the publication in their field of expertise;
2. They take public responsibility for their part of the publication, except for the responsible author who accepts overall responsibility for the publication;
3. There are no other authors of the publication according to these criteria;
4. Potential conflicts of interest have been disclosed to (a) granting bodies, (b) the editor or publisher of journals or other publications, and (c) the head of the responsible academic unit, and
5. They agree to the use of the publication in the student's thesis and its publication on the Australian Digital Thesis database consistent with any limitations set by publisher requirements.

In the case of this chapter:

Raman spectroscopy of the transition of α -gallium oxyhydroxide to β -gallium oxide nanorods

Yanyan Zhao, Jing Yang and Ray L. Frost

Published in the Journal of Raman spectroscopy, (2008), 39(10), 1327-1331

Contributor	Statement of contribution
Yanyan Zhao	Developed experimental design and scientific method; conducted experimental and most of the characterisation work; interpreted data; wrote manuscript.
Jing Yang	Helped with the editing of the manuscript
Ray L. Frost	Assisted with data interpretation and problem solving throughout this research; wrote part of the manuscript, helped with editing of manuscript

Principal Supervisor Confirmation

I have sighted email or other correspondence from all Co-authors confirming their certifying authorship.

Ray L. Frost

11/07/2008

Name

Signature

Data

CHAPTER 9.3

Raman Spectroscopy of the Transition of α -gallium Oxyhydroxide to β -gallium Oxide Nanorods

Yanyan Zhao, Jing Yang and Ray L. Frost

Yanyan Zhao Queensland University of Technology, Faculty of Science,
School of Physical and Chemical Science, Brisbane, Australia

Jing Yang Queensland University of Technology, Faculty of Science,
School of Physical and Chemical Science, Brisbane, Australia

Ray L. Frost Queensland University of Technology, Faculty of Science,
School of Physical and Chemical Science, Brisbane, Australia

ABSTRACT

The thermo-Raman spectra of synthesised α -gallium oxyhydroxide nanorod prove that the transition of α -gallium oxyhydroxide to β -gallium oxide nanorods occurs above 350 °C but below 400 °C. Scanning electron microscopy proves that the morphology of the α -gallium oxyhydroxide nanorods is retained upon calcination to β -gallium oxide. X-ray diffraction patterns show that the nanorods are α -gallium oxyhydroxide converting upon calcination to β -gallium oxide. Intense Raman bands are observed at 190, 262, 275, 430, 520, 605, and 695 cm^{-1} , which undergo a red shift of $\sim 5 \text{ cm}^{-1}$ upon heating to 350 °C. Upon thermal treatment above 350 °C, the Raman spectrum shows a significantly different pattern. Raman bands are observed at 155, 212, 280, 430, 570, and 685 cm^{-1} . The thermo-Raman spectra are in harmony with the TG and DTG patterns, which show that the reaction of α -gallium oxyhydroxide to β -gallium oxide occurs at 365 °C.

KEYWORDS: Gallium oxide; gallium oxyhydroxide; nanorods; nanofibre; Raman spectroscopy

This article is not available here.
Please consult the hardcopy thesis
available from QUT Library



STATEMENT OF CONTRIBUTION

The authors listed below have certified that:

1. They meet the criteria for authorship in that they have participated in the conception, execution, or interpretation, of at least that part of the publication in their field of expertise;
2. They take public responsibility for their part of the publication, except for the responsible author who accepts overall responsibility for the publication;
3. There are no other authors of the publication according to these criteria;
4. Potential conflicts of interest have been disclosed to (a) granting bodies, (b) the editor or publisher of journals or other publications, and (c) the head of the responsible academic unit, and
5. They agree to the use of the publication in the student's thesis and its publication on the Australian Digital Thesis database consistent with any limitations set by publisher requirements.

In the case of this chapter:

XRD, TEM and Thermal Analysis of Yttrium Doped Boehmite Nanofibres and Nanosheets.

Zhao, Yanyan; Frost, Ray L.; Vágvölgyi, Veronika; Waclawik, Eric. R.; Kristóf, János; Horváth, Erzsébet.

Submitted in the Journal of Thermal Analysis and Calorimetry, (2008), 94(1), 219-226

Contributor	Statement of contribution
Yanyan Zhao	Developed experimental design and scientific method; conducted experimental and most of the characterisation work; interpreted data; wrote part of the manuscript.
Ray L. Frost	Assisted with data interpretation and problem solving throughout this research; wrote part of the manuscript, helped with editing of manuscript
Veronika Vágvölgyi	Collecting some of the data
Eric. R. Waclawik	Help with editing
János Kristóf	Gave some advises on the experiment
Erzsébet Horváth	Helped with proof reading

Principal Supervisor Confirmation

I have sighted email or other correspondence from all Co-authors confirming their certifying authorship.

Ray L. Frost

11/07/2008

Name

Signature

Date

CHAPTER 9.4

XRD, TEM and Thermal Analysis of Yttrium Doped Boehmite Nanofibres and Nanosheets

Yanyan Zhao, Ray L. Frost, Veronika Vágvölgyi, E. R. Waclawik, János Kristóf, and Erzsébet Horváth

Yanyan Zhao	Queensland University of Technology, Faculty of Science, School of Physical and Chemical Science, Brisbane, Australia
Ray L. Frost	Queensland University of Technology, Faculty of Science, School of Physical and Chemical Science, Brisbane, Australia
Veronika Vágvölgyi	Department of Analytical Chemistry, University of Pannonia
Eric. R. Waclawik	Queensland University of Technology, Faculty of Science, School of Physical and Chemical Science, Brisbane, Australia
János Kristóf	Department of Analytical Chemistry, University of Pannonia
Erzsébet Horváth	Department of Environmental Engineering and Chemical Technology, University of Pannonia

Copyright 2008 Akadémiai Kiadó

Author version reproduced with the permission of the publisher.

ABSTRACT

Yttrium-doped boehmite nanofibres with varying iron content have been prepared at low temperatures using a hydrothermal treatment in the presence of poly (ethylene oxide) surfactant (PEO). The resultant nanofibres were characterized by X-ray diffraction (XRD) and transmission electron microscopy (TEM). TEM images showed the resulting nanostructures are predominantly nanofibres when Y-doping is less than 5%; in contrast nanosheets were formed if Y-doping was above 5%.

The Y-doped boehmite and the subsequent nanofibres/nanotubes were analyzed by thermoanalytical methods. Boehmite nanofibres decompose at higher temperatures than non-hydrothermally treated boehmite and nano-sheets decompose at lower temperatures than the nanofibres.

KEYWORDS: Boehmite; XRD; TEM; thermogravimetry; nanostructure.

XRD, TEM AND THERMAL ANALYSIS OF YTTRIUM DOPED BOEHMITE NANOFIBRES AND NANOSHEETS

Y. Zhao¹, R. L. Frost^{1*}, Veronika Vágvölgyi², E. R. Waclawik¹, J. Kristóf² and Erzsébet Horváth³

¹Inorganic Materials Research Program, School of Physical and Chemical Sciences, Queensland University of Technology

2 George Street, GPO Box 2434, Brisbane, Queensland 4001, Australia

²Department of Analytical Chemistry, University of Pannonia, 8201 Veszprém, PO Box 158, Hungary

³Department of Environmental Engineering and Chemical Technology, University of Pannonia, 8201 Veszprém PO Box 158, Hungary

Yttrium doped boehmite nanofibres with varying yttrium content have been prepared at low temperatures using a hydrothermal treatment in the presence of poly(ethylene oxide) surfactant (PEO). The resultant nanofibres were characterized by X-ray diffraction (XRD) and transmission electron microscopy (TEM). TEM images showed the resulting nanostructures are predominantly nanofibres when Y-doping is less than 5%; in contrast Y-rich phases were formed when doping was around 10%.

The doped boehmite and the subsequent nanofibres/nanotubes were analyzed by thermogravimetric and controlled rate thermal analysis methods. The boehmite nanofibres produced in this research thermally transform at higher temperatures than boehmite crystals and boehmite platelets. Boehmite nanofibres decompose at higher temperatures than non-hydrothermally treated boehmite.

Keywords: *acicular, boehmite, nanofibre, nanomaterial, nanosheets, nanotube*

Introduction

Recently, the synthesis of inorganic nanoscale materials with special properties has been of great interest in material science [1, 2], because their intrinsic properties at the nanoscale level. Material properties are mainly determined by their composition, structure, crystallinity, size and morphology [3]. In particular, one dimensional (1D) nanoscale inorganic materials including nanofibers, nanowires and nanotubes have attracted extensive interest due to their distinctive geometries, novel physical and chemical properties and potential applications in numerous areas [4].

Boehmite (AlOOH), a principal oxo-hydroxide of aluminium, is a crucial precursor in sol-gel technique for preparing high-purity and high-strength monolithic α -alumina ceramics for use as substrates for electronic circuits, abrasive grains, high-temperature refractory materials, fibres and thin films [5]. Alumina (Al₂O₃) can be obtained from AlOOH by a simple dehydration process from a certain temperature. It has been demonstrated that AlOOH nanostructures undergo an isomorphous transformation to nanocrystalline alumina during heating [6–8]. Therefore, the morphology and size of the resultant alumina can be manipulated by controlling the growth of boehmite. Alumina has been employed as catalyst [9], adsorbent [10, 11], composite materials [12, 13] and ceramics [14–16]. Due to the high surface area of alumina phases, its chemical and thermally stable prop-

erties and mesoporous properties, alumina has been extensively used as carrier and support for a variety of industrial catalysts at high temperature as well as low temperature. It is believed that the high temperature creep deformation of alumina is related to the grain boundary diffusion process in polycrystalline alumina [17]. It has been noticed that high-temperature creep in fine-grained alumina can be controlled by doping with small amounts of rare-earth elements, such as yttrium [18]. Besides, doped with yttrium, the resulting boehmite/alumina nanostructure may have special optical properties which will enable it to further industrial applications.

Thermal analysis has proved most useful for the analysis of minerals and related materials [19–28]. In this work, a series of yttrium doped boehmite nanofibres with varying yttrium content have been synthesised by introducing yttrium as dopant and the properties of the resultant yttrium doped boehmite nanofibres were systematically studied using X-ray diffraction, transmission electron microscopy and both dynamic and controlled rate thermogravimetric techniques.

Experimental

Synthesis of Y-doped boehmite nanofibres

The detailed experimental procedure is as follows. A total amount of 0.2 mol aluminium nitrate and

* Author for correspondence: r.frost@qut.edu.au

yttrium nitrate were mixed before dissolved in ultra-pure water. Mixtures with yttrium molar percentage of 1, 2, 3, 4.5 and 10% were prepared separately and then dissolved in ultra-pure water to form a solution (A) with a metal ion to H₂O molar ratio of 1:100 and heated to 80°C. With stirring in solution A, 5 mol L⁻¹ NaOH solution was then added dropwise at a constant rate of 5 mL min⁻¹ to form precipitate. After that it was aged for two hours with constant stirring at 80°C, the resulting precipitate was recovered by centrifugation, washed with pure water several times to remove sodium nitrate. The washed precipitate was then mixed with water and nonionic PEO surfactant Tergitol 15-S-7 (C₁₂₋₁₄H₂₅₋₂₉O(CH₂CH₂O)₇H, Aldrich) with average molecular mass of ~508 at a metal:H₂O:PEO molar ratio of 0.2:3.2:0.04. The viscous mixture is stirred for 1 h at room temperature and then transferred into an autoclave and kept in oven at 100°C for 6-day hydrothermal treatment. The final product was washed by water and dried in air at 80°C.

X-ray diffraction

XRD analyses were performed on a PANalytical X'Pert PRO X-ray diffractometer (radius: 240.0 mm). Incident X-ray radiation was produced from a line focused PW3373/10 Cu X-ray tube, operating at 45 kV and 35 mA, providing K_{α1} wavelength of 1.540596 Å. The incident beam passed through a 0.04 rad, Soller slit, a 1/2° divergence slit, a 15 mm fixed mask and a 1° fixed anti-scatter slit. After interaction with the sample, the diffracted beam was detected by an X'Celerator RTMS detector. The detector was set in scanning mode, with an active length of 2.022 mm. Samples were analysed utilising Bragg–Brentano geometry over a range of 3–75° 2θ with a step size of 0.02° 2θ, with each step measured for 200 s.

TEM analysis

A Philips CM 200 transmission electron microscopy (TEM) at 200 kV was used to investigate the morphology of the boehmite nanofibres. All samples were dispersed in absolute ethanol solution and then dropped on copper grids coated with carbon film, dried in an oven at 60°C for 10 min for TEM studies.

Thermal analysis

Dynamic experiment

Thermal decomposition of the yttrium doped boehmite samples was carried out in a Derivatograph PC-type thermoanalytical instrument (Hungarian Optical Works, Hungary) capable of recording the thermogravimetric (TG), derivative thermogravimetric (DTG)

and differential thermal analysis (DTA) curves simultaneously. The sample was heated in a ceramic crucible in static air atmosphere at a rate of 5°C min⁻¹.

Controlled rate thermal analysis experiment

Thermal decomposition of the yttrium doped boehmite was carried out in a derivatograph in static air atmosphere (250 cm³ min⁻¹) at a pre-set, constant decomposition rate of 0.15 mg min⁻¹. (Below this threshold value the samples were heated under dynamic conditions at a uniform rate of 1.0°C min⁻¹). The samples were heated in an open ceramic crucible at a rate of 1.0°C min⁻¹. With the quasi-isothermal, quasi-isobaric heating program of the instrument the furnace temperature was regulated precisely to provide a uniform rate of decomposition in the main decomposition stage.

Results and discussion

X-ray diffraction

Figure 1 shows the XRD patterns of doped samples after 6 days hydrothermal treatment at 100°C. All the diffraction peaks of the resultant samples with yttrium doping of 1, 2, 3, 4 and 5% can be assigned to orthorhombic boehmite (AlOOH, JCPDS 00-005-0190). The characteristic diffraction peaks for boehmite at around 14, 28, 38 and 48° 2θ degree indicate an excellent crystallinity of these samples. As for 10% doped sample, yttrium peaks as well as boehmite peaks were presented in the XRD pattern. Peak position, FWHM, lattice parameters and crystal sizes of samples with varying Y-content after 6 days hydrothermal treatment at 100°C are shown in Table 1. Peak position at both 020 and 002 varied with the increase in doped Y%. Variation in lattice parameter *b* was observed whereas lattice parameter *c* remains constant with the increase in Y-content when taking account of calculation errors. Crystallite size along *c* and *b* crystallographic directions varies with the increase in doped Y.

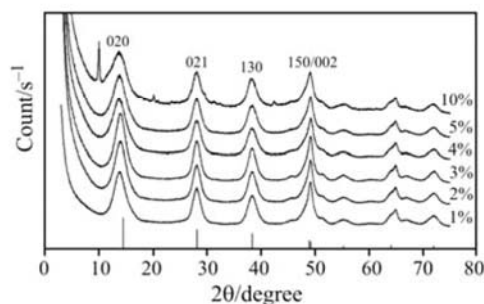


Fig. 1 Powder X-ray diffraction patterns of Y doped boehmite samples with varying Y%

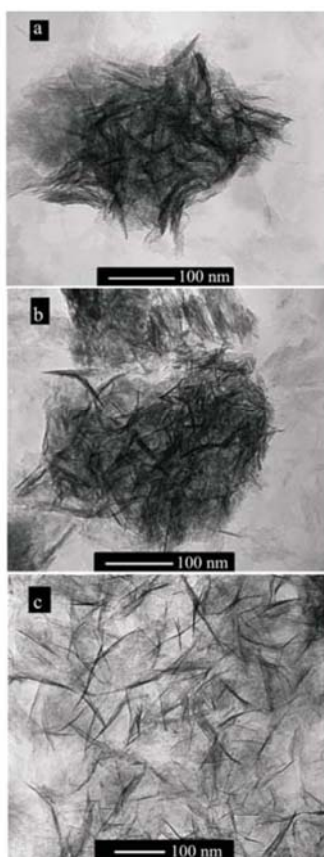
Table 1 Peak position, FWHM, lattice parameters and crystal sizes of samples with varying Y-content after 6 days hydrothermal treatment at 100°C

Added/%	<i>h k l</i>	Peak position	FWHM	Lattice parameter/Å	Crystal size/nm
		2θ/degree			
1	0 2 0	13.820	2.222	12.81	3.6
	0 0 2	49.120	0.672	3.71	13.0
2	0 2 0	13.970	2.180	12.67	3.7
	0 0 2	49.178	0.894	3.70	9.8
3	0 2 0	13.990	1.998	12.65	4.0
	0 0 2	49.157	0.624	3.70	14.0
4	0 2 0	13.754	2.400	12.87	3.3
	0 0 2	49.192	0.726	3.70	12.0
5	0 2 0	13.795	2.386	12.83	3.4
	0 0 2	49.160	0.658	3.70	13.3
10	0 2 0	13.816	2.551	12.81	3.1
	0 0 2	49.115	0.883	3.71	9.9

Transmission electron microscopy

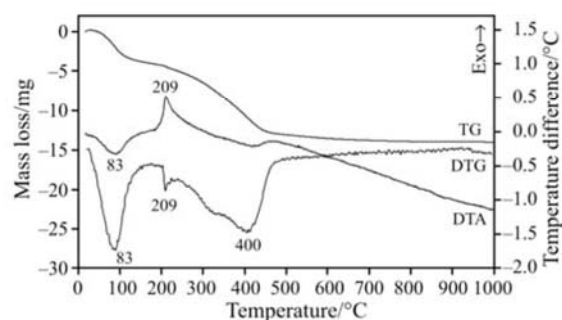
Figure 2 shows the morphology of Y-doped samples after 6 days hydrothermal treatment with Y% of 1, 3 and 5. It was noted that nanofibres, nanotubes with small amount of nanosheets were formed in all these three samples. The overall morphology and size of 1 and 3% doped boehmite are similar. The average length and width of these two samples are approximately 90

and 2.5 nm, respectively. It was noted that the size of 5% Y-doped boehmite was remarkable bigger than the other two doped samples with an average length and width of about 100 and 3.5 nm which is close to the size of pure boehmite synthesized under the same procedure and conditions our early study [29]. As for 10% sample, except for nanofibres with similar size as that formed in 5% sample, large nanorods and square-shaped yttrium rich crystals were observed.


Fig. 2 TEM images of a – 1, b – 3 and c – 5% Y-doped boehmite nanofibres

Thermogravimetric analysis

The dynamic thermal analysis of boehmite is displayed in Fig. 3. The results of the dynamic experiment are reported in Table 2. Due to a yttrium rich phase formed in the 10% sample, samples with added yttrium percentage of 1, 3 and 5 were selected for further investigation by dynamic and controlled rate thermogravimetric techniques. The dynamic thermal analyses of the 1, 3 and 5% yttrium doped boehmite are shown in Figs 4–6. The controlled rate thermal analysis of boehmite is displayed in Fig. 7. The controlled rate thermal analysis of 1, 3 and 5% yttrium doped boehmite are displayed in Figs 8–10. The results of the thermal decomposition of the 1, 3 and 5% yttrium doped boehmite are reported in Table 3.


Fig. 3 Dynamic thermal analysis patterns of boehmite

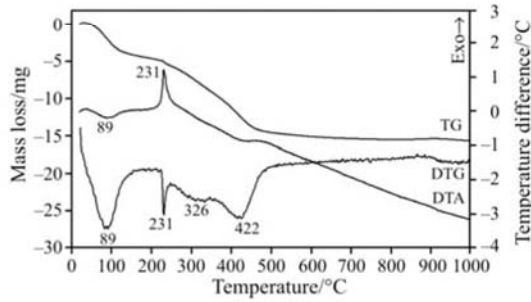


Fig. 4 Dynamic thermal analysis patterns of 1% yttrium doped boehmite

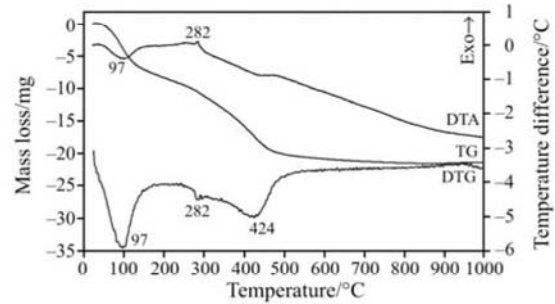


Fig. 6 Dynamic thermal analysis patterns of 5% yttrium doped boehmite

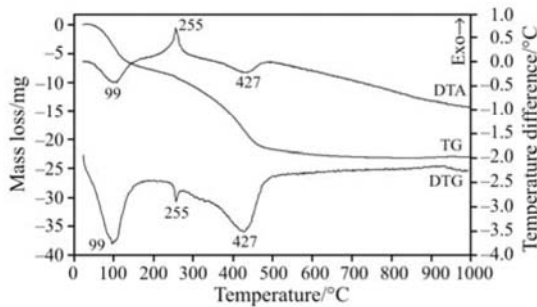


Fig. 5 Dynamic thermal analysis patterns of 3% yttrium doped boehmite

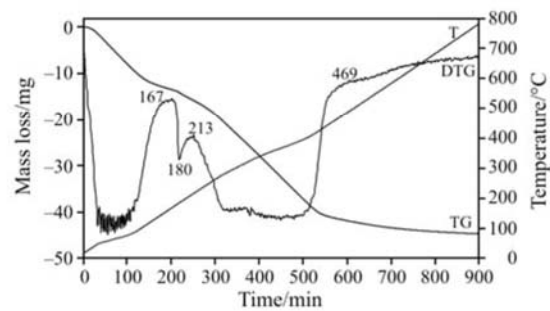
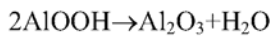


Fig. 7 Controlled rate thermal analysis patterns of 1% yttrium doped boehmite

Pure boehmite with 6 days hydrothermal treatment at 100°C shows four decomposition steps. The step characteristic of boehmite is the broad DTG step at ~397°C with a mass loss of 15.10% (Table 2). The first mass loss occurs at around 83°C with a mass loss of 7.90%. This mass loss step is attributed to adsorbed and intercalated water. The second mass loss step is observed at 209°C and accounts for the major mass loss step of 2.10% mass loss. This mass loss is attributed to interstitial water trapped between the boehmite layers. The theoretical mass loss based upon the equation:



is 15.0% [30].

Undoped boehmite nanofibres/tubes prepared at 100°C for 6 days show at least four separate de-

composition steps. The step which is characteristic of boehmite is the sharp DTG step at 345°C, with a mass loss of 13.23%. The first mass loss occurs at around 50°C, with a mass loss of 1.23%. This mass loss step is attributed to adsorbed water. The second mass loss step is observed in the 176–241°C temperature range and accounts for the major mass loss step with 13.24% mass loss. This mass loss is attributed to the combustion of the surfactant [31].

The 1% Y-doped boehmite DTG curve displays 4 maxima in the DTG curve at 89, 231 (sharp), 326 and 422°C. These DTG peaks are assigned to 9a) dehydration (b) combustion of the surfactant directing agent (c) dehydroxylation of boehmite and (d) further dehydroxylation. The DTA curve for this material shows an endotherm at 89 and around 430 and

Table 2 Decomposition stages under dynamic condition for yttrium doped boehmite

Sample											
Boehmite at 100°C			Boehmite 1% Y-doped			Boehmite 3% Y-doped			Boehmite 5% Y-doped		
$T_{\text{range}}/^\circ\text{C}$	Mass loss (sample mass: 53.11 mg)/		$T_{\text{range}}/^\circ\text{C}$	Mass loss (sample mass: 56.91 mg)/		$T_{\text{range}}/^\circ\text{C}$	Mass loss (sample mass: 88.85 mg)/		$T_{\text{range}}/^\circ\text{C}$	Mass loss (sample mass: 76.02 mg)/	
	mg	%		mg	%		mg	%		mg	%
24–172	4.2	7.9	29–205	4.9	8.6	25–199	8.0	9.0	25–211	8.7	11.4
172–246	1.1	2.1	205–256	1.1	1.9	199–270	1.7	1.9	211–305	2.8	3.7
246–506	8.0	15.1	256–360	3.6	6.3	270–516	12.3	13.8	305–527	9.1	12.0
506–877	0.9	1.7	360–500	5.1	9.0	516–800	1.2	1.4	527–800	1.1	1.4
			500–800	0.9	1.6						

Table 3 Decomposition stages under CRTA conditions for 1, 3 and 5% Y-doped boehmite

Decomposition process	Mass loss (sample mass: 160.00 mg)/		Mass loss (sample mass: 215.14 mg)/		Mass loss (sample mass: 237.99 mg)/		Mass loss (sample mass: 189.03 mg)/		
	$T_{\text{range}}/^{\circ}\text{C}$	mg	%	$T_{\text{range}}/^{\circ}\text{C}$	mg	%	$T_{\text{range}}/^{\circ}\text{C}$	mg	%
Dehydration	22–167	13.4	8.4	22–175	17.9	8.3	21–172	23.5	9.9
Dehydration	167–213	2.2	1.4	175–326	17.4	8.1	172–480	38.2	16.1
Dehydroxylation	213–469	25.8	16.1	326–474	21.2	9.9	480–620	2.9	1.2
	469–764	3.1	1.9	474–667	3.2	1.5	508–716	2.3	1.2

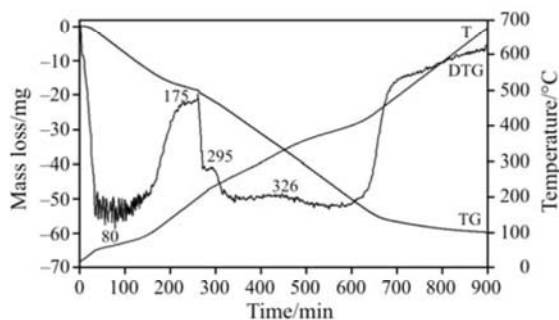


Fig. 8 Controlled rate thermal analysis patterns of 1% yttrium doped boehmite

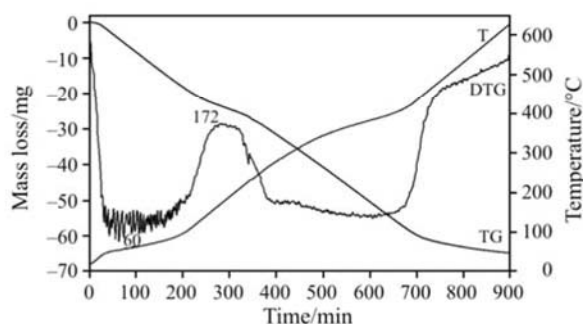


Fig. 9 Controlled rate thermal analysis patterns of 3% yttrium doped boehmite

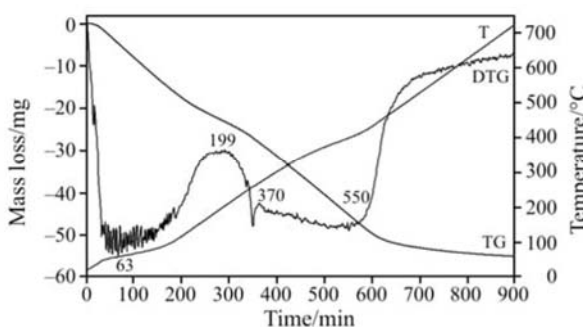


Fig. 10 Controlled rate thermal analysis patterns of 5% yttrium doped boehmite

an exotherm at 231°C. It is proposed that at 427°C the boehmite nanofibres transformed to γ -alumina. The DTG peak and the DTA exotherm at 231°C are assigned to the combustion of the PEO surfactant. In a previous piece of research infrared emission spectroscopy was used to study the dehydroxylation of natural and synthetic boehmite [32]. It was found that dehydroxylation starts at 250 and is complete by 450°C. The dehydroxylation is followed by the loss of intensity of the hydroxyl stretching frequencies observed at 3478, 3319 and 3129 cm^{-1} and by the loss of intensity of the hydroxyl deformation modes at 1140 and 1057 cm^{-1} . A previous study made simulations of the thermal decomposition of boehmite [33]. It was found that the simulations of the non-isothermal experiments.

at constant heating rates show that thermally stimulated transformation of nanocrystalline boehmite into alumina can be accurately modelled by a 4-reaction mechanism involving: (I) the loss of physisorbed water, (II) the loss of chemisorbed water, (III) the conversion of boehmite into transition alumina, (IV) the dehydration of transition alumina (loss of residual hydroxyl groups) [33]. Another study of boehmite precipitates by the authors found that thermal analysis showed five endotherms at 70, 140, 238, 351 and 445°C and these endotherms are attributed to the dehydration and dehydroxylation of the hydrolyzate [34].

The calculation of the water content is given in the appendix. For the 1% yttrium doped boehmite the amount of water was calculated as 0.30 mol mol^{-1} of $\text{AlO}(\text{OH})$. The values for 3 and 5% yttrium doped boehmite are 0.36 and 0.45 moles of water per mole of $\text{AlO}(\text{OH})$. The relationship between the moles of water in the interlayer and the moles of yttrium doping of the boehmite appears linear. The relationship is given as $y=0.375x+0.2575$ with $R^2=0.9868$. In a previous study the authors proposed that water was incorporated into the boehmite structure through folding of the boehmite layers which resulted in changes in the 020 reflection [34]. It was postulated that the structure of the resultant $\text{AlO}(\text{OH})$ formed from cold water hydrolysis of trisecbutoxyaluminium(III) was one of folded boehmite structure along the 020 planes of boehmite. This structure was then proposed to straighten during ageing of the amorphous aluminium oxy(hydroxide), which results in the formation of pseudoboehmite. Such a structure showed an X-ray diffraction pattern with the (020) peak for pseudoboehmite but not other peaks, which was attributed to the disintegration of long range order but preservation of short range order. It should be noted that the temperature of hydrolysis is 75°C. The reason for the selection of this temperature is that at and above this temperature a single phase is formed. If the hydrolyzate is formed at 25°C, an amorphous aluminium oxy(hydroxide) is formed, which on ageing transforms to boehmite and gibbsite. Thus it is proposed that the increase in Y-content in the boehmite results in an increase in the amount of pseudoboehmite and thus more water is incorporated into the pseudoboehmite structure.

The 3% Y doped boehmite shows three DTG peaks at 99, 255 and 427°C. The DTA curve displays two endotherms at 99 and 427°C and an exotherm at 255°C.

The attribution of the DTG peaks is as above. The 5% Y-doped boehmite shows three DTG peaks at 97, 282 and 424°C. The DTA curve of the 5% Y-doped boehmite displays two endotherms at 97 and 427°C and an exotherm at 282°C. It appears that as the yttrium dop-

ing increases the DTG peak at around 427°C becomes significantly broader. This provides an indication of the wide range of nanofibres present in the boehmite nanomaterial. In the work reported by Alphonse and Courty [33] the DTG peak for the nanocrystalline boehmite of platelets of size 10 nm was around 390°C. It is concluded that the boehmite nanofibres produced in this research thermally transform at higher temperatures than boehmite crystals and boehmite platelets.

The CRTA of the pure boehmite (Fig. 7) shows as for the dynamic experiment shows four decomposition steps as per Table 3. These steps are attributed to two dehydration steps the first of which is isothermal at ~70°C and is assigned to adsorbed water. This accounts for a 8.4% mass loss. The second mass loss at 180°C is obviously non-isothermal and accounts for a 1.4% mass loss. In the dynamic experiment a significant exothermic reaction was observed at 209°C. The third mass loss of 16.10% is also isothermal and occurs at ~400°C. In the dynamic experiment a slow mass loss over a wide temperature range occurs, commencing at around 250 and is complete by 470°C.

The CRTA of the 1% yttrium doped boehmite shows a quasi-isothermal dehydration step at 80°C. Similarly to the dynamic experiment, two dehydroxylation stages can be separated in the 175 to 500°C range with the local minimum in the DTG curve at 326°C. Interestingly, the second step of dehydroxylation is approaching a quasi-isothermal course. The shoulder in the DTG curve at about 220°C is assigned to the combustion of traces of the surfactant adsorbed on the surface.

The CRTA of the 3% yttrium doped boehmite shows a quasi-isothermal step of dehydration at around 60°C. The two-stage pattern of dehydroxylation can also be observed in the DTG curve in the 175 to 450°C range. The second (quasi-isothermal) step of dehydroxylation is increased at the expense of the first one. The burning of the surfactant can also be identified at around 220°C. The CRTA of the 5% yttrium doped boehmite shows a quasi-isothermal dehydration step at about 63°C. The combustion of the surfactant can be observed at about 250°C. Although the second part of dehydroxylation is approaching a quasi-isothermal pattern, the separation of the two dehydroxylation processes can no longer be observed in the DTG curve. This is in harmony with the dynamic experiments. In the dynamic experiments the two dehydroxylation steps at 326 and 422°C gradually merged with the increase of yttrium concentration. The anomaly why the initial part of dehydroxylation is non-isothermal, while the second part is getting to be an isothermal process needs further studies on the mechanism of decomposition.

Conclusions

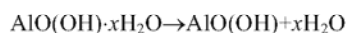
Yttrium doped boehmite nanofibres of some 250 nm in length can be prepared at 100°C using soft chemical hydrothermal methodology using PEO as a surfactant directing agent. The yttrium content in boehmite nanostructures was found to be limited to a maximum of around 5.0%. Fibres or needles were formed at low Y-doping. With the increasing Y-content nanosheets are formed.

Thermal analysis under dynamic and CRTA conditions shows that the steps of dehydroxylation are merged with the increase of the yttrium content. The CRTA experiment revealed that the two steps of dehydroxylation take place according to different mechanisms.

Appendix

Calculation of water content for Y-doped boehmite

using the formula $\text{AlO}(\text{OH}) \cdot x\text{H}_2\text{O}$. Loss of water is calculated according to the reaction:



A) 1% Y-doped boehmite

Composition: $\text{AlO}(\text{OH}) \cdot x\text{H}_2\text{O}$

Loss of water up to 175°C is 17.9 mg (0.993 mmol).

Mass of dehydrated mineral is 197.24 mg (3.288 mmol).

Thus, the amount of crystallization water is 0.30 mol.

B) 3% Y-doped boehmite

Composition: $\text{AlO}(\text{OH}) \cdot x\text{H}_2\text{O}$

Loss of water up to 172°C is 23.5 mg (1.304 mmol).

Mass of dehydrated mineral is 214.49 mg (3.575 mmol).

Thus, the amount of crystallization water is 0.36 mol.

C) 5% Y-doped boehmite

Composition: $\text{AlO}(\text{OH}) \cdot x\text{H}_2\text{O}$

Loss of water up to 193°C is 22.6 mg (1.254 mmol).

Mass of dehydrated mineral is 166.43 mg (2.774 mmol).

Thus, the amount of crystallization water is 0.45 mol.

Acknowledgements

The financial and infra-structure support of the Queensland University of Technology Inorganic Materials Research Program of the School of Physical and Chemical Sciences is gratefully acknowledged. The Australian Research Council (ARC) is thanked for funding the Thermal Analysis facility through a LIEF grant. One of the authors (YZ) is thankful for a Queensland University of Technology international doctoral scholarship (QIDS).

References

- 1 J. H. Fendler and F. C. Meldrum, *Adv. Mater.* (Weinheim, Germany), **7** (1995) 607.
- 2 B. B. Lakshmi, C. J. Patrissi and C. R. Martin, *Chem. Mater.*, **9** (1997) 2544.
- 3 Y. Sun and Y. Xia, *Nature*, **298** (2002) 2176.
- 4 M. S. Gudiksen, L. J. Lauhon, J. Wang, D. C. Smith and C. M. Lieber, *Nature*, **415** (2002) 617.
- 5 C. Kaya, J. Y. He, X. Gu and E. G. Butler, *Microporous Mesoporous Mater.*, **54** (2002) 37.
- 6 Y. Zhao, W. N. Martens, R. L. Frost and H. Y. Zhu, *Langmuir*, **23** (2007) 9850.
- 7 H. Y. Zhu, X. P. Gao, D. Y. Song, S. P. Ringer, Y. X. Xi and R. L. Frost, *Microporous Mesoporous Mater.*, **85** (2005) 226.
- 8 H. Y. Zhu, J. D. Riches and J. C. Barry, *Chem. Mater.*, **14** (2002) 2086.
- 9 J.-L. Le Loarer, H. Nussbaum and D. Bortzmeyer, *Alumina Extrudates, Methods for Preparing and Use as Catalysts or Catalyst Supports*, (Rhodia Chimie, Fr.), Application: WO, 1998, p. 44.
- 10 V. S. Burkat, V. S. Dudorova, V. S. Smola and T. S. Chagina, *Light Metals*, Warrendale, PA, USA 1985, pp. 1443–1448.
- 11 C. Nedez, J.-P. Boitiaux, C. J. Cameron and B. Didillon, *Langmuir*, **12** (1996) 3927.
- 12 Y. Chen, L. Jin and Y. Xie, *J. Sol-Gel Sci. Technol.*, **13** (1998) 735.
- 13 D. S. Xue, Y. L. Huang, Y. Ma, P. H. Zhou, Z. P. Niu, F. S. Li, R. Job and W. R. Fahrner, *J. Mater. Sci. Lett.*, **22** (2003) 1817.
- 14 A. P. Philipse, A.-M. Nechifor and C. Patmamanoharan, *Langmuir*, **10** (1994) 4451.
- 15 K. Okada, A. Tanaka, S. Hayashi, K. Daimon and N. Otsuka, *J. Mater. Res.*, **9** (1994) 1709.
- 16 S. Ananthakumar, V. Raja and K. G. K. Warriar, *Mater. Lett.*, **43** (2000) 174.
- 17 A. H. Heuer, N. J. Tighe and R. M. Cannon, *J. Am. Ceram. Soc.*, **63** (1980) 53.
- 18 J. Cho, M. P. Harmer, H. M. Chan, J. M. Rickman and A. M. Thompson, *J. Am. Ceram. Soc.*, **80** (1997) 1013.
- 19 J. M. Bouzaid, R. L. Frost, A. W. Musumeci and W. N. Martens, *J. Therm. Anal. Cal.*, **86** (2006) 745.
- 20 R. L. Frost, J. M. Bouzaid, A. W. Musumeci, J. T. Klopogge and W. N. Martens, *J. Therm. Anal. Cal.*, **86** (2006) 437.
- 21 R. L. Frost, J. Kristóf, W. N. Martens, M. L. Weier and E. Horváth, *J. Therm. Anal. Cal.*, **83** (2006) 675.
- 22 R. L. Frost, A. W. Musumeci, J. T. Klopogge, M. L. Weier, M. O. Adebajo and W. Martens, *J. Therm. Anal. Cal.*, **86** (2006) 205.
- 23 R. L. Frost, R.-A. Wills, J. T. Klopogge and W. Martens, *J. Therm. Anal. Cal.*, **84** (2006) 489.
- 24 R. L. Frost, R.-A. Wills, J. T. Klopogge and W. N. Martens, *J. Therm. Anal. Cal.*, **83** (2006) 213.
- 25 R. L. Frost, J. Kristóf, M. L. Weier, W. N. Martens and E. Horváth, *J. Therm. Anal. Cal.*, **79** (2005) 721.
- 26 R. L. Frost, M. L. Weier and W. Martens, *J. Therm. Anal. Cal.*, **82** (2005) 115.
- 27 R. L. Frost, M. L. Weier and W. Martens, *J. Therm. Anal. Cal.*, **82** (2005) 373.
- 28 Y.-H. Lin, M. O. Adebajo, R. L. Frost and J. T. Klopogge, *J. Therm. Anal. Cal.*, **81** (2005) 83.
- 29 Y. Zhao, R. L. Frost, W. N. Martens and H. Y. Zhu, *Langmuir*, **23** (2007) 9850.
- 30 Y. Zhao, R. L. Frost, W. N. Martens and H. Y. Zhu, *J. Therm. Anal. Cal.*, **90** (2007) 755.
- 31 Y. Zhao, R. L. Frost and W. N. Martens, *J. Phys. Chem., C* **111** (2007) 5313.
- 32 R. L. Frost, J. T. Klopogge, S. C. Russell and J. Szetu, *Appl. Spectrosc.*, **53** (1999).
- 33 P. Alphonse and M. Courty, *Thermochim. Acta*, **425** (2005) 75.
- 34 W. N. Martens, R. L. Frost, J. Bartlett and J. T. Klopogge, *Thermochim. Acta*, **374** (2001) 31.

Received: January 14, 2008

Accepted: April 1, 2008

OnlineFirst: August 15, 2008

DOI: 10.1007/s10973-008-9002-6



STATEMENT OF CONTRIBUTION

The authors listed below have certified that:

1. They meet the criteria for authorship in that they have participated in the conception, execution, or interpretation, of at least that part of the publication in their field of expertise;
2. They take public responsibility for their part of the publication, except for the responsible author who accepts overall responsibility for the publication;
3. There are no other authors of the publication according to these criteria;
4. Potential conflicts of interest have been disclosed to (a) granting bodies, (b) the editor or publisher of journals or other publications, and (c) the head of the responsible academic unit, and
5. They agree to the use of the publication in the student's thesis and its publication on the Australian Digital Thesis database consistent with any limitations set by publisher requirements.

In the case of this chapter:

Raman spectroscopy and characterization of α -gallium oxyhydroxide and β -gallium oxide nanorods

Yanyan Zhao, Ray L. Frost

Accepted in the Journal of Raman spectroscopy, 2008, 39(10), 1494-1501

Contributor	Statement of contribution
Yanyan Zhao	Developed experimental design and scientific method; conducted experimental and characterisation work; interpreted data; wrote part of manuscript.
Ray L. Frost	Assisted with data interpretation; wrote part of the manuscript, and helped with editing.

Principal Supervisor Confirmation

I have sighted email or other correspondence from all Co-authors confirming their certifying authorship.

Ray L. Frost

11/07/2008

Name

Signature

Date

CHAPTER 9.5

Raman Spectroscopy and Characterization of α -gallium Oxyhydroxide and β -gallium Oxide Nanorods

Yanyan Zhao, Ray L. Frost

Yanyan Zhao Queensland University of Technology, Faculty of Science,
School of Physical and Chemical Science, Brisbane, Australia

Ray L. Frost Queensland University of Technology, Faculty of Science,
School of Physical and Chemical Science, Brisbane, Australia

ABSTRACT

Raman spectroscopy complemented by infrared spectroscopy was used to characterise both gallium oxyhydroxide α -GaO(OH) and gallium oxide β -Ga₂O₃ nanorods synthesised with and without the surfactants using a soft chemical methodology at low temperatures. Nano to micro sized gallium oxyhydroxide and gallium oxide materials were characterised and analysed by both X-ray diffraction and Raman spectroscopy. Rod-like GaO(OH) crystals with average length of ~ 2.5 μm and width of 1.5 μm were obtained. Upon thermally treating gallium oxyhydroxide GaO(OH) to 900°C β -Ga₂O₃ was synthesised retaining the initial GaO(OH) morphology. Raman spectroscopy has been used to study the structure of nanorods of GaO(OH) and Ga₂O₃ crystals.

Raman spectroscopy shows bands characteristic of GaO(OH) at 950 , ~ 1000 cm^{-1} attributed to Ga-OH deformation modes. Bands at 261 , 275 , 433 and 522 cm^{-1} are assigned to vibrational modes involving Ga-OH units. Bands observed at 320 , 346 , 418 and 472 cm^{-1} are assigned to the deformation modes of Ga₂O₆ octahedra. Two sharp infrared bands at 2948 and 2916 cm^{-1} are attributed to the GaO(OH) symmetric stretching vibrations. Raman spectroscopy of Ga₂O₃ provides bands at 630 , 656 and 767 cm^{-1} which are assigned to the bending and stretching of GaO₄ units. Raman bands at 417 and 475 cm^{-1} are attributed to the symmetric stretching modes of GaO₂ units. The Raman bands at 319 and 347 cm^{-1} are assigned to the bending modes of GaO₂ units.

KEYWORDS- Gallium oxide; Gallium oxyhydroxide; nanorods; nanofibre; nanotube; Raman spectroscopy.

This article is not available here.
Please consult the hardcopy thesis
available from QUT Library



STATEMENT OF CONTRIBUTION

The authors listed below have certified that:

1. They meet the criteria for authorship in that they have participated in the conception, execution, or interpretation, of at least that part of the publication in their field of expertise;
2. They take public responsibility for their part of the publication, except for the responsible author who accepts overall responsibility for the publication;
3. There are no other authors of the publication according to these criteria;
4. Potential conflicts of interest have been disclosed to (a) granting bodies, (b) the editor or publisher of journals or other publications, and (c) the head of the responsible academic unit, and
5. They agree to the use of the publication in the student's thesis and its publication on the Australian Digital Thesis database consistent with any limitations set by publisher requirements.

In the case of this chapter:

Dynamic and Controlled rate thermal analysis, surface analysis and infrared emission of Ga doped boehmite nanofibres and nanosheets.

Yanyan Zhao, Jing Yang, Ray L. Frost,
Submitted in Thermochimica Acta

Contributor	Statement of contribution
Yanyan Zhao	Developed experimental design and scientific method; conducted experimental and characterisation work; interpreted data; wrote manuscript.
Jing Yang	Conducted IES data collection
Ray L. Frost	Assisted with data interpretation; contributed to manuscript, and helped with editing.

Principal Supervisor Confirmation

I have sighted email or other correspondence from all Co-authors confirming their certifying authorship.

Ray L. Frost

11/07/2008

Name

Signature

Data

CHAPTER 9.6

Dynamic and Controlled rate Thermal analysis, Surface Analysis and Infrared Emission of Ga Doped Boehmite Nanofibres and Nanosheets

Yanyan Zhao, Jing Yang, Ray L. Frost

Yanyan Zhao Queensland University of Technology, Faculty of Science,
School of Physical and Chemical Science, Brisbane, Australia

Jing Yang Queensland University of Technology, Faculty of Science,
School of Physical and Chemical Science, Brisbane, Australia

Ray L. Frost Queensland University of Technology, Faculty of Science,
School of Physical and Chemical Science, Brisbane, Australia

ABSTRACT

Ga doped boehmite nanofibres with varying Ga content have been prepared at low temperature using hydrothermal treatment in the presence of poly (ethylene oxide) surfactant. The resulting nanofibres were characterized by X-ray diffraction (XRD), transmission electron microscopy (TEM), Energy dispersive X-ray analysis (EDX), N₂ adsorption/desorption, dynamic and controlled rate thermal analysis and Infrared Emission Spectroscopy (IES). TEM results show that nanotubes are dominant when the doped gallium percentage is no more than 5%; nanosheets and amorphous phase are dominant in 10% and 20% gallium doped samples. N₂ adsorption/desorption analysis reveals a large amount of micropores and mesopores are present in the resultant samples. Similar to iron and yttrium doped boehmite nanomaterials, remarkable larger BET specific area were achieved compared to pure boehmite nanomaterials. Both dynamic and controlled thermal analysis show that the gallium doped boehmite nanomaterials dehydrate at higher temperature than that of pure boehmite. Interestingly, the better the crystallinity of the resultant nanotubes is, the higher the dehydration temperature. The IES show that dehydroxylation of the resultant gallium doped boehmite nanomaterials starts at 250 °C and is complete by 450 °C.

KEYWORDS- Doped boehmite, acicular, nanofibre, nanotube, nanosheets.

Dynamic and Controlled rate thermal analysis, surface analysis and infrared emission of Ga doped boehmite nanofibres and nanosheets

Yanyan Zhao, Jing Yang, Ray L. Frost¹

Inorganic Materials Research Program, School of Physical and Chemical Sciences, Queensland University of Technology, 2 George Street, GPO Box 2434, Brisbane, Queensland 4001, Australia

Abstract:

Ga doped boehmite nanofibres with varying Ga content have been prepared at low temperature using hydrothermal treatment in the presence of poly (ethylene oxide) surfactant. The resulting nanofibres were characterized by X-ray diffraction (XRD), transmission electron microscopy (TEM), Energy dispersive X-ray analysis (EDX), N₂ adsorption/desorption, dynamic and controlled rate thermal analysis and Infrared Emission Spectroscopy (IES). TEM results show that nanotubes are dominant when the doped gallium percentage is no more than 5%; nanosheets and amorphous phase are dominant in 10% and 20% gallium doped samples. N₂ adsorption/desorption analysis reveals a large amount of micropores and mesopores are present in the resultant samples. Similar to iron and yttrium doped boehmite nanomaterials, remarkable larger BET specific area were achieved compared to pure boehmite nanomaterials. Both dynamic and controlled thermal analysis show that the gallium doped boehmite nanomaterials dehydrate at higher temperature than that of pure boehmite. Interestingly, the better the crystallinity of the resultant nanotubes is, the higher the dehydration temperature. The IES show that dehydroxylation of the resultant gallium doped boehmite nanomaterials starts at 250 °C and is complete by 450 °C.

Keywords:

boehmite, acicular, nanofibre, nanotube, nanosheets

doped

¹ Corresponding author: Ray Frost
Email address: r.frost@qut.edu.au
Address: 2 George Street, Brisbane Q 4001, Australia
Ph +61 7 3138 2407 F: +61 7 3138 1804

Introduction

Recently, the synthesis of inorganic nanoscale materials with special properties have been of great interest in material science [1, 2], because their intrinsic properties of nanoscale materials are mainly determined by their composition, structure, crystallinity, size and morphology [3]. In particular, one dimensional (1D) nanoscale inorganic materials including nanofibres, nanowires and nanotubes have attracted intensive interest due to their distinctive geometries, novel physical and chemical properties and potential applications in numerous areas [4]. Because of its high surface area, chemical and thermally stable properties and mesoporous properties, alumina has been extensively used as carrier and support for a variety of industrial catalysts at high temperature as well as low temperatures. Alumina can be employed as a catalyst [5], adsorbent [6, 7], composite materials [8, 9] and ceramics [10-12]. Boehmite (γ -AlOOH), a principal oxhydroxide of aluminium, is a crucial precursor in sol-gel technique for preparing high-purity and high-strength monolithic α -alumina ceramics for use as substrates for electronic circuits, abrasive grains, high-temperature refractory materials, fibres and thin films. Boehmite nanofibres were first synthesised by John Bugosh in 1961. Boehmite 1D nanostructures can be used as molecular building units in the preparation of core/shell materials [10, 13]. Also, since the resulting alumina prepared from boehmite can keep the original size and morphology after calcination, great effort has been devoted to the investigation of nanoscale boehmite materials, especially 1D nanostructures, such as nanofibres and nanotubes [14, 15].

Latterly, Zhu et al [16] reported an interesting new synthesis method by using a surfactant. Rather than acting as templates as for the synthesis of mesoporous materials, the surfactant was able to direct formation of boehmite fibres. It was also reported that a much higher Al concentration and lower temperatures can be used, compared to traditional methods for the synthesis of boehmite nanofibres. This is an efficient approach for producing nanofibres in large quantities. Metal ion doping is a promising technique to fabricate and control the properties of materials. Enhanced or new properties can be achieved by introducing Ga to the target materials [17-21]. Therefore, doped with Ga, the resulting boehmite nanostructure may have promising optical, electronic and other properties which will enable further industrial applications.

It is well known that the surface properties including surface area, pore volume and pore size distribution are very important for materials in the applications of catalysts, adsorbents and so on. Thermal analysis has proved to be another most important and useful for the analysis and application exploration of minerals and related materials. In this work, a series of gallium doped boehmite nanotubes with varying gallium content have been synthesized and the morphology and most importantly the detailed properties of the resultant materials were investigated by using TEM, XRD, EDX, N₂ adsorption/desorption, t-plot analysis and distribution analysis, TG

techniques and Infrared Emission Spectroscopy.

Experimental

Synthesis of Ga doped boehmite nanofibres

The detailed experimental procedure is as follows. A total amount of 0.2 mol aluminium nitrate and gallium nitrate were mixed before dissolved in ultra-pure water. Mixtures with gallium molar percentage of 0%, 1%, 2%, 3%, 4%, 5%, 10% and 20% were prepared separately and then dissolved in ultra-pure water to form a solution (A) with a metal ion to H₂O molar ratio of 1:100 and heated to 80 °C. With stirring in solution A, 6 mol·L⁻¹ NaOH solution was then added drop-wise at a constant rate of 5 ml·min⁻¹ to form precipitate. After that it was aged for two hours with constant stirring at 80°C, the resulting precipitate was recovered by centrifugation, washed with pure water several times to remove sodium nitrate. The washed precipitate was then mixed with water and nonionic PEO surfactant Tergitol 15-S-7 (C₁₂₋₁₄H₂₅₋₂₉O (CH₂CH₂O)₇H , Aldrich) with average molecular weight of ~508 at a metal: H₂O: PEO molar ratio of 1:16:0.4. The viscous mixture is stirred for one hour at room temperature and then transferred into an autoclave and kept in oven at 100°C for 6 day hydrothermal treatment. The final product was washed by water and dried in air at 80°C.

X-ray diffraction

XRD analyses were performed on a PANalytical X'Pert PRO X-ray diffractometer (radius: 240.0 mm). Incident X-ray radiation was produced from a line focused PW3373/10 Cu X-ray tube, operating at 45 kV and 35 mA, providing K α 1 wavelength of 1.540596Å. The incident beam passed through a 0.04 rad, Soller slit, a ½° divergence slit, a 15 mm fixed mask and a 1° fixed anti scatter slit. After interaction with the sample, the diffracted beam was detected by an X'Celerator RTMS detector. The detector was set in scanning mode, with an active length of 2.022 mm. Samples were analyzed utilizing Bragg-Brentano geometry over a range of 3-75° 2 θ with a step size of 0.02° 2 θ , with each step measured for 200 seconds.

TEM Analysis

A Philips CM 200 transmission electron microscopy (TEM) at 200 kV was used to investigate the morphology of the Ga doped boehmite nanofibres. All samples were dispersed in absolute

ethanol solution and then dropped on copper grids coated with carbon film, dried in an oven at 60 °C for 10 mins for TEM studies.

Energy dispersive X-ray analysis (EDX)

The EDX analysis procedure for Ga doped samples before hydrothermal treatment is as follows: The samples were crushed into tablets and then coated with a thin layer of evaporated carbon to enhance surface conductivity. After this preparation, EDX analysis was carried out in a JEOL 840A analytical scanning electron microscope (SEM) at a 15 kV accelerating voltage using a JEOL 2300 microanalyzer. The EDX analysis for Ga doped samples after hydrothermal treatment was performed via TEM using an Oxford Instruments Link ISIS microanalysis system. At least five analyses at different spots were performed for each sample to obtain an average value.

N₂ adsorption/desorption

Surface area analysis based up N₂ adsorption/desorption techniques were analysed on a Micrometrics Tristar 3000 automated gas adsorption analyser after the sample was pre-treated at 110°C under the flow of N₂ on a Micrometrics Flowprep 060 degasser.

Thermal analysis

Dynamic experiment

Thermal decomposition of the gallium doped boehmite samples was carried out in a Derivatograph PC-type thermoanalytical instrument (Hungarian Optical Works, Budapest, Hungary) capable of recording the thermogravimetric (TG), derivative thermogravimetric (DTG) and differential thermal analysis (DTA) curves simultaneously. The sample was heated in a ceramic crucible in static air atmosphere at a rate of 5° C/min.

Controlled Rate Thermal analysis experiment

Thermal decomposition of the gallium doped boehmite was carried out in a Derivatograph in static air atmosphere (250 cm³/min) at a pre-set, constant decomposition rate of 0.15 mg/min. (Below this threshold value the samples were heated under dynamic conditions at a uniform rate of 1.0 °C/min). The samples were heated in an open ceramic crucible at a rate of 1.0 °C/min⁻¹. With the quasi-isothermal, quasi-isobaric heating program of the instrument the furnace

temperature was regulated precisely to provide a uniform rate of decomposition in the main decomposition stage.

Infrared Emission Spectroscopy

FTIR emission spectroscopy was carried out on a Nicolet Nexus 870 FTIR spectrometer equipped with a TGS detector, which was modified by replacing the IR source with an emission cell. A description of the cell and principles of the emission experiment have been published elsewhere . Approximately 0.2 mg of boehmite was spread as a thin layer (approximately 0.2 microns) on a 6 mm diameter platinum surface and held in an inert atmosphere within a nitrogen-purged cell during heating.

Band component analysis was undertaken using the Jandel 'Peakfit' (Erkrath, Germany) software package which enabled the type of fitting function to be selected and allows specific parameters to be fixed or varied accordingly. Band fitting was done using a Lorentz-Gauss cross-product function with the minimum number of component bands used for the fitting process. The Lorentz-Gauss ratio was maintained at values greater than 0.7 and fitting was undertaken until reproducible results were obtained with squared correlations (r^2) greater than 0.995. Band fitting of the spectra is quite reliable providing there is some band separation or changes in the spectral profile.

Results and Discussion

X-ray diffraction

The X-ray diffraction patterns of the Ga doped samples before and after hydrothermal treatment are shown in Figures 1a and b. Figure 1a shows the XRD patterns of the Ga doped samples before hydrothermal treatment but after ageing. (These are referred to as precipitate samples). The main peaks in patterns for the undoped and 1% Ga doped samples match well the standard reference pattern for boehmite [00-005-0190]. Bayerite phase was also formed in pure boehmite sample whereas no bayerite phase was observed in the 1% sample. As for precipitate samples with Ga content between 2 and 5%, although the overall diffraction patterns are broad indicating small particle size in the resulting sample, boehmite as well as bayerite phases can be clearly seen in the patterns. Nearly no boehmite phase can be observed in the patterns for precipitate samples with 10 and 20% Ga doping. A broad diffraction peak at around $8^\circ 2\theta$ can also be clearly observed for the precipitate samples with Ga varying from 2 to 20%. Those broad peaks are attributed to a poorly diffracting phase. The peak at around $8^\circ 2\theta$ is pseudoboehmite

[22]. It was noted that the peak position for the precipitate samples shifted to a higher degree 2θ with increasing Ga content, ranging from 7.72 to $8.56^\circ 2\theta$. It can be concluded that during precipitation, the formation of boehmite is more favourable at low Ga doping, whereas bayerite and pseudoboehmite phases are more favourable at high Ga doping.

Figure 1b displays the XRD patterns for Ga doped samples after 6 days hydrothermal treatment. Very broad diffraction peaks for 20% Ga doped boehmite treated at 100°C were observed indicating a poorly diffracting phase which is in agreement with TEM results where $\sim 90\%$ of the entire sample is amorphous phase. Except for the pattern of 20% sample treated at 100°C , all the peaks in the other patterns can be assigned to boehmite [00-005-0190] indicating boehmite phase is more stable than bayerite phase under the reaction conditions employed in this work. The crystallite sizes of 1% Ga doped sample with 0, 2, 4, 6 days hydrothermal treatment were calculated by the Debye-Scherrer equation showing a gradual increase from 7.42, 21.74, 20.56 nm to 11.03, 27.75, 38.50 nm along 020, 002, 200 crystallographic directions; Whereas the peak width decreased gradually with the increase in hydrothermal time, indicating a gradual increase in crystallinity of the nanostructures during the soft chemical treatment. Lattice cell parameters a, b and c and crystallite size for Ga doped samples with varying Ga content after 6 days hydrothermal treatment at 100°C were calculated based on the XRD results. There is no obvious relationship between doped Ga% and peak width, and consequential calculated crystal size. It was observed that when Ga content is $\leq 10\%$, lattice parameter a and b remain constant, whereas b varies from 12.23 to 12.71 Å with the change in composition and decreases during hydrothermal treatment. The change in b is related to the hydration of the boehmite basal spacing where large values indicating a high amount of hydration as compared to small values. A gradual increase in crystallite dimension with increasing Ga content along the b (from 6.3 to 20.8 nm) crystallographic direction was also observed indicating Ga doping increases the crystallite size of the resultant materials. Similarly as for the precipitate samples, a broad peak at around $8^\circ 2\theta$ was observed in each sample when Ga content is above 2%. Interestingly, instead of shifting to higher degree 2θ as is observed for the precipitate samples, the peak position for samples after hydrothermal treatment shift to a low degree 2θ with the increase in Ga content, ranging from 8.25 to $8.98^\circ 2\theta$.

Transmission electron microscopy and EDX analysis

The typical TEM images of Ga doped samples are shown in Figure 2. As can be seen in Figure 2a, 2b, 2c, 2d and 2e, at low concentrations up to 5% Ga doping, except for the formation of a small amount of platelike angular crystals in the 1% sample, the only Ga-boehmite morphology is that of nanotubes. The internal and external diameters of Ga doped nanotubes are around 2-5 nm and 3-7 nm, respectively. The average lengths of nanotubes with varying Ga content are

~90 nm ranging from 30-140 nm which are similar to those of pure boehmite nanotubes. The average width of the nanotubes increased slightly with the increase in Ga content while there was minimal difference in the average length.

Above 5%, a mixture of nanotubes, nanoribbons nanosheets and amorphous phases are formed. Nanosheets, which have bevelled ends, are dominant in the 10% sample, and accounted for ~80% of the entire sample. The detailed nanosheets in 10% sample are shown in Figure 2g. It was noted that the length of nanosheets formed in the 10% samples was similar to that of nanotubes, and some of the partially rolled nanosheets were also observed in the 10% sample, which indicates a mechanism of rolling up of the sheets for the formation of nanotubes in this material. Nanoribbons in the 10% sample were up to 220 nm in length, while their width varied from 11 to 16 nm, which is several times larger than the size of the resulting nanotubes. The characteristic morphology of the 20% Ga doped sample is amorphous phase which is accounted for ~90% of the entire sample. The detailed investigation and discussion on the morphology of Ga doped boehmite nanostructures was presented in one of our study [23].

The relationship between added Ga content and observed Ga content for precipitate samples and for samples after 6 days hydrothermal treatment are compared and shown in Figure 3. Similar to the Ga doped boehmite nanostructures which was discussed in our early study [23], a linear relationship between the added and actual Ga content for precipitate samples was also observed indicating the difference in solubility and miscibility between Ga and Al reactants.

Recently, a miscibility gap was observed in an iron doped boehmite study [21]. No miscibility gap was found for Ga doped boehmites. One of the possible reasons could be that Fe and Al are partially miscible whereas Ga and Al are totally miscible. Interestingly, the line slope for precipitate is 1.0461 which is more than one indicating Al ion is more soluble than Ga ion. The line slope for nanostructure indicates that only 60-70% of the added Ga content can substitute for the Al to form Ga-doped boehmite nanotubes for both low and high Ga content.

It was reported nanofibres and nanosheets were formed in high percentage iron doped boehmite samples where nanosheets were dominant [21]. A similar phenomenon is observed in this work. The iron content in nanosheets was nearly 50% higher than that in nanofibres[21]. However, in this work, the average Ga content in nanosheets (5.17%) is lower than that in nanotubes/nanoribbons (6.48%). As for 20% Ga doped sample after hydrothermal treatment, an average Ga content of 16.72% for both large crystal and nanoribbons was observed, which indicates that those large nanoribbons may be built up from large nanoribbons. The average Ga content for the amorphous phase, accounted for ~90% of the entire sample, was 16.95% which is remarkable higher than that for nanotube (13.95%) and also a bit higher than the other

nanostructures including nanoribbons and layered large crystals. It indicated at high Ga content, most of the Ga stayed in the amorphous phase, proving a Ga source to the growth of nanotubes, relatively large nanoribbons and layered larger crystals.

N₂ adsorption/desorption

Nitrogen adsorption/desorption studies, t-plot analysis, and cumulative pore volume and pore size distribution studies were performed to measure the surface areas and porosities of the resulting Ga doped boehmite samples. The effect of hydrothermal duration on the BET specific surface area, pore volume and BET pore diameter were also investigated by studying 1% Ga doped boehmite samples shown in Figure 4, the increase in hydrothermal time from 0 to 6 days resulted in dramatically decline in BET specific surface area and remarkable increase in BET average diameter; whereas the pore volume jumped in the first two days hydrothermal duration from 0.291 to 0.508 cm³·g⁻¹ and then slightly rose to 0.536 cm³·g⁻¹ in the following two days and dropped to 0.499 cm³·g⁻¹ during the last two days. The results shown in Figure 4a and 4b indicated that the fast growth of Ga doped boehmite nanotubes mainly occurred in the first two days and the growth rate slowed down afterwards. The decrease in pore volume during the last two days may be due to the formation of secondary particles which was also denoted as agglomerates in a peer study [24].

As for samples after 6 days hydrothermal treatment, Ga doped samples have remarkable larger BET specific surface area but much smaller BET average pore diameter (except for 1% Ga doped sample) when compared to pure boehmite sample. Pore volume of Ga doped samples at low Ga content ($\leq 5\%$) ranged from 0.405 to 0.511 cm³·g⁻¹ which is close to that of pure boehmite sample; Ga doped samples at high Ga content ($\geq 10\%$) exhibited very low pore volume, such as 0.102 cm³·g⁻¹ for 20% Ga doped sample. It was noted that there was little difference in pore volume when doped Ga% is within 3% and there was an obvious gradual decline in pore volume when doped Ga% increase from 3 to 20%. A gradual increase in BET specific surface area when doped Ga% $\leq 3\%$ and a gradual decrease in BET specific surface area when doped Ga% $\geq 3\%$ were also observed.

N₂ adsorption/desorption isotherms can provide useful information on the mesoporous and microporous property change of the resultant samples. It was reported that adsorption strongly depends on the porosity of solids [24]. The detailed discussion on N₂ adsorption-desorption isotherms for 1% Ga doped sample with 2, 4, 6 days hydrothermal treatment and samples with varying doped Ga% after 6 days hydrothermal treatment were reported in our early study. A gradual change in the shape of N₂ adsorption-desorption curves for 1% Ga doped samples was observed. the N₂ adsorption-desorption curves for 1% Ga doped sample without hydrothermal

treatment (Referred as precipitate sample) is very much different from the other three 1% Ga doped samples with 2, 4 and 6 days hydrothermal treatment, which indicated a significant changes in the texture of the resulting nanostructures (Figure 5). The 1% Ga doped precipitate sample has an adsorption capacity of $\sim 200 \text{ cm}^3 \cdot \text{g}^{-1} \text{ STP}$, whereas the other three 1% Ga doped samples regardless the duration of hydrothermal treatment have a similar adsorption capacity of $\sim 350 \text{ cm}^3 \cdot \text{g}^{-1} \text{ STP}$, indicating a larger volume of mesopores were formed in the hydrothermally treated samples. Capillary condensation predominated in Ga doped samples with Ga percentage no more than 10% indicating the presence of well formed cylindrical pores is characteristic of the nanotubes in these samples and also these samples displayed a similar moderate hysteresis effects. No hysteresis effects were observed for 20% Ga doped boehmite sample.

Based on the new classification of hysteresis loops recommended in IUPAC manual, the isotherms for 1, 2, 3, 4, 5, 10% Ga doped samples after hydrothermal treatment exhibited type H3 hysteresis loops that reflected the presence of micropores and mesopores [24]. It was reported that the type H3 loop is often associated with slit-like pores as a result of the aggregates of plate-like particles [25], which was in agreement with TEM results that nanotube clusters were observed throughout the entire samples. Whereas the isotherms for 1% Ga doped precipitate sample exhibited a mixture shape of type H2 and H4, in particular, more close to type H2 loop. Type H2 loop occurs in some corpuscular systems such as certain silica gels and type H4 normally can be obtain with adsorbents having slit-shape pores or plate-like particles [24]. Therefore, it would be reasonable to assume that the 1% Ga doped precipitate sample process the morphology of tiny particles and plate-like particles where those tiny particles dominate in the entire sample, which is consistent with TEM results that amorphous phase dominated except for a tiny amount of nanotubes were also formed in the precipitate sample. Samples with 20% Ga content can be assigned to type H4 associated with type I indicating 1) slit-shape pores or plate-like particles; 2) low mesoporosity; 3) posses microporosity.

t-plot analysis were undertaken to provide more information on the mesoporous and microporous property of the resultant Ga doped samples. Figure 6a shows the *t*-plots of 1% Ga doped samples with and without hydrothermal treatment. Figure 6b shows the *t*-plots of samples with varying Ga content after 6 days hydrothermal treatment. *t*-plot analysis reveals much more information regarding the pore structure. For microporous materials, the *t*-plot is characteristic with two linear regions, the first region being associated with micropore filling and monolayer coverage, whereas the second region represents layer-by-layer adsorption in the mesopores [26]. The linearity portion of *t*-plot indicates the micropores property while the remaining portion at higher thickness region corresponds to slit shaped pores between the layers of boehmite [27]. As shown in Figure 6a, 1% Ga doped precipitate sample exhibited excellent microporosity but remarkable low mesoporosity. A gradual decrease in microporosity and increase in mesoporosity

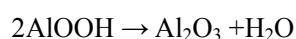
with the increase in hydrothermal treatment duration for 1% Ga doped samples can be clearly observed. As shown in Figure 6b, pure boehmite and 1% Ga doped boehmite sample exhibit remarkable larger mesoporous than 2, 3, 4, 5, 10 and 20% Ga doped samples, in particular, 20% Ga doped samples have a very low mesoporosity.

The effect of hydrothermal treatment duration, dopant and the percentage of Ga on the pore size distribution of resultant samples were investigated and shown in Figure 7. As can be seen in Figure 7a, the pore size for 1% Ga doped precipitate sample concentrated in the range of 1.4~2.0 nm in radius with a sharp peak at around 1.8 nm showing a pore volume of $0.68 \text{ cm}^3 \cdot \text{g}^{-1} \text{STP}$. After two days hydrothermal shown in Figure 7b, the pore size distribution changed dramatically where the volume of micropores dropped significantly and a large amount of mesopores were formed. There were two sharp peaks in the pore size distribution curves for all the 1% Ga doped samples with different hydrothermal treatment duration, indicating a considerable number of micropores with radius of $\sim 1.8 \text{ nm}$ and mesopores with radius of $3\sim 8$ were presented in those samples. As shown in Figure 7b, 7c and 7d, the sharp peak at around 1.8 nm in the microporous region decrease gradually from ~ 0.075 to 0.043 and $0.027 \text{ cm}^3 \cdot \text{g}^{-1} \text{STP}$ after 2, 4, 6 days hydrothermal treatment; whereas the centre of the other sharp peak in the mesoporous region shift from ~ 0.53 to 0.67 nm with the maximum pore volume changing from ~ 0.095 to $0.845 \text{ cm}^3 \cdot \text{g}^{-1} \text{STP}$ when compared sample with 2 days hydrothermal treatment and sample with 6 day hydrothermal treatment. The pore size distribution results for 1% Ga doped sample with different hydrothermal treatment duration are in consistent with that of *t*-plot analysis that micropores decreased and mesopores increased with the elongation of hydrothermal treatment duration. A sharp peak at $\sim 1.6 \text{ nm}$ and a broad peak in the range of $3.5 \sim 6.5 \text{ nm}$ were also observed in pure boehmite sample after 6 days hydrothermal treatment. Interestingly, when doped Ga percentage was in the range of 2~10 %, A sharp peak at $\sim 1.8 \text{ nm}$ with a large pore volume of $0.24\sim 0.50 \text{ cm}^3 \cdot \text{g}^{-1} \text{STP}$ was observed in each samples but no obvious peaks presented in the mesoporous region indicating micropores with radius of $\sim 1.8 \text{ nm}$ were dominant which is in agreement with *t*-plot results. Figure 7e shows the pore size distribution of 10% Ga doped sample after 6 days hydrothermal treatment and all the other Ga doped sample with Ga percentage ranging from 2 to 5% have a similar shape as 10% Ga doped sample. The remarkable difference in pore size distribution between samples with Ga percentage of 0, 1% and 2, 3, 4, 5, 10% may be one of the main reasons for the difference in the shape of N_2 adsorption-desorption isotherms. 20% Ga doped sample after 6 days hydrothermal treatment was also presented in Figure 7f showing an extremely small volume of microporosity and mesoporosity for this sample which is in consistent with N_2 adsorption/desorption analysis results.

Thermal analysis

The dynamic thermal analysis of Ga doped boehmite is displayed in Figure 8a to 8e. The results of the dynamic experiment are reported in Table 1. Samples with added yttrium percentage of 1, 3, 5, 10 and 20% were selected for further investigation by dynamic and controlled thermogravimetric techniques. The dynamic thermal analyses of the 1, 3, 5, 10 and 20% gallium doped boehmites are shown in Figures 8a, 8b, 8c 8d and 8e.

The dynamic thermal analysis of pure boehmite nanomaterials prepared via the same synthesis route was reported in an early study [28]. It was found that undoped boehmite show four decomposition steps. The characteristic step of boehmite is the broad DTG step at ~397 °C with a mass loss of 15.10 %. The theoretical mass loss based upon the equation:



is 11.5 % [29] . In a previous piece of research infrared emission spectroscopy was used to study the dehydroxylation of natural and synthetic boehmite[30]. It was found that dehydroxylation starts at 250 °C and is complete by 450 °C. The dehydroxylation is followed by the loss of intensity of the hydroxyl stretching frequencies observed at 3478, 3319 and 3129 cm^{-1} and by the loss of intensity of the hydroxyl deformation modes at 1140 and 1057 cm^{-1} . A previous study made simulations of the thermal decomposition of boehmite [31]. It was found that the simulations of the non-isothermal experiments. at constant heating rates show that thermally stimulated transformation of nanocrystalline boehmite into alumina can be accurately modelled by a 4-reaction mechanism involving: (I) the loss of physisorbed water, (II) the loss of chemisorbed water, (III) the conversion of boehmite into transition alumina, (IV) the dehydration of transition alumina (loss of residual hydroxyl groups [31]. Another study of boehmite precipitates by the authors found that thermal analysis showed five endotherms at 70, 140, 238, 351 and 445°C and these endotherms are attributed to the dehydration and dehydroxylation of the hydrolyzate [32].

As shown in Figure 8a, the 1% Ga doped boehmite DTG curve displays four maxima in the DTG curves at 97, 277, 380 and 448°C (sharp). The mass losses are 3.4, 7.2, 4.2 and 11.1% over the temperature ranges 28-173, 173-334, 334-339 and 399-556, respectively. There are two endothermic peaks observed at 97, 448°C and an exothermic peak at 277°C. These DTG peaks are assigned to a) dehydration (b) combustion of the surfactant directing agent (c) dehydroxylation of boehmite and (d) further dehydroxylation.

The 3% Ga doped boehmite DTG curve shows at least three mass loss steps at 105, 210 and 432°C. The DTA curve displays two endotherms at 110 and 435°C and an exotherm at 210°C. The mass losses are 10.2, 4.8, 14.7 and 1.3% over the range of 30-181, 181-269, 269-542 and 542-895°C. The attribution of the DTG peaks is as above. The 5% Ga doped boehmite shows four DTG peaks at 107, 217, 293 and 438°C. The DTA curves of 5% Ga doped boehmite displays

two endotherms at 107 and 438°C and an exotherm at 217°C. It appears that at low gallium content as the gallium doping increases the DTG peak at around 435°C becomes significantly broader and the dehydroxylation temperature of boehmite decreases.

The 10% Ga doped boehmite DTG curve display three mass loss steps at 128, 227 and 438°C. The mass loses are 10.4, 13.6 and 7.1% over the range of 27-192, 192-368 and 368-537°C. Two endotherms and one exotherm are also observed at around 128, 445 and 235°C, respectively. The 20% Ga doped boehmite shows at least two DTG peaks at 143 and 234°C. The DTG peak at round 416°C are almost too broad to be observed. The DTA curves of 20% Ga doped boehmite displays two endothermic peaks and one exothermic peak at around 140, 365 and 242°C.

Compared with undoped boehmite nanomaterials, gallium doped boehmite nanomaterials have higher the dehydration temperatures of absorbed water and boehmite. In particular, the first mass loss occurred at a gradually increased temperature from 83 to 143°C with the increase in Ga doping from 0 to 20% indicating gallium has stronger interaction with the adsorbed water. The characteristic thermal decomposition step of Ga doped boehmites varies from 416 to 448°C. It appears that at low Ga doping ($Ga \leq 5\%$) where nanotubes are dominant, there is a linear relationship between the FWHM along 020 direction and the characteristic decomposition temperatures ($y = -1046.1x + 473.37$, $R^2=0.95$). Since FWHM reflects the crystallinity of the resultant Ga doped boehmite, it can be proposed that the better crystallinity of the doped boehmite nanotubes, the higher thermal dehydration temperature.

The controlled rate thermal analysis experiment

The controlled thermal analyses (CRTA) of the 1, 3, 5, 10 and 20% gallium doped boehmites are shown in Figures 9a, 9b, 9c 9d and 9e. The results of the calculations are reported in Table 2. It was reported that the controlled thermal analysis of pure boehmite prepared at 100°C showed three main decomposition steps: the first step is isothermal at ~70 °C and is assigned to adsorbed water accounted for a 8.4% mass loss; the second step at 180 °C is non-isothermal accounted for 1.4% mass loss; the third step is also isothermal accounted for 16.1% and occurred at ~400 °C [].

The controlled rate thermal analysis (CRTA) of the 1% Ga doped boehmite (Fig. 9a) shows a number of thermal analysis features. A quasi-isothermal step is observed at 57°C, and two dehydroxylation steps are observed over the temperature range 200 to 700 °C. The CRTA of the 3% Ga doped boehmite shows a different pattern (Fig. 9b). The quasi-isothermal step assigned to dehydration of the 3 % Ga doped boehmite is observed at 63 °C and dehydroxylation occurs over an extended period of time over the temperature range 144 to 377 °C. The CRTA of the 5% Ga doped boehmite shows a quasi-isothermal dehydration step at about 66 °C. The

dehydration and dehydroxylation steps can no longer be separated in the CRTA experiment. This continuous mass loss becomes even clearer in the 10% Ga doped boehmite (Fig. 9d) and is also observed for the 20 % Ga doped boehmite. .

Infrared emission spectroscopy

Natural boehmites studied show hydroxyl stretching bands at 3413, 3283, 3096 and 2977 cm^{-1} . Some variation in the band positions is observed and attributed to variations in the boehmite structure. This structure consists of parallel sheets of octahedra with aluminium ions at the centers of the octahedra. These octahedra are joined through hydrogen bonds between the hydroxyls of one sheet and the oxygens of the adjacent parallel sheet. The octahedra are joined in continuous chains. . It is proposed that some variation in the parallel sheets as with kaolinite structures results in the variation of the frequencies of the component bands. The higher frequency band at 3413 cm^{-1} is attributed to the non-hydrogen bonded hydroxyl groups that occur on the edge of the sheets. The band is quite broad with bandwidths of $\sim 250 \text{ cm}^{-1}$. The two bands at 3283 and 3096 cm^{-1} may be attributed to the stretching hydroxyl stretching frequencies of the hydroxyl groups within the structure.

The infrared emission spectra of the 5, 10 and 20% Ga doped boehmite in the 650 to 4000 cm^{-1} region are shown in Figures 10a, 10b and 10c. These figures show the change in intensity of the infrared bands as a function of temperature. The figures clearly show the changes in the molecular structure as determined by the infrared emission spectra as the boehmite is thermally treated. Dehydroxylation may be observed by the decrease in intensity of the hydroxyl-stretching region and also by the decrease in intensity of the hydroxyl deformation modes in the 1000 to 1100 cm^{-1} region. It should be noted that the spectra at 200 °C are noisy. This is due to the low thermal energy at this temperature. Three bands in the IE spectra of the 5% Ga doped boehmite at 100 °C (Fig. 10a) are observed in the OH stretching region at 3118, 3330 and 3670 cm^{-1} . There is a very strong shift to higher wavenumbers upon thermal treatment. The bands are observed at 3200, 3390 and 3680 cm^{-1} at 300 °C. The intensity of these bands decreases with temperature increase. It is apparent that the intensity of the high wavenumber band remains even at 700 °C. The IE spectra of the 10% Ga doped boehmite (Fig. 10b) are similar to that of the 5 % Ga doped boehmite. The IE spectra of the 20% Ga doped boehmite are different in that the differentiation of the OH stretching bands is lost. The characteristic OH deformation modes are also not observed for this nanostructure.

Infrared absorption spectra of boehmite show bands at 1080 and 1160 cm^{-1} . The infrared emission spectra of synthetic at 200 °C show two bands centered at 1140 and 1057 cm^{-1} for the synthetic boehmite and at 1155 and 1064 cm^{-1} for the natural boehmite. In the IES spectra at

200 °C, two bands are observed at 1070 and 1150 cm^{-1} . This later band is weak in the IR spectra. These bands show a shift to lower wavenumbers with increased temperature and the intensity of these bands is lost by 400 °C.

Prominent bands in the low wavenumber region of Gallium doped boehmite are observed at 740 and 835 cm^{-1} for boehmite. These bands are attributed to hydroxyl deformation modes of the boehmite lattice. The bands at 1320 and 1500 cm^{-1} are attributed to surfactant impurities. These bands are lost by ~600 °C.

Conclusions

The formation of boehmite nanofibres and nanotubes are favourable under low hydrothermal temperature with minor percentage ($\leq 5\%$) of doped gallium in the presence of surfactant PEO. Similar to iron and yttrium doped boehmites, high doped gallium percentage resulted in the formation of large fraction of nanosheets and amorphous phase. Hydrothermal treatment converted the initially formed bayerite phase during precipitation reaction to boehmite phase. A linear relationship between added and actual gallium substituted in boehmite was observed, however, no miscibility gap appears at high gallium doped percentage which is different from that of iron and yttrium doped boehmite nanostructures.

After hydrothermal treatment, a large amount of micropores and mesopores presented in the resultant gallium doped boehmite samples. Compared to pure boehmite nanostructure, gallium doped boehmite nanostructure have remarkable larger BET specific area but much smaller BET average pore diameter. The dramatically decline in BET specific surface area and remarkable increase in pore volume after two days hydrothermal treatment demonstrate that the fast growth of Ga doped boehmite nanotubes mainly occurred in the first two days hydrothermal duration. There is little effect of dopant gallium on the pore volume and BET specific area at low doped gallium percentage ($\leq 3\%$). The pore volume and BET specific surface area gradually decreased with the increase in doped gallium percentage from 3 to 20%.

Similar as iron and yttrium doped boehmites, gallium doped boehmite nanomaterials have higher the dehydration temperature of absorbed water and boehmite. Interestingly, gallium doped boehmite nanotubes with better crystallinity tend to dehydration at higher temperatures.

Dehydroxylation of samples of Ga doped boehmite has also been studied by infrared emission spectroscopy. Dehydroxylation of boehmite is followed by the decrease in intensity of the hydroxyl stretching and hydroxyl deformation modes. Hydroxyl stretching frequencies are observed at 3478, 3319 and 3129 cm^{-1} . The hydroxyl deformation modes are observed at 1140

and 1057 cm^{-1} . Dehydroxylation starts at $250\text{ }^{\circ}\text{C}$ and is complete by $450\text{ }^{\circ}\text{C}$. No difference was found between the synthetic and natural boehmite dehydroxylation. The hydroxyl stretching modes all show a strong blue shift and the hydroxyl deformation modes all show a pronounced red shift. The hydroxyl translation modes show a blue shift to higher frequencies.

Acknowledgments

The financial and infra-structure support of the Queensland University of Technology Inorganic Materials Research Program of the School of Physical and Chemical Sciences is gratefully acknowledged. The Australian Research Council (ARC) is thanked for funding the Thermal Analysis facility through a LIEF grant. One of the authors (YZ) is thankful for a Queensland University of Technology international doctoral scholarship (QIDS). Professor Janos Kristof and Dr. Thor Bostrom are thanked for collecting the CRTA data and taking the TEM images.

References

- [1] J. H. Fendler and F. C. Meldrum, *Adv. Mater. (Weinheim, Germany)* 7 (1995) 607-632
- [2] B. B. Lakshmi, C. J. Patrissi and C. R. Martin, *Chem. Mater.* 9 (1997) 2544-2550
- [3] Y. Sun and Y. Xia, *Nature* 298 (2002) 2176-2179
- [4] M. S. Gudiksen, L. J. Lauhon, J. Wang, D. C. Smith and C. M. Lieber, *Nature* 415 (2002) 617-620
- [5] J.L. Le Loarer, H. Nussbaum and D. Bortzmeyer Alumina extrudates, methods for preparing and use as catalysts or catalyst supports, 98-FR1186 9856499
- [6] V. S. Burkat, V. S. Dudorova, V. S. Smola and T. S. Chagina, *Light Met. (Warrendale, PA, United States)* (1985) 1443-1448
- [7] C. Nedez, J.-P. Boitiaux, C. J. Cameron and B. Didillon, *Langmuir* 12 (1996) 3927-3931
- [8] Y. Chen, L. Jin and Y. Xie, *J. Sol-Gel Sci. Technol.* 13 (1998) 735-738
- [9] D. S. Xue, Y. L. Huang, Y. Ma, P. H. Zhou, Z. P. Niu, F. S. Li, R. Job and W. R. Fahrner, *J. Mater. Sci. Lett.* 22 (2003) 1817-1820
- [10] A. P. Philipse, A.-M. Nechifor and C. Patmamanoharan, *Langmuir* 10 (1994) 4451-4458
- [11] K. Okada, A. Tanaka, S. Hayashi, K. Daimon and N. Otsuka, *J. Mater. Res.* 9 (1994) 1709-1713
- [12] S. Ananthakumar, V. Raja and K. G. K. Warriar, *Mater. Lett.* 43 (2000) 174-179
- [13] M. P. B. Van Bruggen, *Langmuir* 14 (1998) 2245-2255
- [14] D. Kuang, Y. Fang, H. Liu, C. Frommen and D. Fenske, *J. Mater. Chem.* 13 (2003) 660-662
- [15] H. Y. Zhu, Gao. X. P., D. Y. Song, Y. Q. Bai, S. P. Ringer, Z. Gao, Y. X. Xi, W. Martens, J. D. Riches and R. L. Frost., *J. Phys. Chem. B* 108 (2004) 4245-4247
- [16] H. Y. Zhu, J. D. Riches and J. C. Barry., *Chem. Mater.* 14 (2002) 2086-2093
- [17] J. Jansons, P. Kulis, Z. A. Rachko, M. Springis, I. Tale and J. Valbis, *Phys. Status Solidi B: Basic Research* 120 (1983) 511-518
- [18] K. I. Shimizu, A. Satsuma and T. Hattori, *Appl. Catal., B: Environmental* 16 (1998) 319-326
- [19] T. Minami, *Mater. Res. Bull.* 25 (2000) 38
- [20] E. Fernandez, P. Sanchez, M. Panizza, V. Sanchez, J. M. Gallardo-Amores, G. Busca, E. Tejedor and C. Resini, *Boletin de la Sociedad Espanola de Ceramica y Vidrio* 43 (2004) 132-134
- [21] Y. Zhao, W. N. Martens, T. E. Bostrom, H. Y. Zhu and R. L. Frost, *Langmuir* 23 (2007) 2110-2116
- [22] W. N. Martens, J. T. Klopogge, R. L. Frost and J. R. Bartlett, *J. Colloid Interface Sci.* 247 (2002) 132-137
- [23] Y. Zhao, R. L. Frost and W. N. Martens, *J. Phys. Chem. C* 111 (2007) 5313-5324
- [24] S. J. Gregg and K. S. W. Sing Adsorption, surface area and porosity, Academic Press, 1982
- [25] K. S. W. Sing, D. H. Everett, R. A. W. Haul, L. Moscou, R. A. Pierotti, J. Rouquerol and T. Siemieniowska, *Pure Appl.Chem* 57 (1985) 603-619
- [26] B. Be Whitte, K. Vercruyse, K. Aernouts, P. Verwimp and J.B. Utterhoeven, *J. Porous Mater.* 2 (1996) 307
- [27] A. C. Pierce, *Introduction to Sol-Gel Processing*, Kluwer Academic Publishers, 1998
- [28] Y. Zhao, R. L. Frost, V. Vágvölgyi, E. R. Waclawik, J. Kristóf and E. Horváth, *J. Therm. Anal. Cal.* 94 (2008) 219-226
- [29] Y. Zhao, R. L. Frost, W. N. Martens and H. Y. Zhu, *J. Therm. Anal. Cal.* 90 (2007) 755-760
- [30] R. L. Frost, J. T. Klopogge, S. C. Russell and J. Szetu, *Appl Spectrosc* 53 (1999)
- [31] P. Alphonse and M. Courty, *Thermochim. Acta* 425 (2005) 75-89
- [32] W. N. Martens, R. L. Frost, J. R. Bartlett and J. T. Klopogge, *Thermochim. Acta* 374 (2001) 31-43

1 **Table 1 Decomposition stages under dynamic conditions for gallium doped boehmite nanostructures**

2

Sample: Boehmite 1% Ga doped			Sample: Boehmite 3% Ga doped			Sample: Boehmite 5% Ga doped			Sample: Boehmite 10% Ga doped			Sample: Boehmite 20% Ga doped		
Temperature range (°C)	Mass loss (Sample mass: 195.89 mg)		Temperature range (°C)	Mass loss (Sample mass: 124.11 mg)		Temperature range (°C)	Mass loss (Sample mass: 127.55 mg)		Temperature range (°C)	Mass loss (Sample mass: 195.13 mg)		Temperature range (°C)	Mass loss (Sample mass: 183.77 mg)	
	mg	%		mg	%		mg	%		mg	%		mg	%
28-173	6.6	3.4	30-81	12.7	10.2	29-179	12.5	9.8	27-192	20.3	10.4	27-196	26.0	14.1
173-334	14.1	7.2	18-269	6.0	4.8	179-274	9.3	7.3	192-368	26.6	13.6	196-288	18.8	10.2
334-399	8.2	4.2	269-542	18.3	14.7	274-344	5.6	4.4				288-420	26.7	7.6
399-556	21.7	11.1				344-519	11.7	9.2	368-537	13.9	7.1	420-547	4.2	2.3
556-921	2.5	1.3	542-895	1.6	1.3	519-800	1.7	1.3	537-873	2.2	1.1	547-864	1.9	1.0

3

4

1
2
3

Table 2 Decomposition stages under CRTA conditions for gallium doped boehmite nanostructures.

Sample: Boehmite 1% Ga doped			Sample: Boehmite 3% Ga doped			Sample: Boehmite 5% Ga doped			Sample: Boehmite 10% Ga doped			Sample: Boehmite 20% Ga doped		
Temperature range (°C)	Mass loss (Sample mass: 274.23 mg)		Temperature range (°C)	Mass loss (Sample mass: 186.54 mg)		Temperature range (°C)	Mass loss (Sample mass: 194.69 mg)		Temperature range (°C)	Mass loss (Sample mass: 228.70 mg)		Temperature range (°C)	Mass loss (Sample mass: 215.65 mg)	
	mg	%		mg	%		mg	%		mg	%		mg	%
21-147	9.1	3.3	21-144	17.0	9.1	22-130	15.9	8.2	21-135	19.2	8.4	20-149	28.2	13.1
147-244	15.8	5.8	144-593	39.5	21.2	130-307	24.5	12.6	135-305	31.3	13.7	149-361	37.8	17.5
244-334	15.6	5.7				307-482	19.0	9.8	305-564	21.8	9.5			
334-525	31.2	11.4				482-670	2.3	1.2						

4

List of Figures

Figure 1a X-ray diffraction patterns of Ga doped samples at 1, 2, 3, 4, 5, 10 and 20% loadings collected after 2 hours ageing but before hydrothermal treatment.

Figure 1b X-ray diffraction patterns of Ga doped boehmite nanostructures at 1, 2, 3, 4, 5, 10 and 20% loadings.

Figure 2 TEM images showing the morphology of Ga doped boehmite samples after 6 days hydrothermal treatment at 100 °C with varying Ga content. a) 1%; b) 2%; c) 3%; d) 4%; e) 5%; f) and g) 10%; h) 20%.

Figure 3 EDX analyses of Ga doped boehmite before and after hydrothermal treatment

Figure 4a BET-Specific Surface Area (S_{BET}) and BET Mean Pore Diameter as a function of hydrothermal treatment duration for 1% Ga doped boehmite samples.

Figure 4b BET Pore volume as a function of hydrothermal treatment duration for 1% Ga doped boehmite samples.

Figure 5 N_2 adsorption/desorption isotherms for the 1% Ga doped samples with 0, 2, 4, 6 days of hydrothermal treatment at 100°C.

Figure 6a t -plot of 1% Ga doped boehmite samples with different hydrothermal treatment duration.

Figure 6b t -plot of Ga doped boehmite samples with varying Ga percentage after 6 days hydrothermal treatment.

Figure 7 Pore size distributions for a) 1% Ga doped precipitate sample after ageing but before hydrothermal treatment; b) 1% Ga doped sample after 2 days hydrothermal treatment; c) 1% Ga doped sample after 4 days hydrothermal treatment; d) 1% Ga doped sample after 6 days hydrothermal treatment; e) 10% Ga doped boehmite sample after 6 days hydrothermal treatment; f) 20% Ga doped boehmite sample after 6 days hydrothermal treatment.

Figure 8 Dynamic thermal analysis of a) 1%; b) 3%; c) 5%; d) 10% and e) 20% Ga doped boehmite nanostructures

Figure 9 Controlled rate thermal analysis of a) 1%; b) 3%; c) 5%; d) 10% and e) 20% Ga doped boehmite nanostructures

Figure 10 Infrared emission spectra of a) 5%; b) 10% and c) 20% Ga doped boehmite in the 650 to 3900 cm^{-1} region

List of Tables

Table 1 Decomposition stages under dynamic conditions for gallium doped boehmite nanostructures

Table 2 Decomposition stages under CRTA conditions for gallium doped boehmite nanostructures

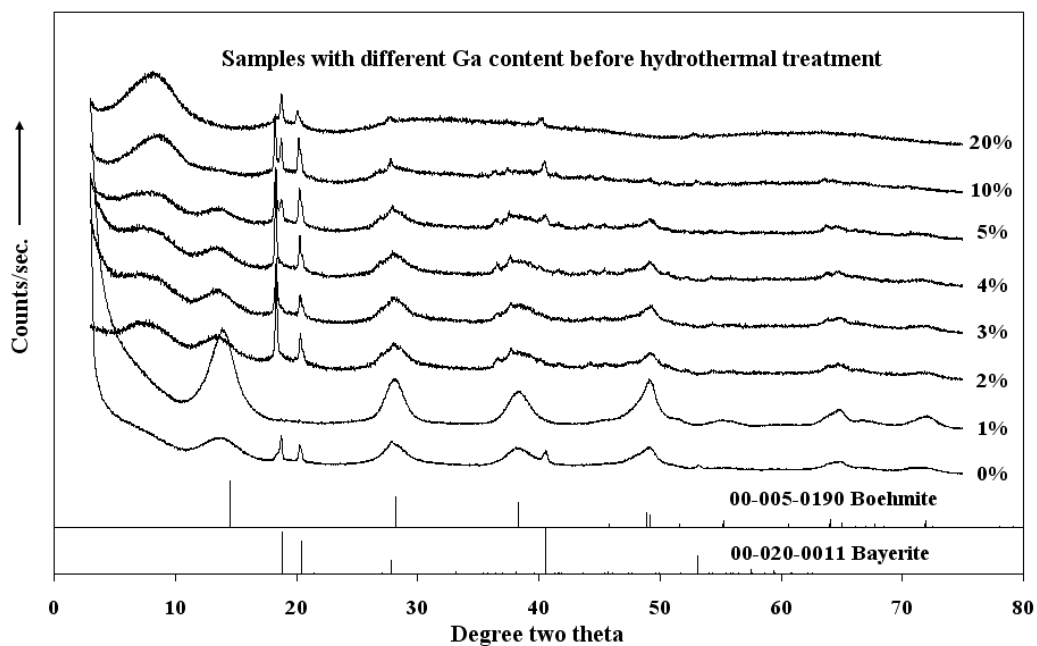


Figure 1a X-ray diffraction patterns of Ga doped samples at 1, 2, 3, 4, 5, 10 and 20% loadings collected after 2 hours ageing but before hydrothermal treatment.

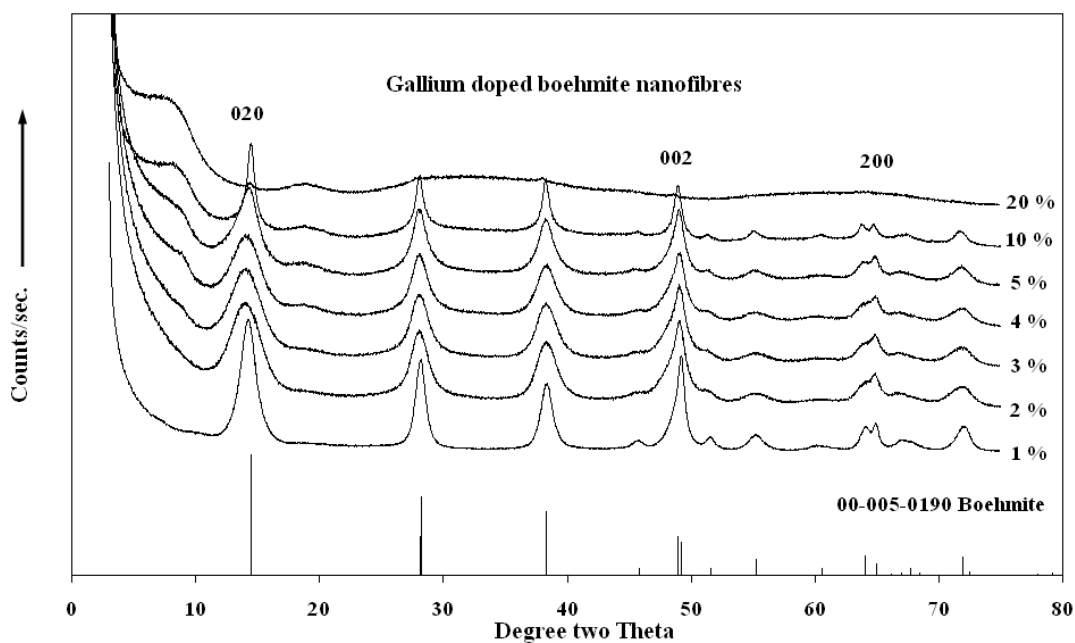


Figure 1b X-ray diffraction patterns of Ga doped boehmite nanostructures at 1, 2, 3, 4, 5, 10 and 20% loadings.

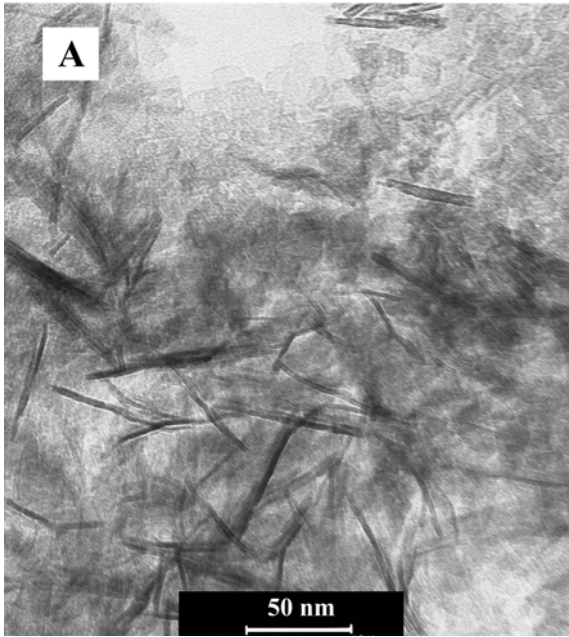


Figure 2a 1% Ga doped

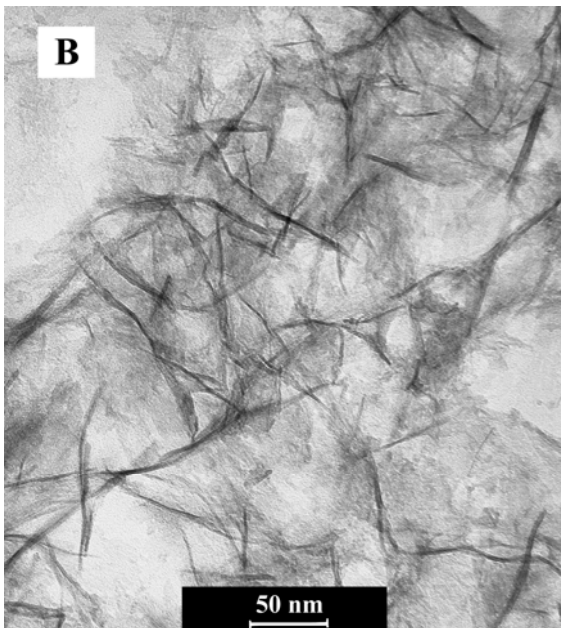


Figure 2b 2% Ga doped

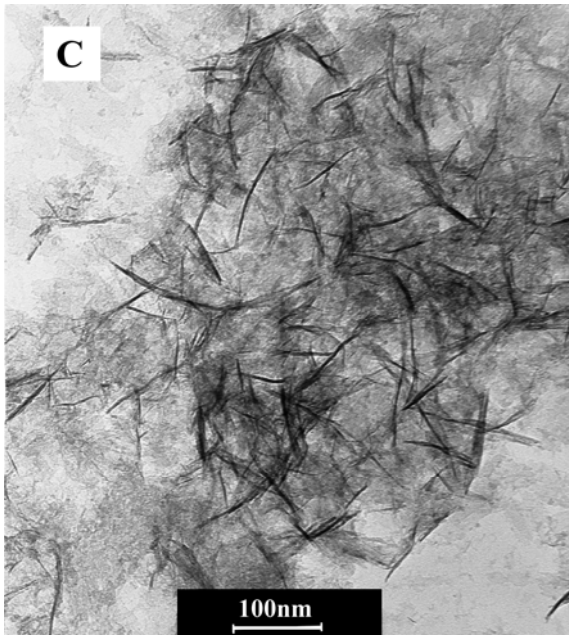


Figure 2c 3% Ga doped

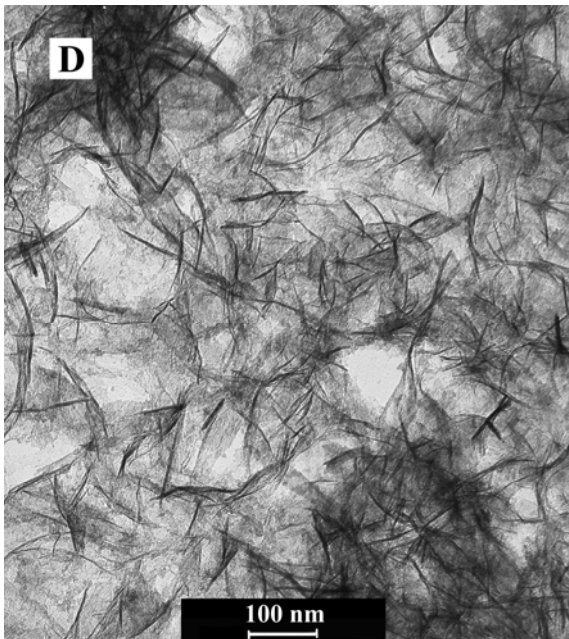


Figure 2d 4% Ga doped

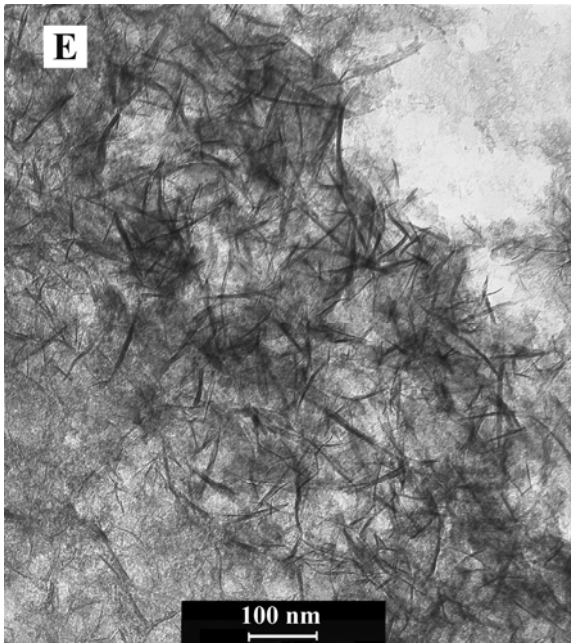


Figure 2e **5% Ga doped**

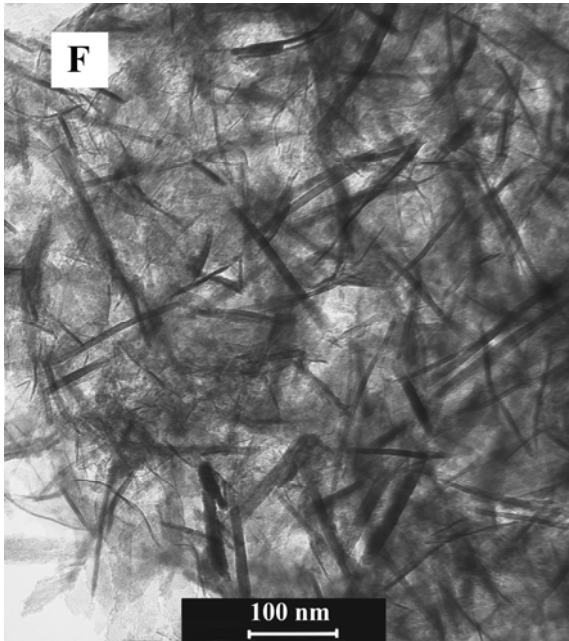


Figure 2f 10% Ga doped

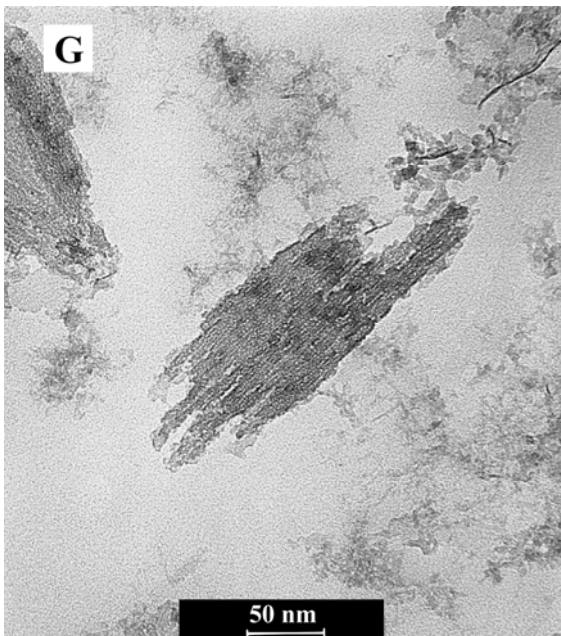


Figure 2g 10% Ga doped

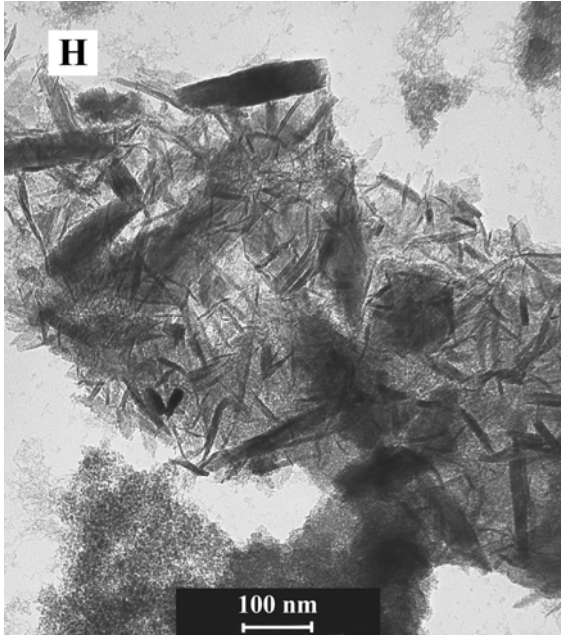


Figure 2h 20% Ga doped

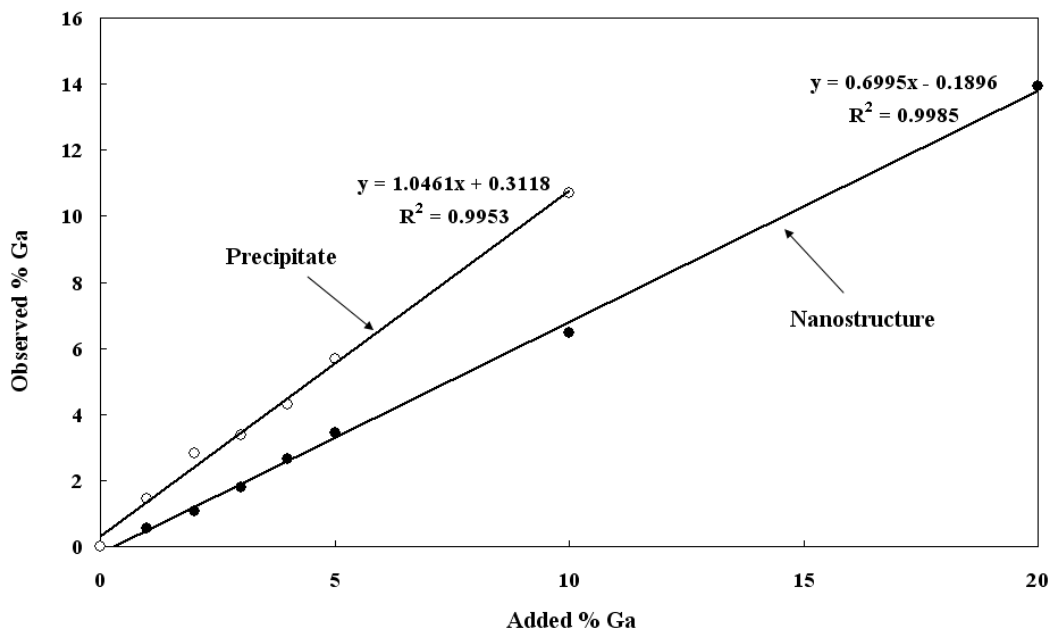


Figure 3 EDX analyses of Ga doped boehmite before and after hydrothermal treatment

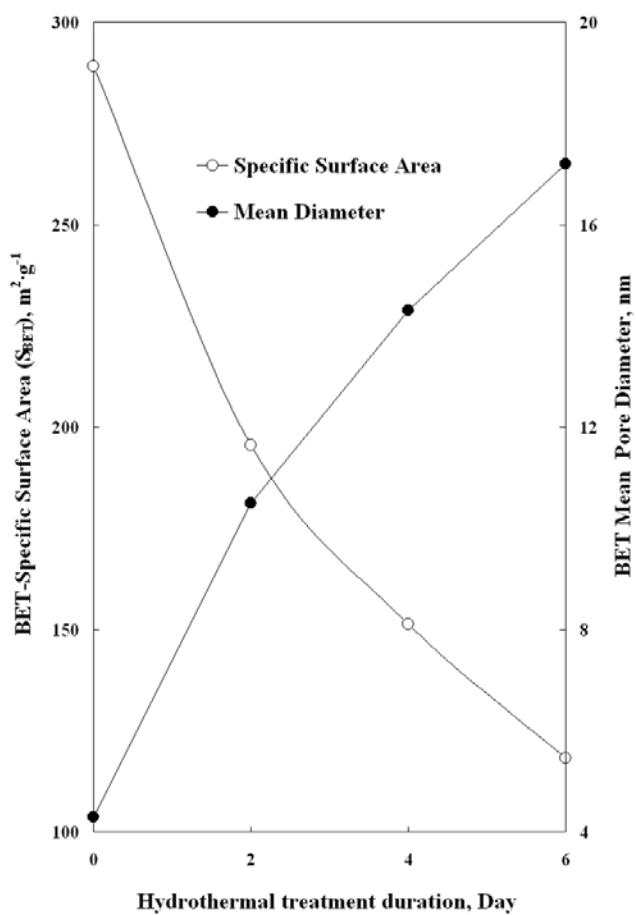


Figure 4a BET-specific surface area (S_{BET}) and BET mean pore diameter as a function of hydrothermal treatment duration for 1% Ga doped boehmite samples.

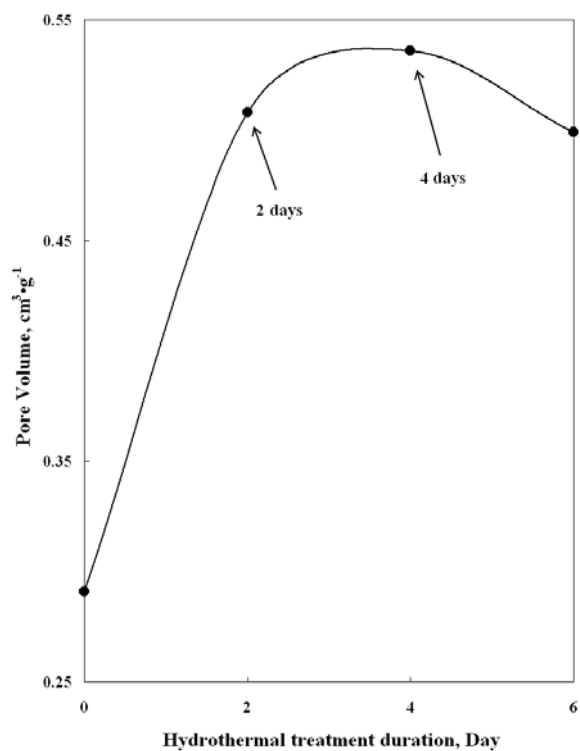


Figure 4b BET pore volume as a function of hydrothermal treatment duration for 1% Ga doped boehmite samples.

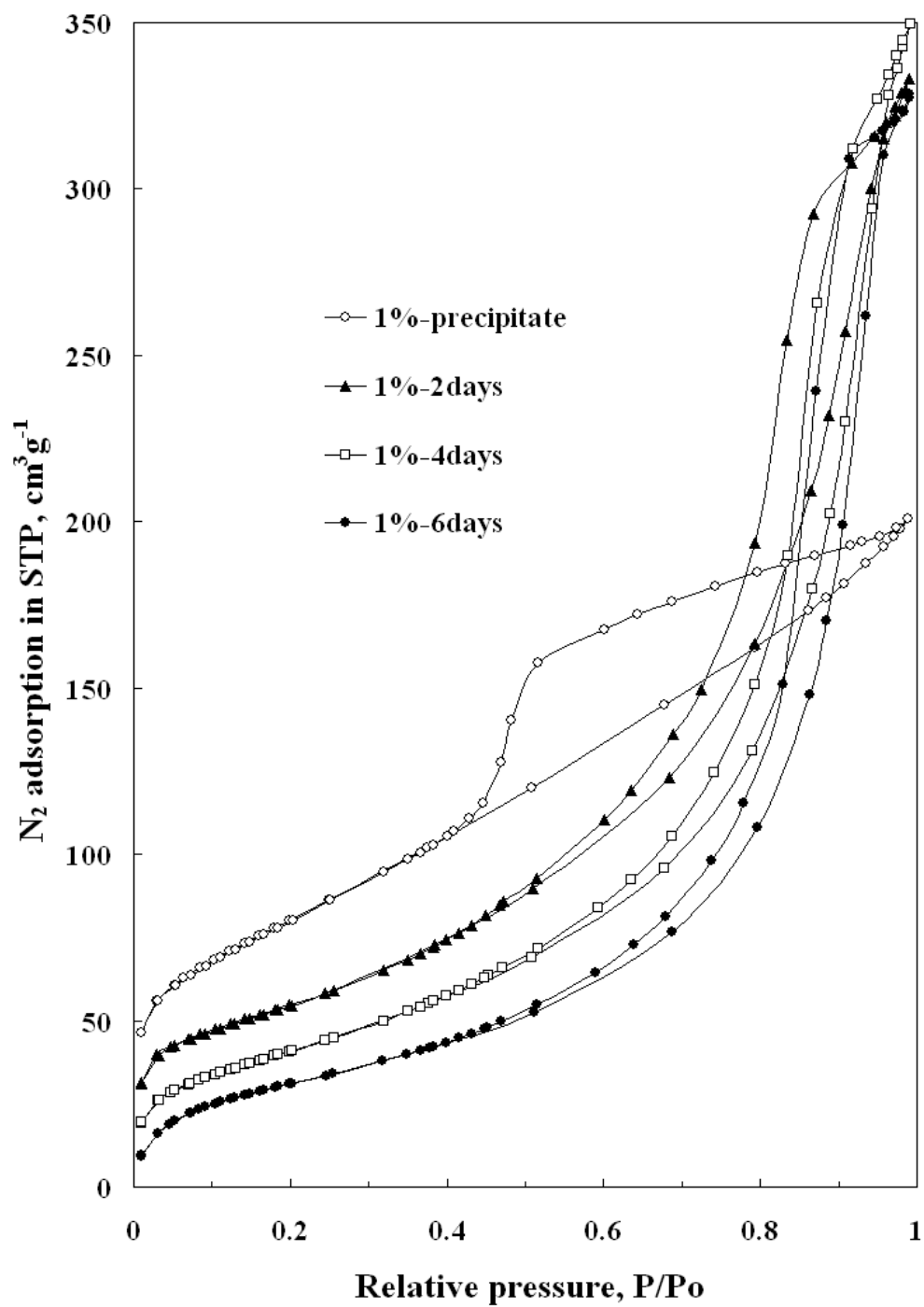


Figure 5. N_2 adsorption/desorption isotherms for the 1% Ga doped samples with 0, 2, 4, 6 days of hydrothermal treatment at 100°C .

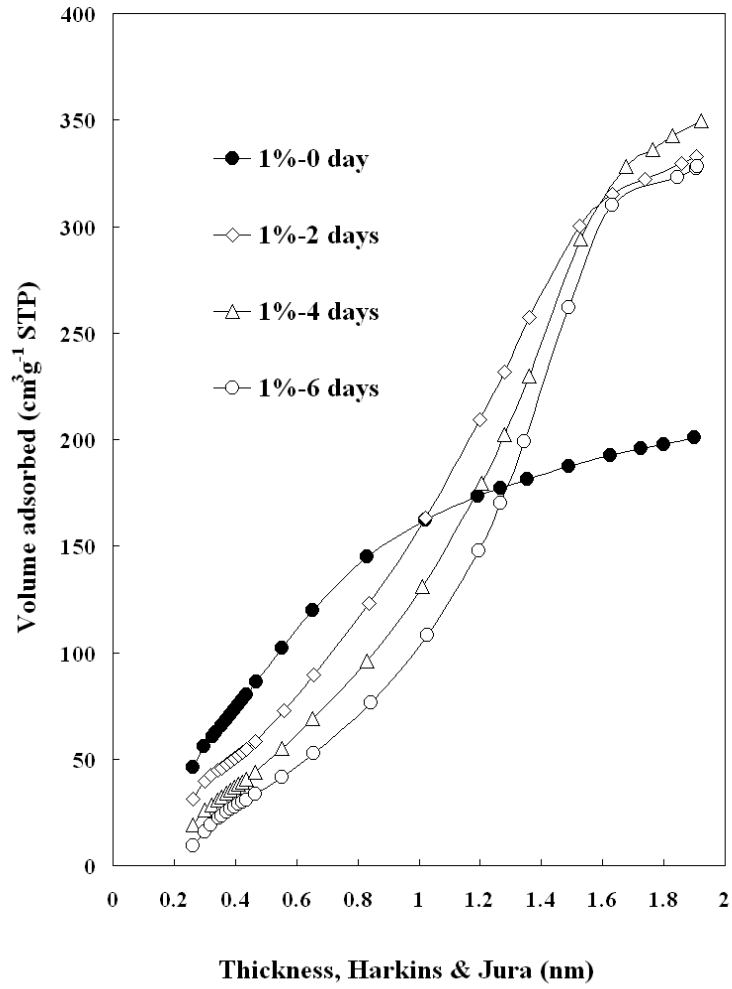


Figure 6a. *t*-plot of 1% Ga doped boehmite samples with different hydrothermal treatment duration.

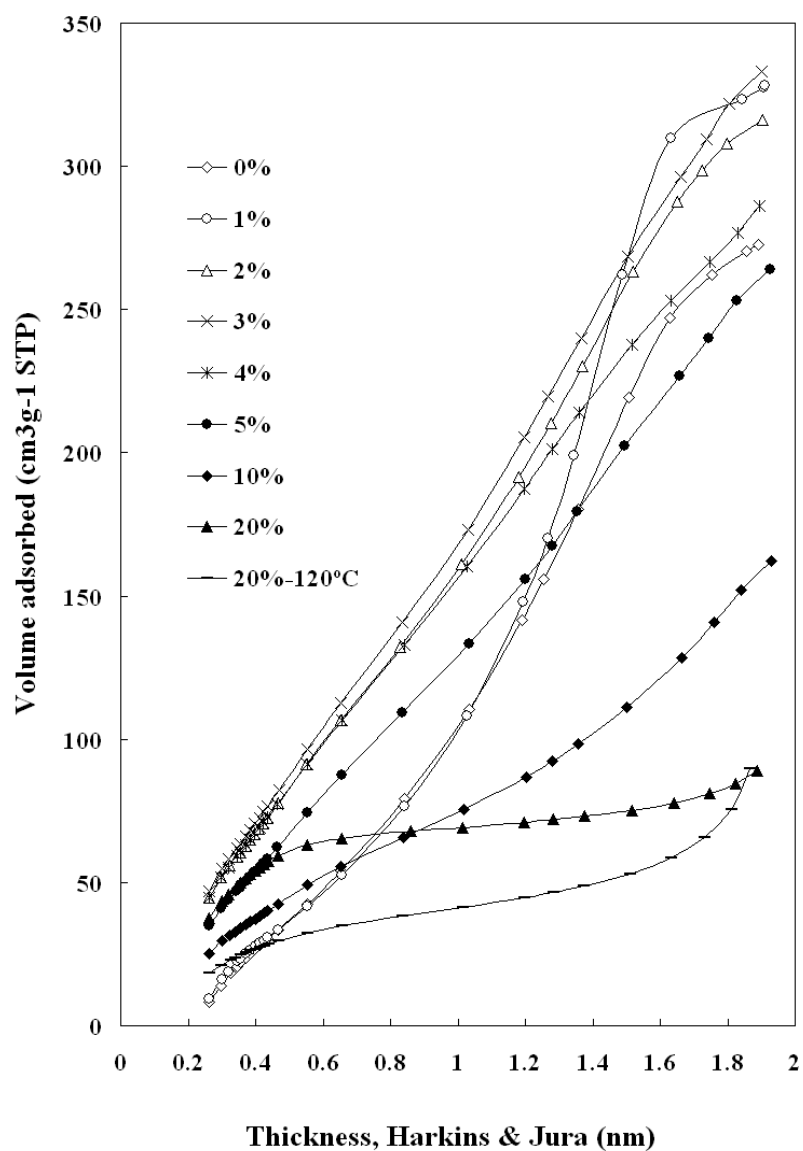


Figure 6b. *t*-plot of Ga doped boehmite samples with varying Ga percentage after 6 days hydrothermal treatment.

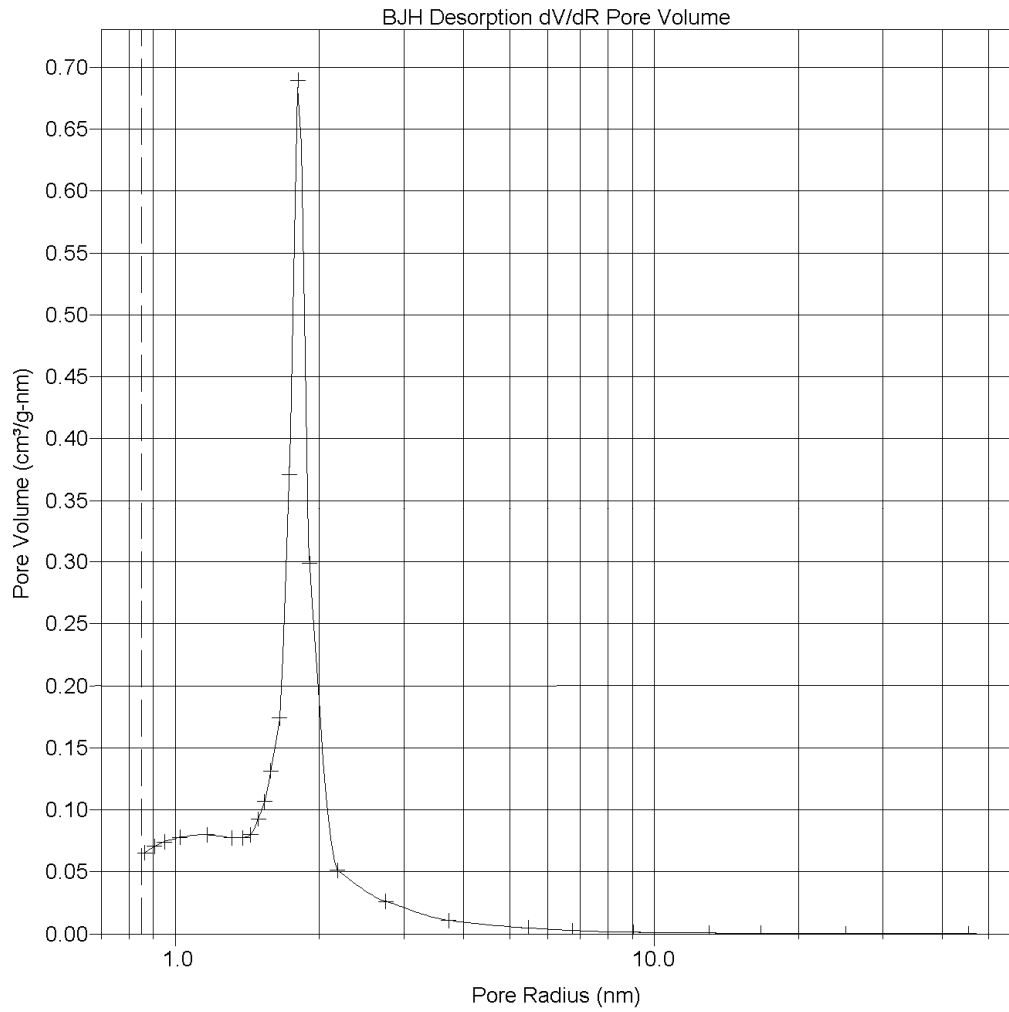


Figure 7a Pore size distribution for 1% Ga doped precipitate sample after ageing but before hydrothermal treatment.

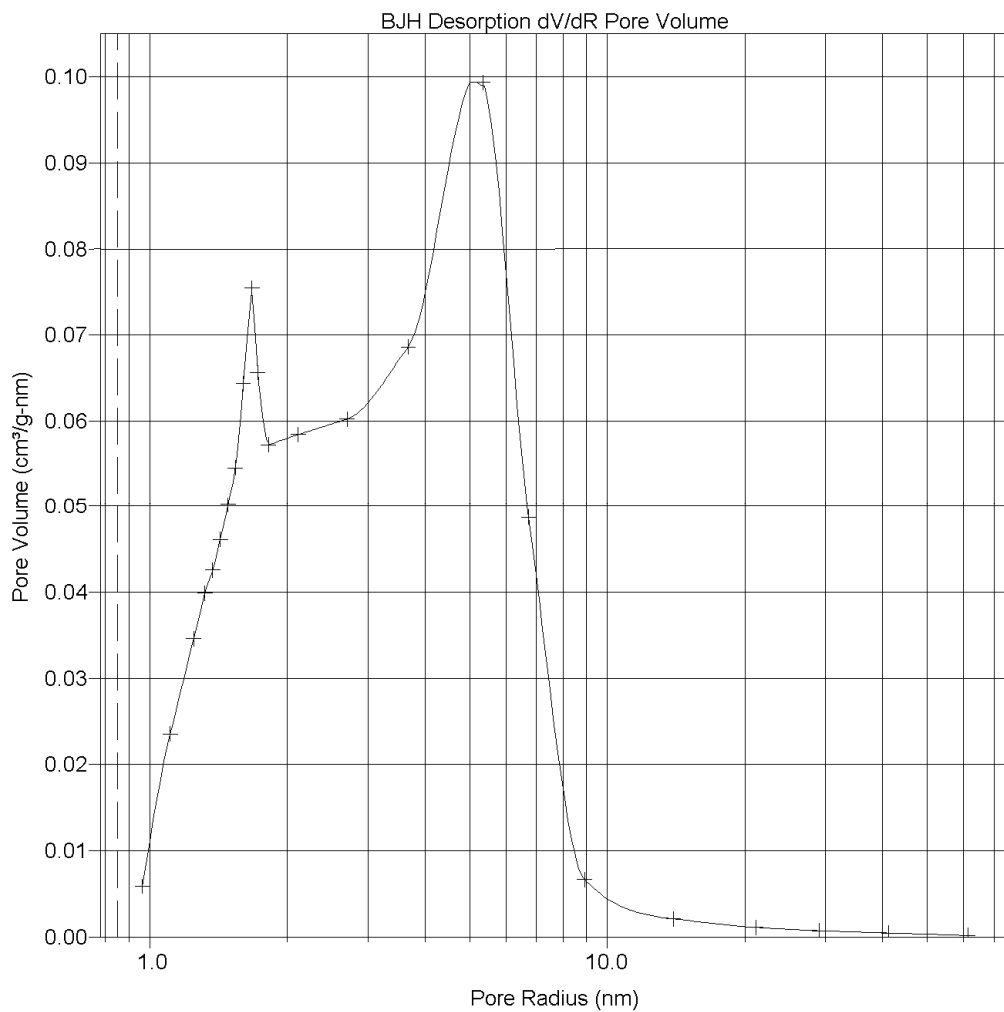


Figure 7b Pore size distribution for 1% Ga doped boehmite sample after 2 days hydrothermal treatment.

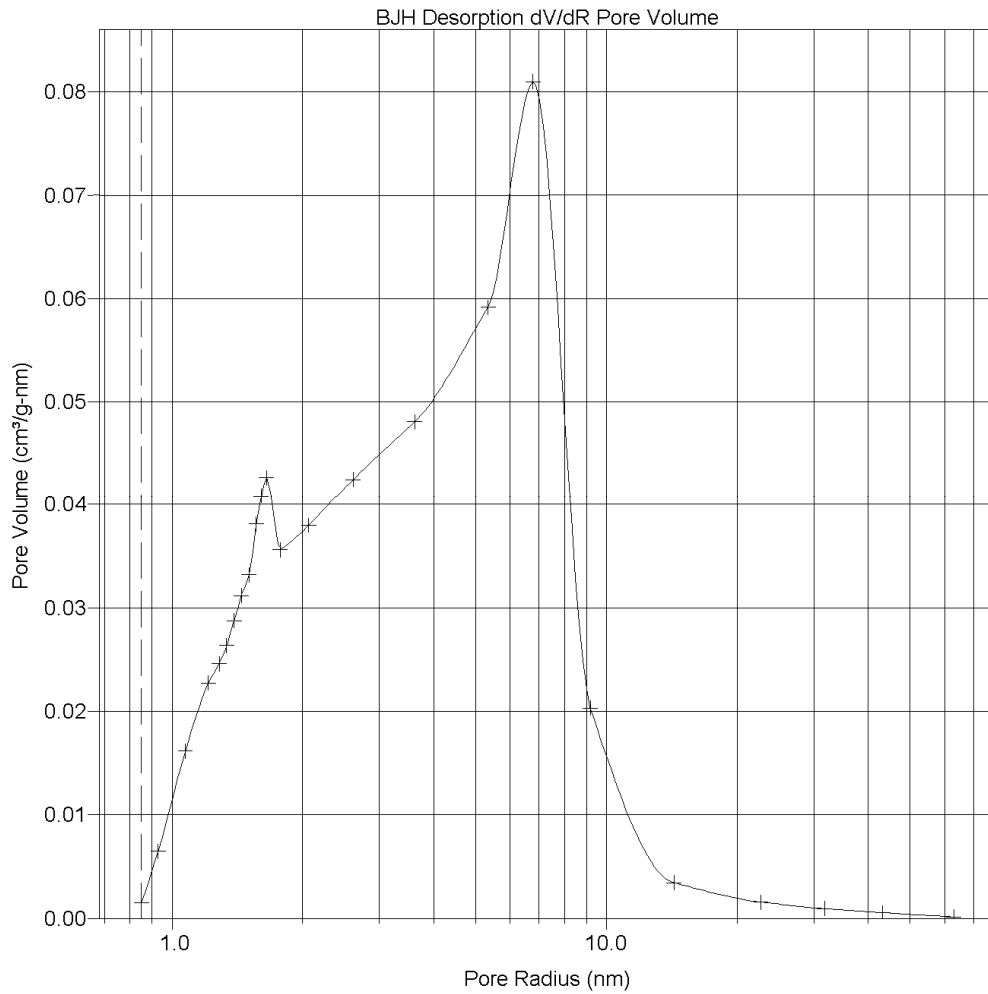


Figure 7c Pore size distribution for 1% Ga doped boehmite sample after 4 days hydrothermal treatment.

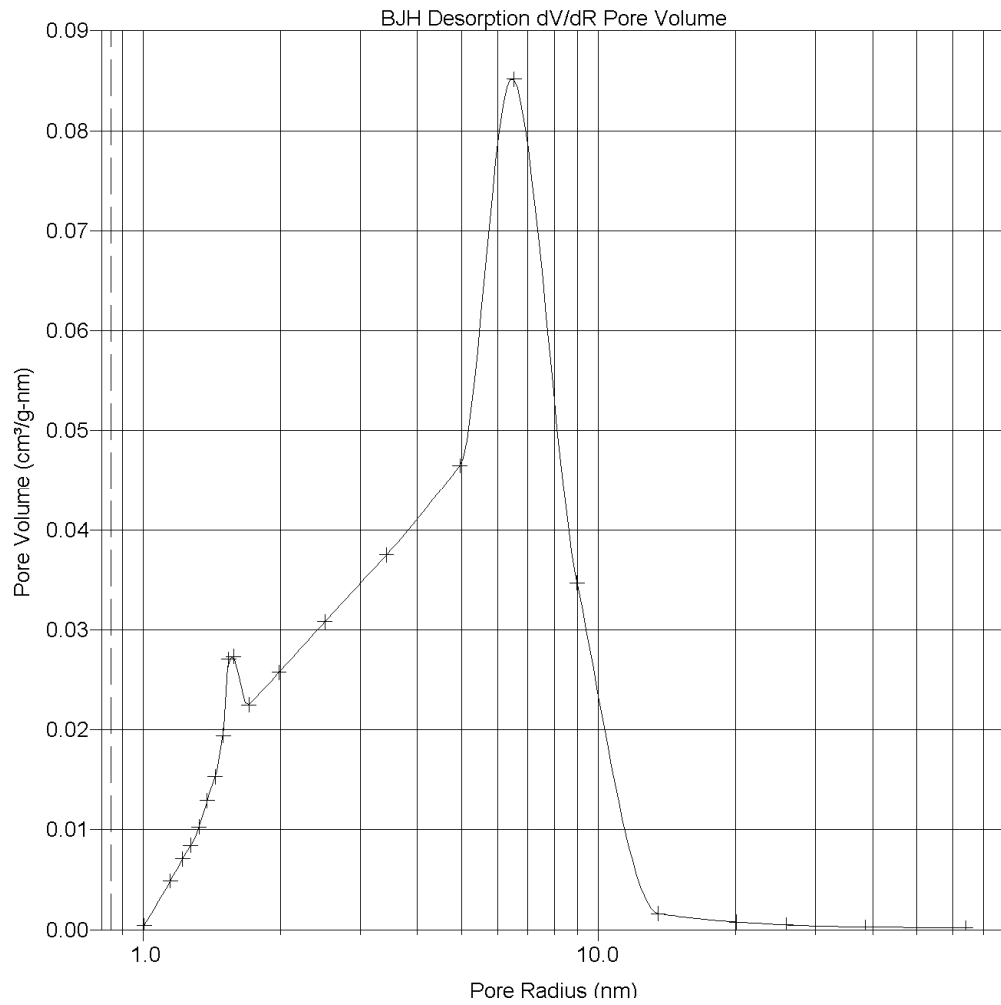


Figure 7d Pore size distribution for 1% Ga doped boehmite sample after 6 days hydrothermal treatment.

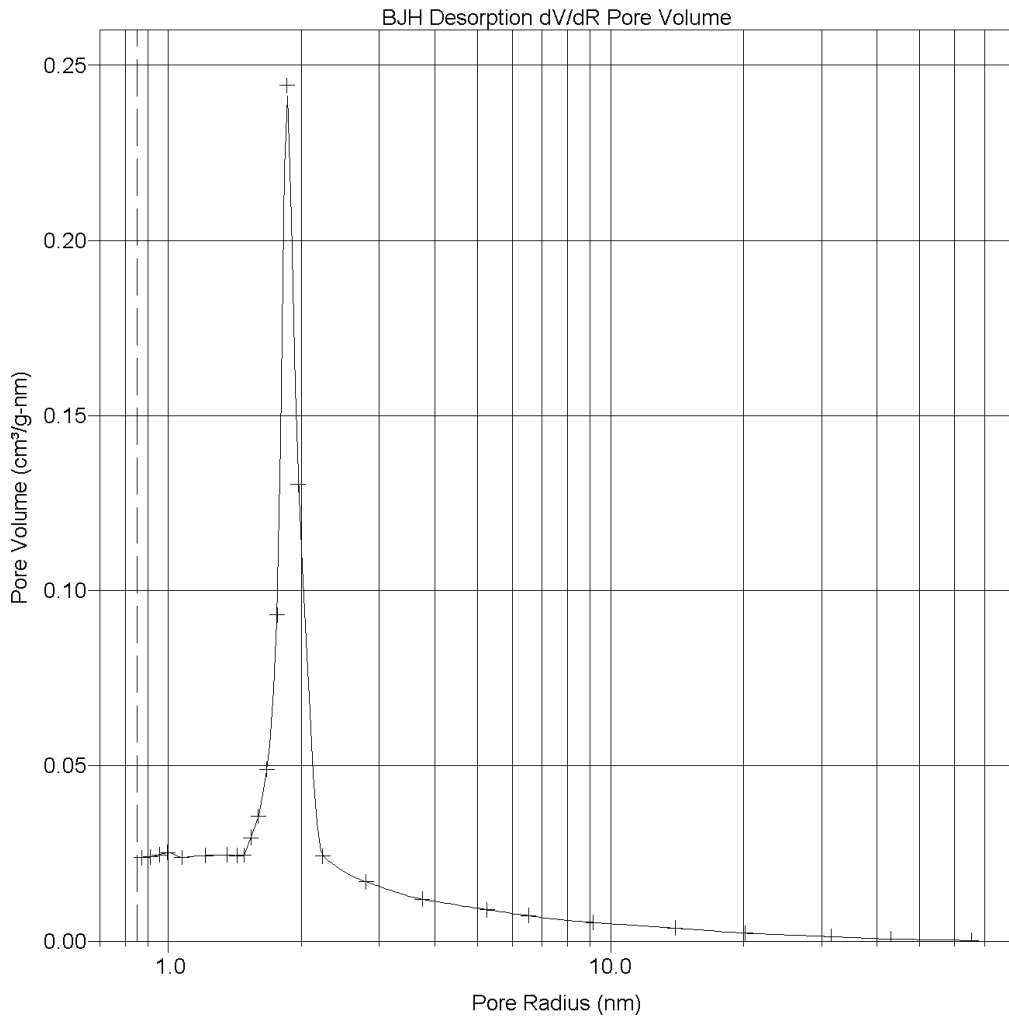


Figure 7e Pore size distribution for 10% Ga doped boehmite sample after 6 days hydrothermal treatment.

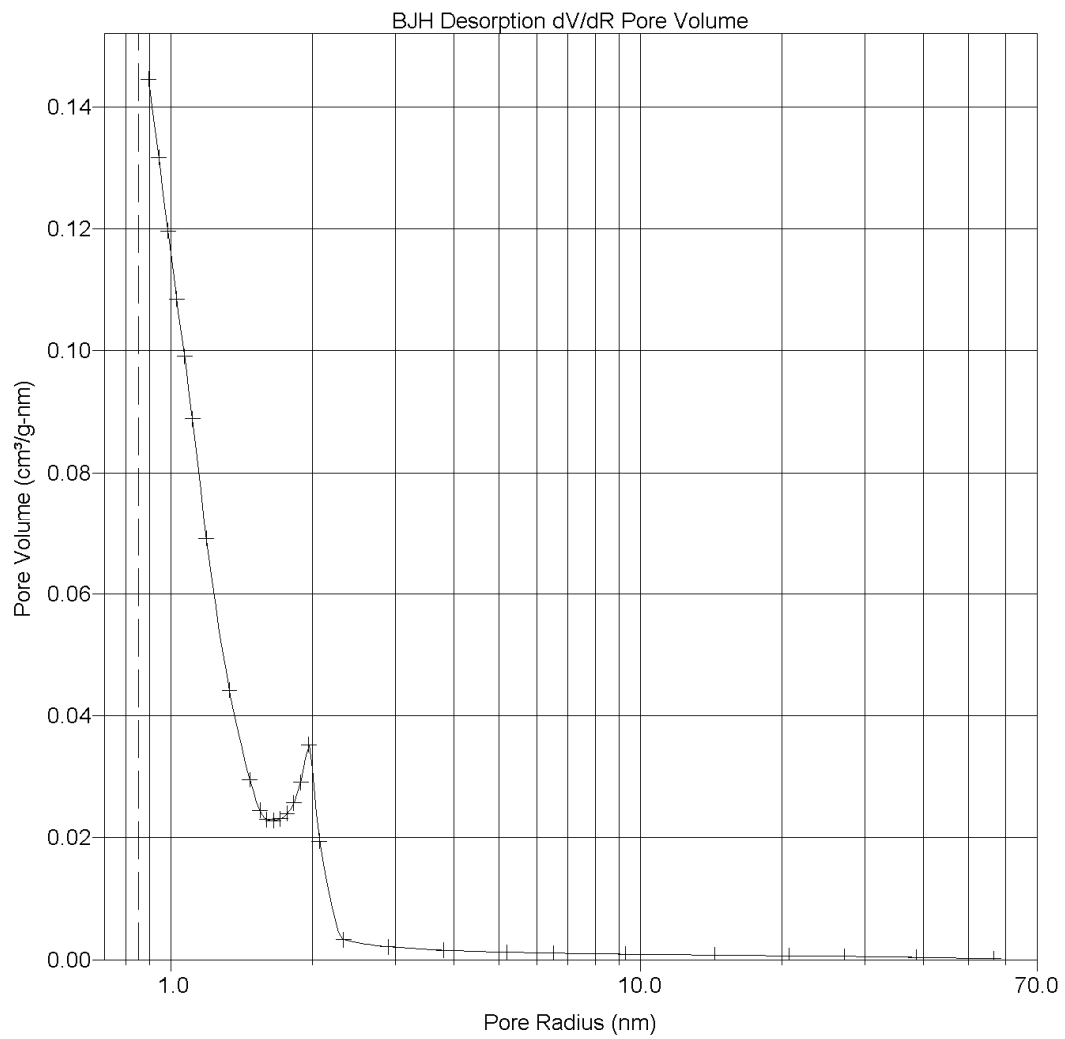


Figure 7f Pore size distribution for 20% Ga doped boehmite sample after 6 days hydrothermal treatment.

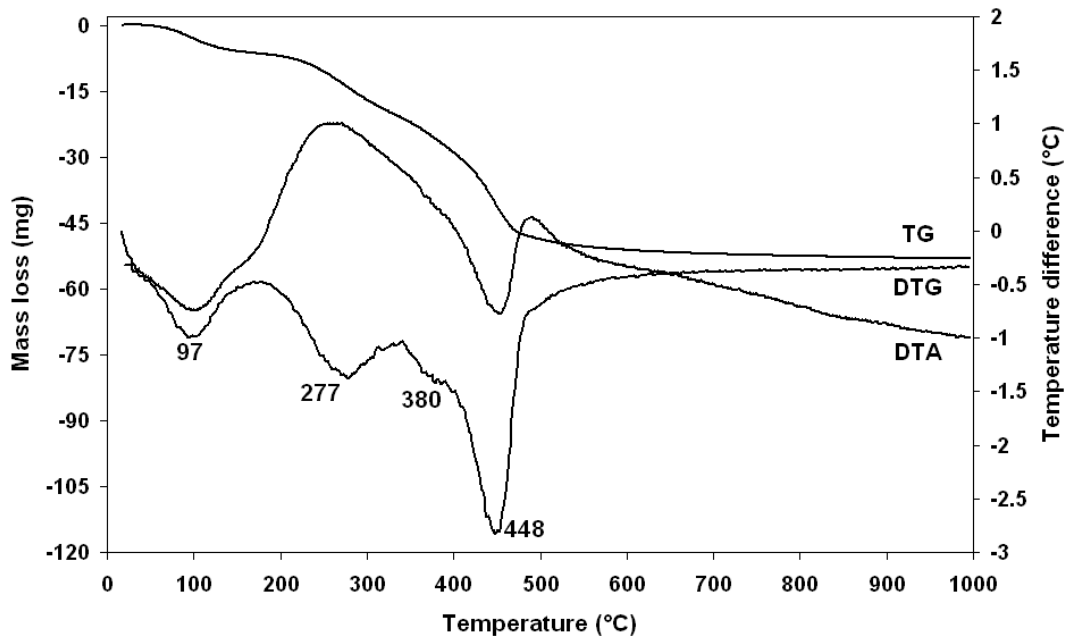


Figure 8a 1% Ga doped

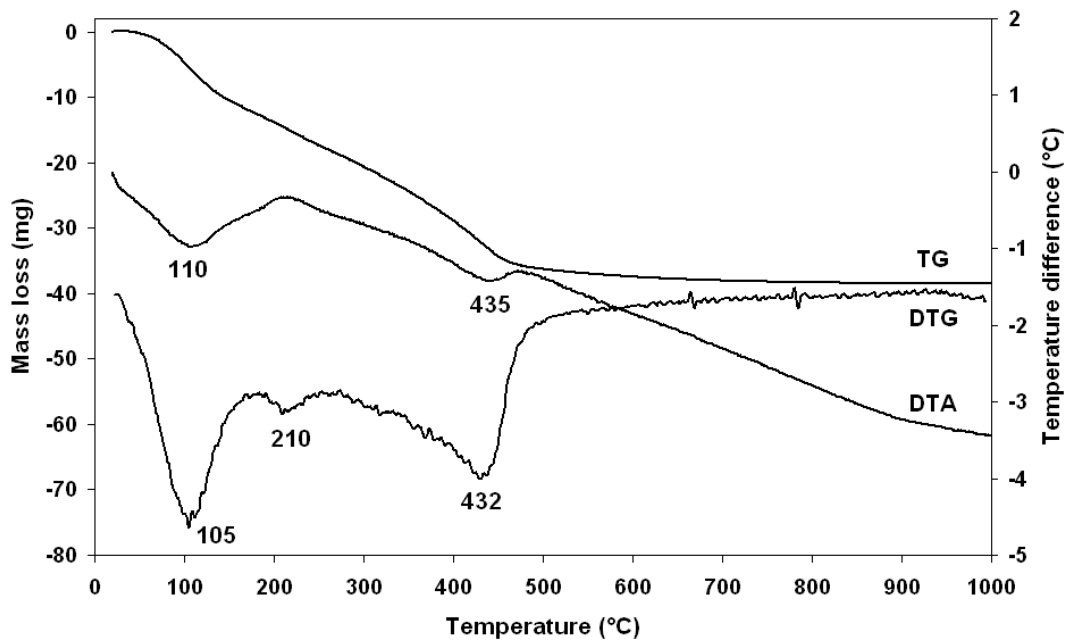


Figure 8b 3% Ga doped

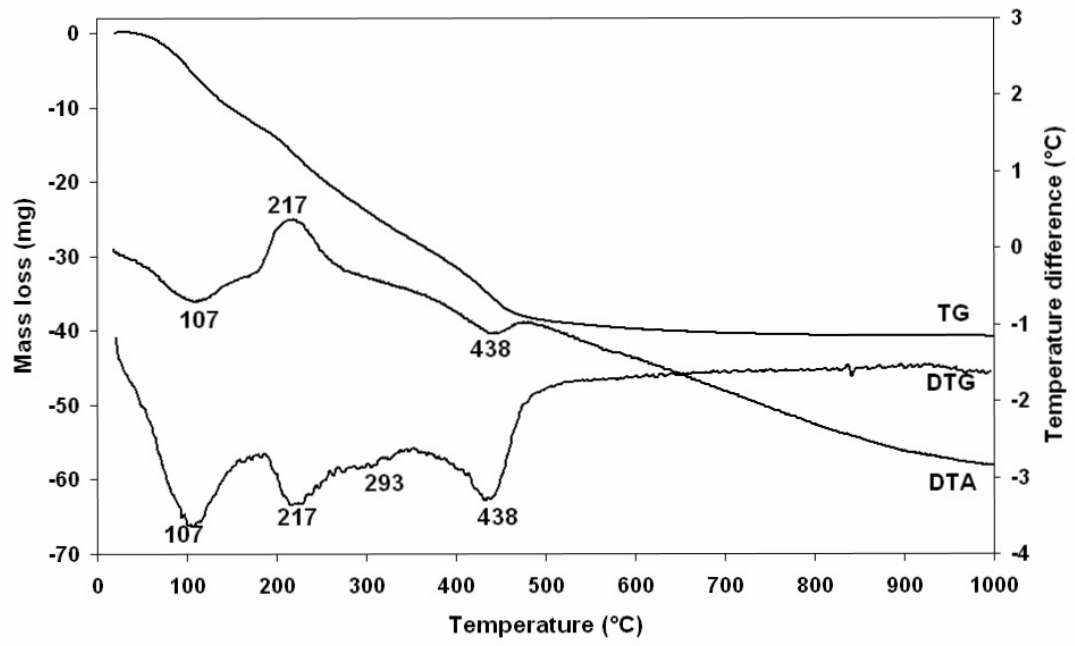


Figure 8c 5% Ga doped

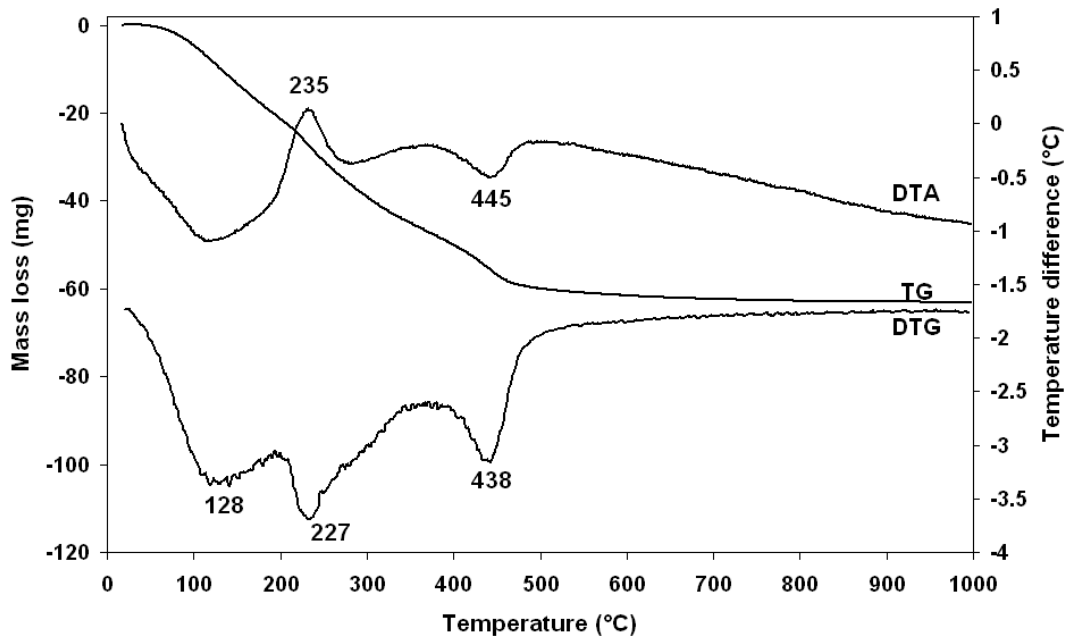


Figure 8d 10% Ga doped

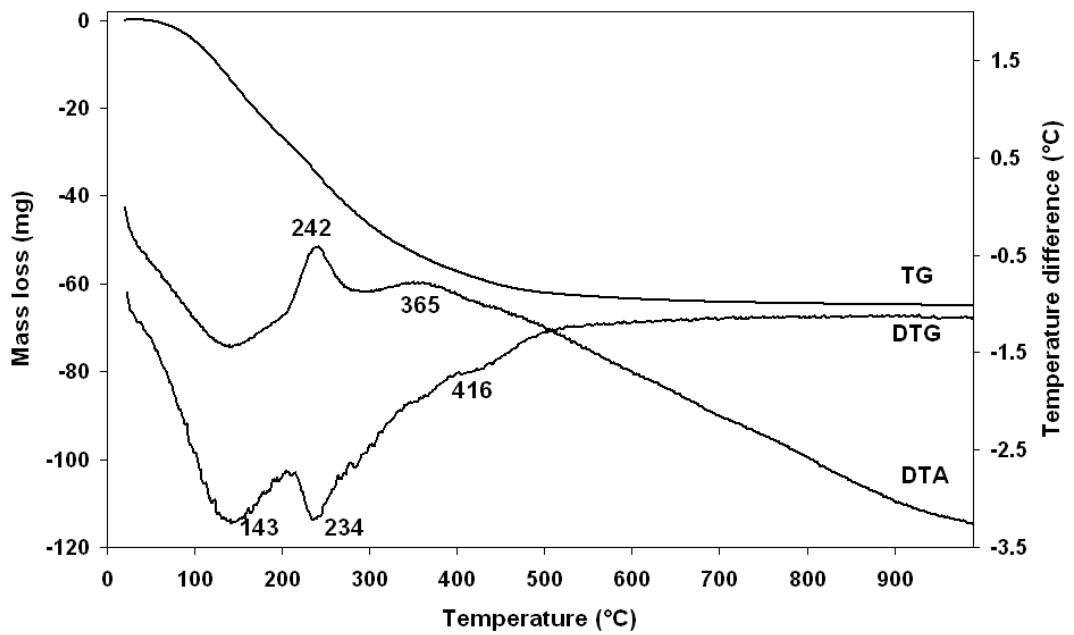


Figure 8e 20% Ga doped

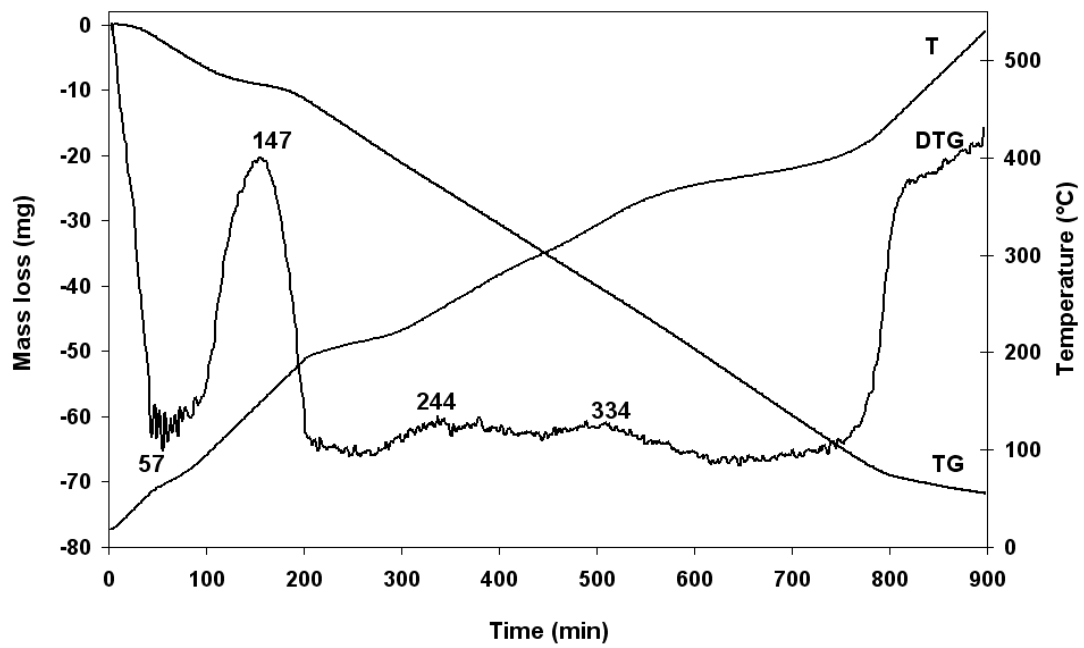


Figure 9a CRTA patterns of 1% gallium doped boehmite

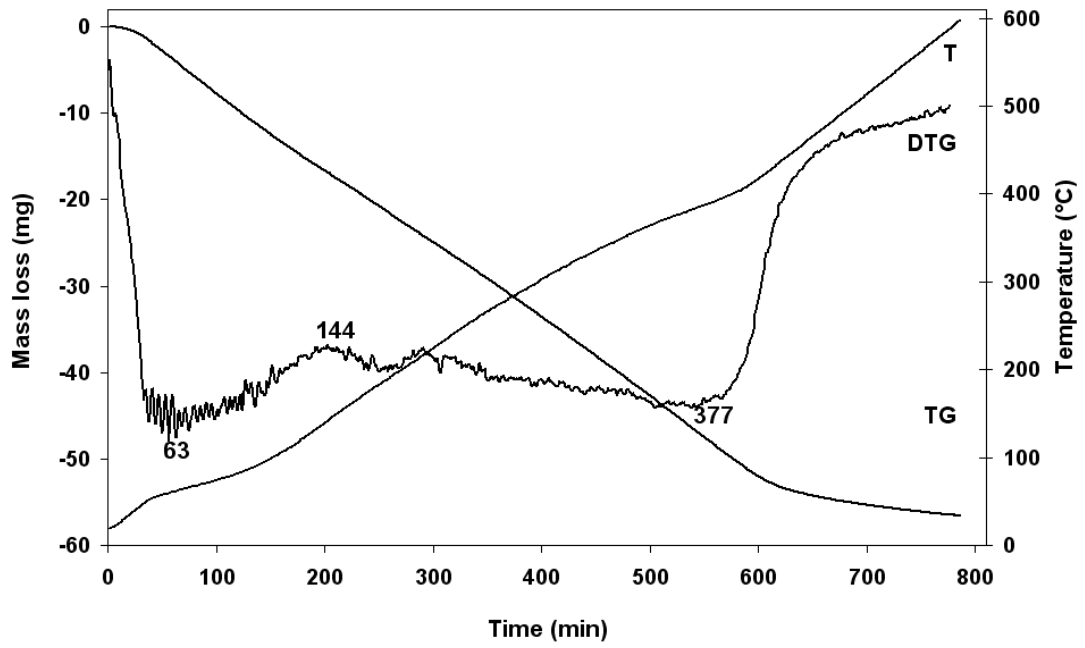


Figure 9b CRTA patterns of 3% gallium doped boehmite

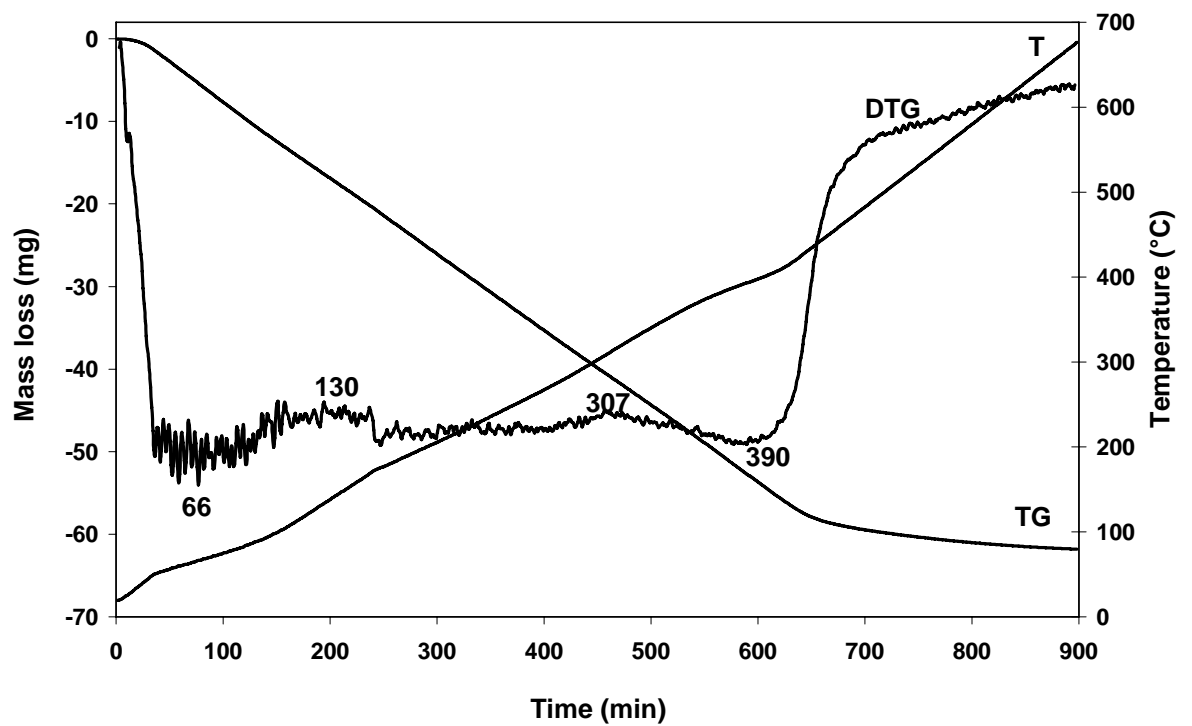


Figure 9c CRTA patterns of 5% gallium doped boehmite

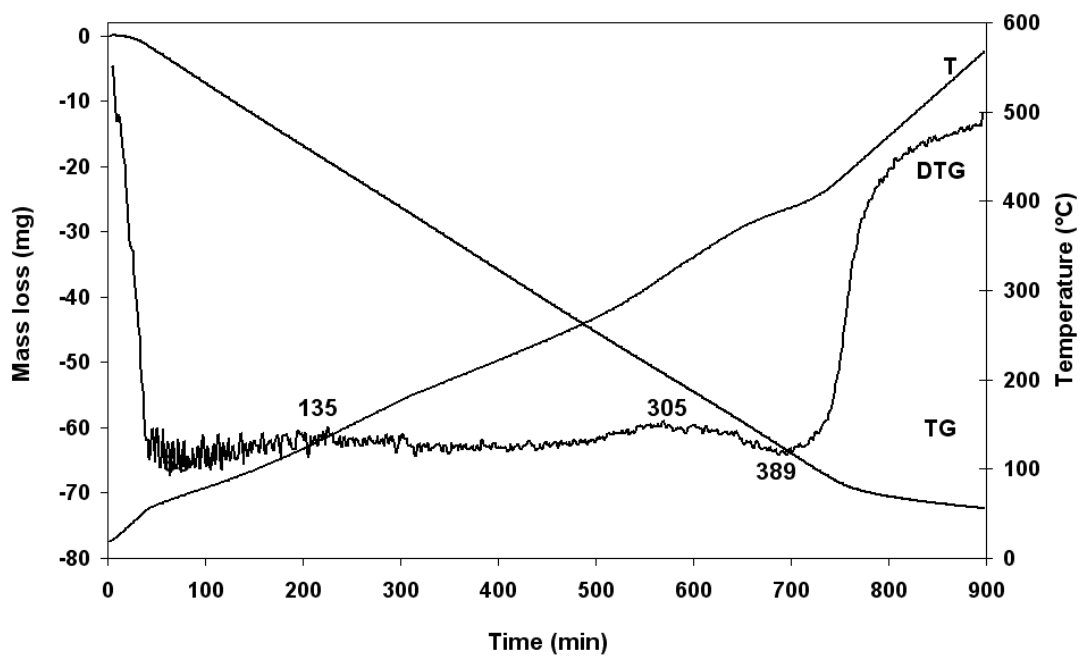


Figure 9d CRTA patterns of 10% gallium doped boehmite

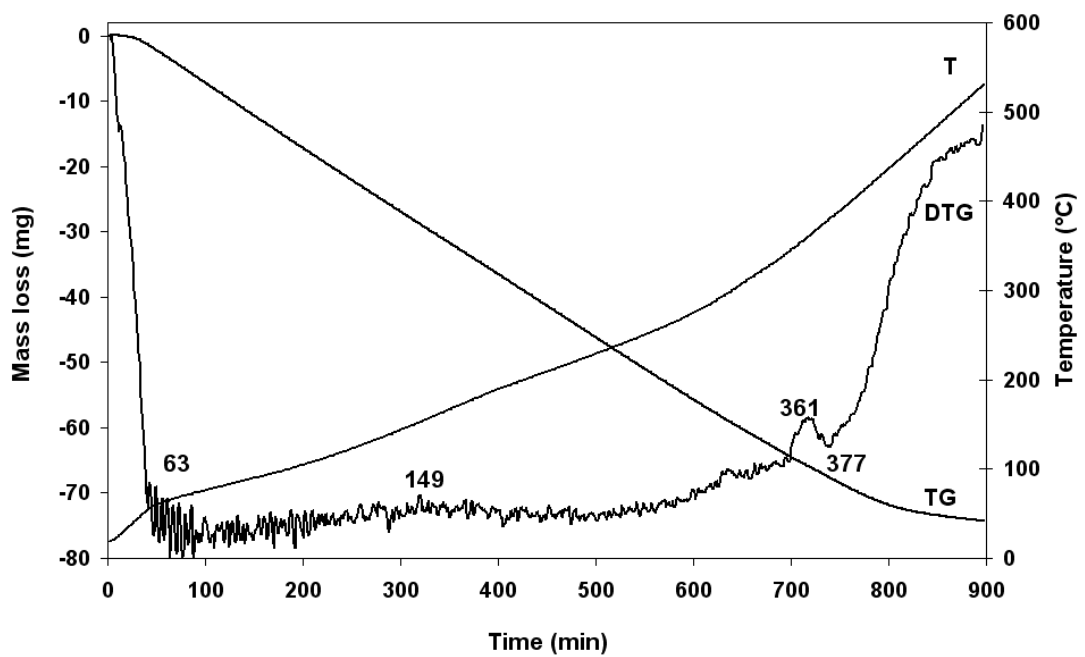


Figure 9e CRTA patterns of 20% gallium doped boehmite

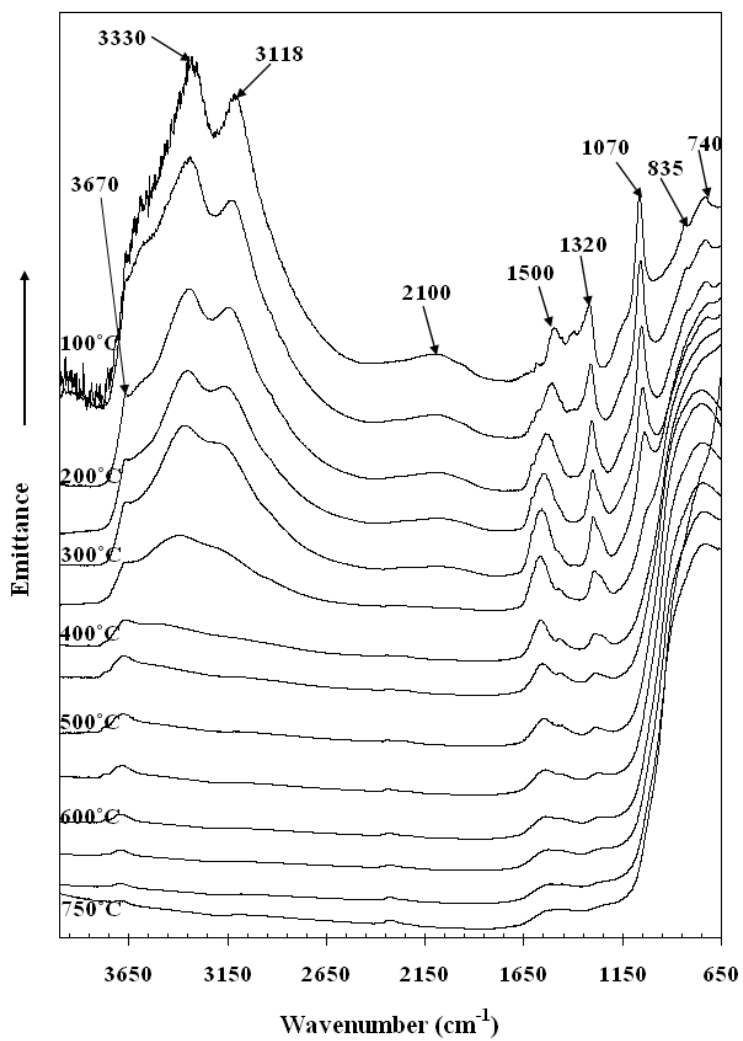


Figure 10a 5% Ga doped boehmite

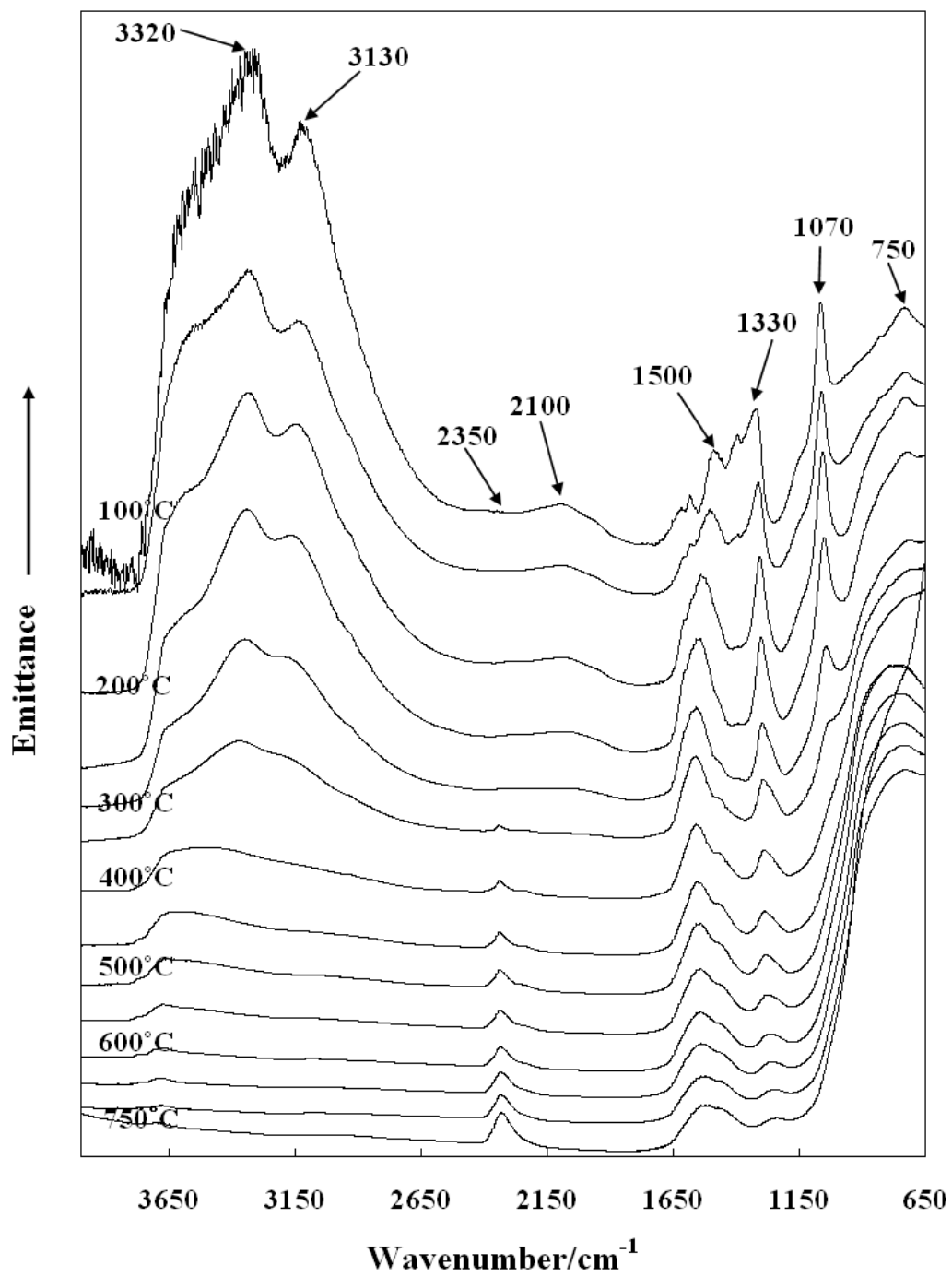


Figure 10b 10% Ga doped boehmite

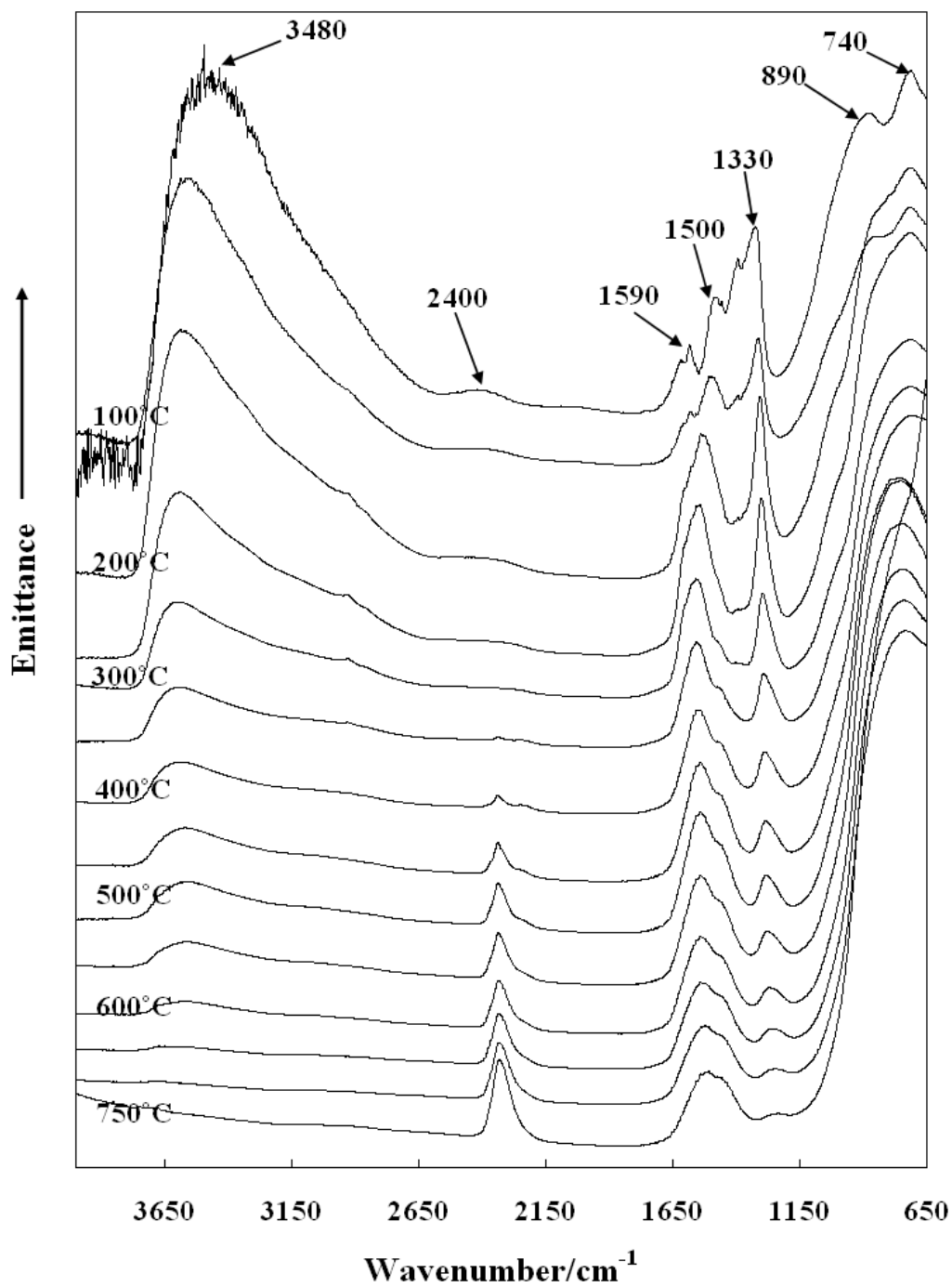


Figure 10c 20% Ga doped boehmite